Classical and quantum properties of φ Josephson junctions

Dissertation

der Mathematisch-Naturwissenschaftlichen Fakultät
der Eberhard Karls Universität Tübingen
zur Erlangung des Grades eines
Doktors der Naturwissenschaften
(Dr. rer. nat.)

vorgelegt von
Rosina Menditto
aus Piedimonte Matese

Tübingen
2017

Gedruckt mit Genehmigung der Mathematisch-Naturwissenschaftlichen Fakultät der Eberhard Karls Universität Tübingen.

Tag der mündlichen Qualifikation:	21.07.2017
Dekan:	Prof. Dr. Wolfgang Rosenstiel
1. Berichterstatter:	Prof. Dr. Reinhold Kleiner
2. Berichterstatter:	Prof. Dr. Dieter Kölle

Abstract

Josephson junctions (JJs) with nontrivial current phase relation (CPR) have attracted a large interest over the last 20 years, due to the new fundamental physics and their potential for many applications in both classical and quantum circuits, *e.g.*, as phase batteries or memory elements.

In this thesis, the properties of φ Josephson junctions in the classical and in the quantum domain are studied. A φ JJ is a junction with a doubly degenerate ground state phase $\phi = \pm\varphi$, where $0 < \varphi < \pi$. Such a system can be obtained combining a 0 and a π JJ, with phases $\phi = 0$ and $\phi = \pi$ in the ground state, respectively. The two segments should not be very different, with a small asymmetry either in the geometrical lengths ($L_0 \neq L_\pi$) or in the different critical currents densities ($j_{c0} \neq j_{c\pi}$).

The experiments presented here have been performed on φ junctions fabricated with two different technologies. The first one is based on superconductor-insulator-ferromagnet-superconductor (SIFS) JJs with a tailored ferromagnetic barrier. Realization of the φ state with such a technology was already proven in the past. In the thesis, SIFS φ junctions were used for two main experiments in the classical limit. First, we studied the retrapping dynamics of the Josephson phase upon returning from the resistive to the zero-voltage state. Since a φ JJ has two possible ground state phases, it is not obvious where the phase ends when the junction jumps back to the zero-voltage state. Second, we demonstrated the operation of the φ JJ as a deterministic ratchet. The energy $U(\phi)$ of a φ JJ is tunable by an external magnetic field, and a ratchet potential with no reflection symmetry can be easily obtained.

In the quantum regime a φ JJ can be regarded as macroscopic two-level system. Hence, it would also be interesting to investigate its quantum properties. However, several technological drawbacks affecting the SIFS φ JJs (*e.g.*, low j_c and high damping) prevented experiments in this domain. As a first attempt to improve our technology, we fabricated SIFS JJs with an additional thin superconducting interlayer s, obtaining SIsFS structures. It was proposed that such junctions can have parameters (*e.g.*, j_c, characteristic voltage V_c) comparable to conventional superconductor-insulator-superconductor (SIS) junctions. Although we actually detected an improvement with respect to the SIFS JJs, the typical parameters obtained did not fulfill our purposes. A more successful technology was attained with SIS JJs, where the phase discontinuity is artificially created

by means of the current I_{inj} circulating through two microinjectors attached to the junction. In this thesis, I present the experiments carried out on such JJs in the quantum regime, where we investigated the escape mechanism of the Josephson phase from both ground states $\pm\varphi$.

Finally, I give an outlook on measurements to be performed in the near future, where we want to create a φ JJ with an energy profile which is fully tunable electronically. Simulations predict that such a junction can be realized out of a SIS JJ with three pairs of injectors. The Josephson potential can be then controlled by adjusting the current through the two additional injector pairs, I_{inj2} and I_{inj3}, and the external magnetic flux Φ. Preliminary experimental characterization of such multiple injector junctions in the classical limit, together with numerical fits, are shown.

Kurzfassung

Josephsonkontakte (JK) mit nichttrivialer Strom-Phasen-Beziehung (SPB) haben, dank ihrer neuen grundlegenden Physik und ihrer vielen Anwendungsmöglichkeiten in klassischen und Quanten-Schaltkreisen, wie z.B. als Phasenbatterien oder Speicherelemente, in den letzen zwanzig Jahren ein großes Interesse geweckt.

In dieser Doktorarbeit werden die Eingenschaften von φ-Josephsonkontakten im klassischen und im quantenmechanischen Regime studiert. Ein φ-JK ist ein Kontakt, der eine zweifach entartete Grundzustandsphase $\phi = \pm\varphi$ hat, wobei $0 < \varphi < \pi$. Ein φ-JK kann durch die Kombination eines 0- und eines π-JKs hergestellt werden, deren Grundzustandsphasen $\phi = 0$ bzw. $\phi = \pi$ sind. Die zwei Teile sollen nicht zu unterschiedlich sein, mit einer kleinen Asymmetrie etweder in den geometrischen Längen ($L_0 \neq L_\pi$) oder in den kritischen Stromdichten ($j_{c0} \neq j_{c\pi}$). Die hier präsentierten Experimente wurden mit φ-Kontakten durchgeführt, die mit zwei verschiedenen Technologien hergestellt wurden. Die erste basiert auf Supraleiter-Isolator-Ferromagnet-Supraleiter-Josephson-Kontakten (SIFS-JK) mit einer maßgeschneiderten ferromagnetischen Barriere. Die Realisierung von φ-Kontakten mithilfe dieser Technologie wurde bereits in der Vergangenheit demonstriert. Im Rahmen meiner Doktorarbeit wurden solche Kontakte für zwei Hauptexperimente im klassischen Regime benutzt. Erstens studierten wir die Dynamik des Retrapping-Prozesses der Josephsonphase bei der Rückkehr aus dem resistiven in den spannungslosen Zustand. Da der φ-JK zwei Grundzustandsphasen hat, ist es nicht ersichtlich, welche Phase sich einstellt, wenn der Kontakt in den Spannungslosen Zustand zurückspringt. Zweitens demonstrierten wir den Betrieb eines φ-JK als deterministische Ratsche. Die Energie $U(\phi)$ eines φ-JKs kann mithilfe eines äußeren Magnetfelds gesteuert werden, und ein Ratschenpotential mit gebrochener Reflektionssymmetrie kann auf einfache Art realisiert werden.

Im quantenmechanischen Regime kann der φ-JK als ein makroskopisches zwei-Niveau-System aufgefasst werden, was Untersuchungen im Quantenregime interessant macht. Experimente in diesem Regime waren jedoch wegen mehrerer technologischer Nachteile für SIFS-φ-JK (z.B. niedriges j_c und hohe Dämpfung) nicht möglich. In einem ersten Versuch, unsere Technologie zu verbessern, stellten wir SIFS-JK mit einer zusätzlichen dünnen supraleitenden Zwischenschicht s her, was SIsFS-Strukturen ergab.

Es wurde vermutet, dass solche Kontakte vergleichbare Parameter (z.B. j_c, charakteristische Spannung V_c) wie Supraleiter-Isolator-Supraleiter-Kontakte (SIS-JK) haben können. Obwohl wir tatsächlich eine Verbesserung gegenüber der vorherigen SIFS-Technologie erzielen konnten, erfüllten die typischerweise erreichten Parameter nicht unsere Anforderungen. Eine erfolgreichere Technologie wurde mit SIS-JK entwickelt, wobei die Phasendiskontinuität künstlich mithilfe eines in einem mit dem Kontakt verbundenen Injektorpaar fließenden Stromes erzeugt wurde. In dieser Arbeit präsentiere ich die Versuche, die mit solchen JK im quantenmechanischen Regime durchgeführt wurden, wobei wir das Entkommen der Josephsonphase aus beiden Grundzuständen $\pm\varphi$ untersuchten.

Abschließend gebe ich einen Ausblick auf Geometrien, die einen φ-JK mit vollständig elektronisch steuerbarem Energieprofil verwirklichen können. Simulationen sagen vorher, dass ein solcher Kontakt aus einem SIS-JK mit drei Injektorpaaren realisiert werden kann. In diesem System kann das Josephsonpotenzial gesteuert werden, indem man den Strom durch zwei zusätzliche Injektorpaare, I_{inj2} und I_{inj3}, sowie den äußeren magnetischen Fluss Φ anpasst. Die vorläufige experimentelle Charakterisierung und die numerische Analyse von solchen Kontakten mit Multiinjektoren im klassischen Regime werden vorgestellt.

List of publications

This cumulative thesis is based on the work published in the four papers listed below. A fifth manuscript is in preparation. The publications are attached at the end of the thesis.

Publications

- **Publication 1**

  R. Menditto, H. Sickinger, M. Weides, H. Kohlstedt, M. Žonda, T. Novotný, D. Koelle, R. Kleiner, and E. Goldobin
  "Phase retrapping in a φ Josephson junction: Onset of the butterfly effect"
  Phys. Rev. B **93**, 174506 (2016)

- **Publication 2**

  E. Goldobin, **R. Menditto**, D. Koelle and R. Kleiner
  "Model I–V curves and figures of merit of underdamped deterministic Josephson ratchets"
  Phys. Rev. E **94**, 032203 (2016)

- **Publication 3**

  R. Menditto, H. Sickinger, M. Weides, H. Kohlstedt, D. Koelle, R. Kleiner and E. Goldobin
  "Tunable φ Josephson junction ratchet"
  Phys. Rev. E **94**, 042202 (2016)

- **Publication 4**

  N. Ruppelt, H. Sickinger, **R. Menditto**, E. Goldobin, D. Koelle, R. Kleiner, O. Vavra, H. Kohlstedt
  "Observation of 0–π transition in SIsFS Josephson junctions"
  Appl. Phys. Lett. **106**, 022602 (2015)

Manuscript in preparation

- **R. Menditto**, M. Merker, M. Siegel, D. Koelle, R. Kleiner and E. Goldobin
  "An artificial φ Josephson junction: Evidence of macroscopic quantum tunneling from both ground states." (preliminary title)

Publications not included in this thesis

- **Publication 1**

  I. Ottaviani, M. Lucci, **R. Menditto**, V. Merlo, M. Salvato, M. Cirillo, F. Müller, T. Weimann, M. G. Castellano, F. Chiarello *"Characterization of anomalous pair currents in Josephson junction networks"*
  J. Phys.: Condens. Matter **26**, 215701 (2014)

- **Publication 2**

  L. Persichetti, **R. Menditto**, A. Sgarlata, M. Fanfoni and A. Balzarotti *"Hugh-like island growth of Ge on strained vicinal Si(111) surfaces"*
  Appl. Phys. Lett. **99**, 161907 (2011)

Contents

1 Introduction

The *Josephson effect*, first predicted by B. Josephson [1], is a quantum coherent phenomenon that describes the transfer of *Cooper pairs* (electrons correlated in momentum space) across a thin barrier separating two superconductors. The barrier can be an insulator (I), a normal metal (N) or a ferromagnet (F). More recently barriers based on semiconducting and organic materials have been explored, *e.g.*, semiconducting nanowires, quantum dots, carbon nanotubes and graphene. Such a device, known as a *Josephson junction* (JJ), represents the building block of superconducting electronics.

The physics and the properties of a JJ are derived from the *first Josephson relation* linking the (super)current I_s through the junction to the difference of the phases $\phi = \phi_2 - \phi_1$ of the wave functions $\Psi_{1,2}$ describing the two superconductors. The equation is also known as *current–phase relation* (CPR). For most type of JJs, the CPR is a 2π-periodic function of the phase. Below, I will refer to only one of the periods.

Generally, for *conventional JJs*, the CPR is $I_\mathrm{s}(\phi) = I_\mathrm{c}\sin(\phi)$, where $I_\mathrm{c} > 0$ is the highest current that can flow without dissipation. In this case, the junction energy $U(\phi)$, calculated as the integral of the CPR with respect to ϕ, has a minimum at $\phi = 0$. Therefore the junction is called a 0 JJ.

In the past four decades, *unconventional JJs* with different CPRs [2] and a non-zero phase energy minimum have been proposed and were intensively investigated, due to the potential for new applications in classical and quantum superconducting circuits. These types of junctions are π JJs, φ_0 JJs and φ JJs.

In a π JJ the phase difference ϕ carries an additional shift of π in the CPR with respect to the 0 JJ, *i.e.* $I_\mathrm{s}(\phi) = I_\mathrm{c}\sin(\phi + \pi)$. Hence the Josephson energy has a minimum at $\phi = \pi$. The interesting aspect of a π JJ is evident when such a junction is closed into a superconducting ring. In order to satisfy the fluxoid quantization, a spontaneous current carrying a half flux quantum $\pm\Phi_0/2$ (called a "Semifluxon") may be generated in the ring [3, 4]. This current can be used to feed other circuits, thus one creates a *phase battery*. Predicted in 1977 by Bulaevskiĭ [5], in the last twenty years, π JJs have been realized with several technologies, [6–21], and found application in both classical [22] and quantum circuits [23, 24].

Similarly to the π JJ, one defines a φ_0 JJ as a junction exhibiting an

arbitrary finite phase shift in the CPR, *i.e.* $I_s(\phi) = I_c \sin(\phi + \varphi_0)$. In this case, the energy profile shows a minimum at $\phi = \varphi_0 \neq 0, \pi$. These kind of junctions have been intensively studied from the theoretical point of view [25–27], but realized for the first time in a quantum interference device (SQUID) based on a nanowire quantum dot only recently [28].

In my thesis I focus on the third type of the listed novel JJs: the φ JJ. A φ JJ can be realized by a CPR with two harmonics, $I(\phi) = I_{c1} \sin(\phi) + I_{c2} \sin(2\phi)$, with $I_{c2} < -|I_{c1}|/2$ [29, 30]. The distinctive feature of such a junction is that the energy $U(\phi)$ has *two degenerate ground states* at $\phi = \pm\varphi$ within each 2π-period, where $0 < \varphi < \pi$. As a consequence, the junction has two critical currents (with different amplitude), corresponding to the escape of the Josephson phase from the $+\varphi$ and the $-\varphi$ well. The two phase states can be used to store information [31] or, in the quantum limit, to study quantum coherence, since the junction can be pictured as a quantum mechanical two-level system. Furthermore, similarly to the π JJ, a φ JJ can be used to realize a phase battery.

It was theoretically predicted that a JJ with an effective negative second harmonic I_{c2} in the CPR can be realized out of a 0-π JJ [32, 33]. Experimentally, such a junction was realized for the first time in 2012 by the Tübingen group in collaboration with Forschungszentrum Jülich using a SIFS junction with a stepped ferromagnetic layer [34].

In the first part of my thesis I show results obtained in the investigation of φ JJs fabricated with SIFS technology. In particular, we studied the process of the retrapping of the Josephson phase. Since the φ JJ has two energy minima, it is interesting to understand in which one the phase will be trapped when the JJ returns from the finite to the zero-voltage state, and to find which parameters may play a role. To this purpose, we performed measurements of switching current distributions as a function of temperature and compared the results to the theory [35]. Furthermore, since the reflection symmetry of the energy profile $U(\phi)$ of a φ JJ can be broken upon application of an external magnetic field H [32], we demonstrate the operation of the φ JJ as a voltage rectifier (ratchet) in the idle regime and in the presence of a counterforce. A theoretical model describing the ratchet is derived and main figures of merit are estimated.

The realization of a φ JJ based on the SIFS technology is quite challenging and it is affected by several problems. The balance between the 0 and π segments is rather complicated, and a precision of less than 1 Å is required in the thickness of the ferromagnetic layers $d_{F,0}$ and $d_{F,\pi}$ for

short junctions (the length L is smaller than the Josephson penetration depth λ_J). Moreover, the presence of the F-layer causes a low critical current density ($j_c \lesssim 60\text{A/cm}^2$), that translates into a classical-to-quantum crossover temperature $T^\star$ of only a few mK, and a strong dissipation. As a consequence, the SIFS junctions are not suitable to study the properties of φ JJs in the quantum limit. Our attempt to increase j_c to typical values of the SIS JJs (*i.e.* $j_c \sim \text{kA/cm}^2$) by inserting a thin superconducting interlayer in the structure (SIsFS JJs) as proposed in [36–40] was not successful. The highest critical current density achieved in the π region was only $60\,\text{A/cm}^2$ for an s-layer 11 nm thick. SIsFS JJs with thicker d_s showed a much higher j_c. However, no 0-π phase transition was observed by varying d_F.

In the second part of my thesis I present the investigation of a φ JJ realized with the conventional SIS technology, where a 0-π phase discontinuity is artificially induced by two tiny leads (*aka* current injectors) attached to one of the junction electrodes [41, 42]. The technology has been developed in collaboration with the Karlsruhe Institute of Technology, and it has been improved in the past few years to provide high quality junctions with very narrow injectors. Up to now, the tiniest working injectors have a width of 1 μm. Further progress is needed in order to get sub-μm dimensions. SIS junctions exhibit many advantages with respect to the ferromagnetic ones. Firstly, they have typically very low dissipation, and secondly, they can be realized with high j_c — up to a few kA/cm^2 — by simply controlling the oxidation of the insulating barrier. A larger j_c results in a crossover temperature $T^\star$ of hundreds of mK. In this way, at $T = 20\,\text{mK}$ (the base temperature of a dilution refrigerator), one is deep in the quantum regime. In the frame of my Ph.D. project, such junctions were used to investigate the quantum dynamics of the Josephson phase in the φ JJ potential. I will present here evidence of macroscopic quantum tunneling (MQT) from the $\pm\varphi$ wells.

The thesis is organized as follows. The **first chapter** reviews the basics of conventional Josephson junctions. The properties of a φ JJ are described in **chapter two**. The **third chapter** concerns the investigation of the retrapping of the Josephson phase in a SIFS φ JJ. Here, I summarize the experimental results published in Publication 1. In the **fourth chapter**, I summarize the content of two of my papers (Publication 2 and 3) that report on a Josephson ratchet. Publication 2 illustrates a simple and generic theoretical model that describes and derives main key figures

of a ratchet based on JJ systems. In Publication 3, I show the experimental demonstration of a voltage rectifier realized from a single SIFS φ JJ, and apply the theoretical model to it. In the **fifth chapter**, I present the experimental investigation of the 0-π transition in SIsFS JJs that we performed in order to realize a φ JJ with a higher j_c. The work is the subject of Publication 4. The **sixth chapter** deals with the realization of a φ JJ with current injectors. Experimental characterization in the classical and quantum domain is shown (manuscript in preparation). The thesis closes with a **Summary** and an **Outlook**, where I discuss unsolved problems and possible new experiments. The **Bibliography** precedes the reprints of all my publications at the very end of the thesis.

2 Fundamentals of Josephson junctions

2.1 Superconductivity

Superconductors (SCs) are materials exhibiting zero electrical resistance [43] and a perfect diamagnetic state [44] below a critical temperature T_c and below some critical magnetic field (B_{c1} for type-II SCs). Their discovery in 1911 [43] opened a new and exotic field in physics, that fascinates scientists ever since.

It took almost 50 years for physicists to find a microscopic explanation to the phenomenon of superconductivity, that is elegantly described in the Bardeen-Cooper-Schrieffer (BCS) theory [45]. According to this theory, superconductivity arises due to the formation of pairs of weakly interacting electrons (*Cooper pairs*). At the transition to the superconducting state, the Cooper pairs (CPs) condense in the same quantum state, that can be described by a single macroscopic wave function

$$\Psi(\mathbf{r}) = \Psi_0(\mathbf{r})e^{i\phi(\mathbf{r})} \tag{2.1}$$

where $\Psi_0(\mathbf{r})$ is linked to the density of pairs and $\phi(\mathbf{r})$ describes the center of mass motion of all pairs. The function Ψ is also called the *superconducting order parameter* [46].

The nature of the electron interaction in superconductors is of fundamental importance as it determines their properties. In conventional SCs, such as niobium and many other low-temperature SCs, the Cooper pairing is mediated through the excitations of the crystal lattice (phonons). In these materials, the CPs have total spin $S = 0$ (spin singlet) and total angular momentum $L = 0$, which define an isotropic wave function Ψ in the k-space (*s-wave symmetry*), *i.e.* Ψ has the same sign in all directions. In unconventional SCs, the pairing mechanism is non-phononic and the symmetry of the superconducting order parameter may not be s-wave-like. High temperature cuprate superconductors, for instance, have $S = 0$ and $L = 2$, that correspond to a wave function with a $d_{x^2-y^2}$ *symmetry*, with Ψ changing sign going from the k_x to the k_y direction. For most of these materials, the way pairing of electrons occurs is still a matter of debate.

In the following, I will describe one of the most striking applications of superconductivity, *i.e.* the Josephson junction. Here the combination of conventional and unconventional SCs may lead to novel junctions with unique properties.

2.2 Josephson relations

A Josephson junction is a contact composed of two superconductors coupled through a weak link, as sketched is Fig. 2.1. The weak link is generally a thin layer of another material. In his historical paper [1], B. Josephson considered an insulator. Since then, a large variety of materials have been explored. The superconducting order parameter of the two superconductors $\Psi_{1,2}$ decays into the barrier (see Fig. 2.1), but if the barrier is thin enough for $\Psi_{1,2}$ to overlap, coherence is preserved and CPs can flow through the barrier. This results in a supercurrent flowing through the junction with no voltage drop.

The physics of JJs is described by two main relations that can be derived by solving the Schrödinger equation of the system [1]. The *first Josephson relation*, also denoted as *current-phase relation*, is given by

$$I_{\mathrm{s}}(\phi) = I_{\mathrm{c}} \sin(\phi_2 - \phi_1) = I_{\mathrm{c}} \sin(\phi) \tag{2.2}$$

and it describes the variation of the supercurrent I_{s} crossing the junction as a function of the difference of the phases ϕ_1 and ϕ_2 of the two superconductors. I_{s} is zero for $\phi = 0$, while it reaches its maximum value $I_{\mathrm{s}} = I_{\mathrm{c}}$ at $\phi = \pi/2$. The amplitude of I_{c} is determined by the strength of the coupling of the two superconductors. The Josephson phase ϕ evolves in time according to the *second Josephson relation*:

$$\frac{d\phi}{dt} = \frac{2\pi V}{\Phi_0}, \tag{2.3}$$

with $\Phi_0 = 2.07 \times 10^{-15}$ Wb being the flux quantum. Assuming a time-independent voltage V, by integrating Eq. (2.3) and substituting the result in Eq. (2.2), one gets a supercurrent oscillating in time with the Josephson frequency $f_{\mathrm{J}} = V/\Phi_0 \approx V \cdot 483.6\,\mathrm{MHz}/\mu\mathrm{V}$. From Eq. (2.2) and Eq. (2.3), one can calculate the coupling energy of a JJ:

$$U(\phi) = \int_0^t I_{\mathrm{s}} V dt = \frac{I_{\mathrm{c}}\Phi_0}{2\pi} \int_0^{\phi} \sin(\phi) d\phi = E_{\mathrm{J}}[1 - \cos(\phi)]. \tag{2.4}$$

The energy is a 2π-periodic function of the phase. Its minima represent the ground state of the JJ. For conventional junctions, the minimum occurs at $\phi = 0 \mod 2\pi$, therefore they are generally named "0 JJs". Further in the thesis, I will discuss the more general case of junctions where $U_{\min} = U(\phi \neq 0)$.

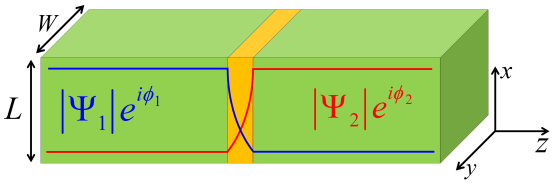

Figure 2.1: Cartoon of a Josephson junction: two superconductors (green) separated by a barrier (yellow). The superconducting order parameters $\Psi_{1,2}$ decay into the barrier. The junction has length L and width W.

2.3 The RCSJ Model

The phase dynamics of a JJ is well described by the *Resistively and Capacitively Shunted Junction (RCSJ) Model* [47, 48]. The theory represents the JJ as an ideal non-linear element in parallel with a resistance R and a capacitance C, as sketched in Fig. 2.2(a). The ideal JJ sustains the current I_s of Eq. (2.2). The resistance accounts for the quasiparticle transport through the junction, that causes the current I_n. In the simplest picture, the dependence of I_n on the applied voltage is approximated to be ohmic. Eventually, one can extend the model to a more general $I_\mathrm{n}(V)$ (non-linear RCSJ model). The capacitance defines a displacement current $I_\mathrm{d} = C\dot{V}$. Thus, the total current crossing the junction is:

$$I = I_\mathrm{s} + I_\mathrm{n} + I_\mathrm{d} = I_\mathrm{c}\sin\phi + \frac{V}{R} + C\dot{V}, \tag{2.5}$$

that together with Eq. (2.3) and Eq. (2.4) leads to:

$$E_\mathrm{J}\frac{d}{d\phi}\Big[\gamma\phi - (1-\cos\phi)\Big] = \frac{1}{R}\Big(\frac{\Phi_0}{2\pi}\Big)^2\frac{d\phi}{dt} + C\Big(\frac{\Phi_0}{2\pi}\Big)^2\frac{d^2\phi}{dt^2}, \tag{2.6}$$

where $\gamma = I/I_\mathrm{c}$. The equation above is equivalent to the equation of a particle of mass $M = C(\Phi_0/2\pi)^2$, moving with a friction $\eta = (\Phi_0/2\pi)^2R^{-1}$ in a washboard potential $U \propto (1-\cos\phi) - \gamma\phi$ (see Fig. 2.2 (b)). Eq. (2.6) is often rewritten in a dimensionless form by normalizing the time t to the inverse of the eigenfrequency of the junction $\omega_{\mathrm{p}0}^{-1}$, obtaining

$$\gamma = \sin(\phi) + \frac{1}{\sqrt{\beta_c}}\frac{d\phi}{dt} + \frac{d^2\phi}{dt^2}, \tag{2.7}$$

where $\beta_c = 2\pi I_c R^2 C/\Phi_0$ is called the *Stewart-McCumber parameter* and it describes the damping of the JJ. More often, in literature, one refers to the dimensionless damping with the parameter $\alpha = 1/\sqrt{\beta_c}$. The frequency ω_{p0}, also called *plasma frequency* for historical reasons, is defined as

$$\omega_{p0} = \sqrt{\frac{2\pi I_c}{\Phi_0 C}} \tag{2.8}$$

and it corresponds to the frequency of the eigenoscillations of the Josephson phase at the bottom of the energy minimum at zero bias (*i.e.* untilted potential).

The dynamics of a JJ strongly depends on β_c. Commonly, if $\beta_c < 1$ the junction is called *overdamped*, whereas for $\beta_c > 1$ is called *underdamped*. In the former, the fictitious particle representing the Josephson phase has a small mass M and it is subject to a large friction. In the latter, the particle is heavy (large M) and it moves less viscously. The two types of JJs have different current-voltage characteristics (IVCs), as shown Fig. 2.2(c). Here, I is the bias current applied to the junctions and $\overline{V}$ is the time averaged voltage detected across it. Three main transport regimes can be distinguished in both IVCs. (I) Starting from zero bias current $I = 0$, a supercurrent with zero voltage is measured across the junctions up to the value $I = I_c$. In the picture of the washboard potential, the fictitious particle is pinned in the metastable minimum of the potential $U(\phi)$. (II) For $I \geq I_c$, the junctions switch to the voltage state. For these values of the bias, the energy well disappears (*cf.* Fig. 2.2(b)) and the phase-particle escapes and rolls down the washboard. As the phase varies in time, a voltage appears according to Eq. (2.3). For large I, both IVCs approach a linear behavior, with the slope given by the inverse of the normal resistance of the junction. In the experiments, due to the presence of thermal fluctuations, the phase can actually escape from the energy minimum already for $I < I_c$, therefore the measured critical current (*aka* switching current) of the junction is always somewhat smaller than the noise-free I_{c0}. By lowering the temperature of the JJ, one can achieve a better estimation of I_c, that will approach I_{c0} as $T \to 0$. (III) As the bias current is reduced back to zero (*i.e.* the washboard is brought back to the untilted configuration), the overdamped and underdamped JJ behave very differently. For $\beta_c < 1$, the IVC follows the same curve measured for increasing bias and the junction returns to the zero voltage state at $I \leq I_c$.

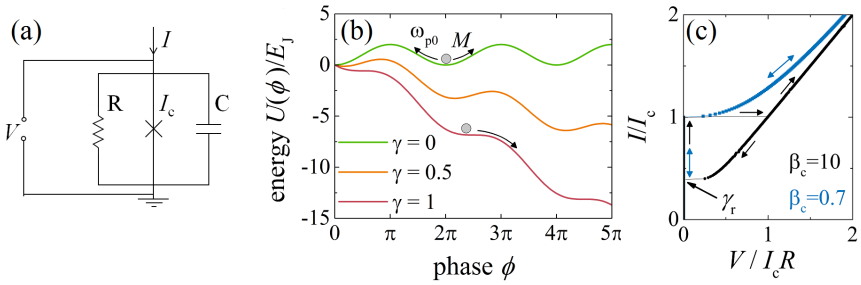

Figure 2.2: (a) Sketch of the equivalent circuit of a Josephson junction according to the RCSJ model. (b) Josephson washboard potential for different values of the normalized bias current γ. The particle of mass M represents the particle-like Josephson phase. (c) Simulated IVCs (from Eq. (2.13)) of a JJ in the underdamped (black curve) and in the overdamped (blue curve) regime. The arrows indicate the sweeping direction of the bias current.

For $\beta_c > 1$, a hysteresis appears in the IVC and the voltage jumps back to zero at a value of the current I_r (return current) smaller than I_c.

2.4 Josephson junctions in a magnetic field

The phase difference across the junction changes in space in the presence of an external magnetic field H, applied in the plane of the junction in the y direction (see Fig. 2.1). In order to derive the $\phi(x)$ dependence, one has to consider the phase spatial variation induced by the field between two infinitesimally close points x and $x + dx$. Since the Josephson phase is a gauge invariant variable, the variation can be expressed as follows:

$$\phi(x + dx) - \phi(x) = \frac{2\pi}{\Phi_0} \mu_0 H \Lambda dx, \tag{2.9}$$

with the effective magnetic thickness Λ and the vacuum permeability μ_0. Integration of Eq. (2.9), under the assumption that (i) the magnetic field penetrates the barrier uniformly and (ii) the critical current density is homogeneous, leads to:

$$\phi(x) = \frac{2\pi}{\Phi_0} \Lambda \mu_0 H x + \phi_0. \tag{2.10}$$

Therefore, substituting this in the first Josephson relation $j_s = j_c \sin\phi(x)$ and integrating in space to get the total current, one finds that the critical current oscillates with the magnetic field according to a Fraunhofer pattern:

$$I_c(H) = I_c \left| \frac{\sin \pi \frac{\Phi}{\Phi_0}}{\pi \frac{\Phi}{\Phi_0}} \right|, \tag{2.11}$$

with the total flux through the junction $\Phi = \Lambda \mu_0 H L$.

2.5 Sine-Gordon equation

The RCSJ model and the $I_c(H)$ dependence derived in the previous sections apply in the limit of a short JJ, that is for a junction with length small compared to the Josephson penetration depth λ_J, *i.e.* $L \lesssim \lambda_J$. In this geometrical configuration, self-field effects — generation of magnetic fields caused by the Josephson and the screening currents — are negligible. However, this condition does not hold in the case of long JJs, *i.e.* $L > \lambda_J$.

In this section I introduce the sine-Gordon model, that is a more general model describing the phase dynamics in a long JJ. The model takes as equivalent circuit of the junction RCSJ cells connected in parallel through an inductance. Calculations based on the Kirchhoff laws lead to the following spatial variation of the Josephson phase:

$$\frac{2\pi j_c \lambda_J^2}{\Phi_0} \mu_0 \Lambda \frac{\partial H(x)}{\partial x} - j_c \lambda_J^2 \frac{\partial^2 \phi}{\partial x^2} = j_b - j(x), \tag{2.12}$$

where j_b is the bias current density and j is the current density across the barrier. Eq. (2.12) together with Eq. (2.6) gives the *perturbed sine-Gordon equation*, that reads:

$$\frac{\partial^2 \phi}{\partial x^2} - \frac{\partial^2 \phi}{\partial t^2} - \sin\phi = \alpha \frac{\partial \phi}{\partial t} - \gamma + \frac{\partial h(x)}{\partial x}, \tag{2.13}$$

with x normalized to λ_J, the time t to the inverse of the plasma frequency ω_{p0}^{-1}, and the field to the critical field $H_{c1} = \Phi_0 / 2\pi \lambda_J \mu_0 \Lambda$.

Later, I will use Eq. (2.13) to numerically simulate some characteristic dependences, *e.g.*, $I_c(H)$. By comparing numerical results obtained for different sets of parameters with the experimental curves, one can determine λ_J and β_c that are not measurable directly.

2.6 Macroscopic quantum tunneling

Consider the Josephson energy potential tilted by a bias current I just below the critical value I_c, *i.e.* $I_c - I \ll I_c$. In these conditions, the height of the energy barrier ΔU (*cf.* see Fig. 2.3) is small and the phase may escape to the voltage state either due to thermal fluctuations or due to quantum tunneling through the energy barrier. In the first case, one talks about *thermal activation* (TA) or *classical escape* process, while in the second case one has *macroscopic quantum tunneling* (MQT). The rate at which the two processes occur depends on the applied bias current via the energy barrier $\Delta U(\gamma)$ [49]

$$\begin{aligned}\Delta U(\gamma) &= 2E_J[\sqrt{(1-\gamma^2)} - \gamma \arccos\gamma] \\ &\approx \frac{4}{3}\sqrt{2}E_J(1-\gamma)^{3/2} \quad , \quad (1-\gamma) \ll 1,\end{aligned}$$

and the plasma frequency

$$\omega_p(\gamma) = \omega_{p0}(1-\gamma^2)^{1/4}. \tag{2.14}$$

At high temperature, the escape mechanism is dominated by TA. The escape rate in this regime is given by the Kramers formula [50]

$$\Gamma_t = a_t \frac{\omega_p(\gamma)}{2\pi} \exp\left(-\frac{\Delta U(\gamma)}{k_B T}\right), \tag{2.15}$$

with $a_t \lesssim 1$ being a damping-dependent parameter. For strong damping α, a_t can significantly deviate from one, *i.e.* Γ decreases. The case of low, intermediate and high α in the escape process has been discussed in several works and expressions for a_t have been derived in each regime [50–53].

The escape rate in the classical domain depends exponentially on the temperature T. Hence, activation over the barrier is suppressed as T is lowered. For sufficiently low T, MQT can be observed, with a rate for finite damping given by [54]

$$\Gamma_q = a_q \frac{\omega_p(\gamma)}{2\pi} \exp\left[-7.2\frac{\Delta U(\gamma)}{\hbar\omega_p(\gamma)}\left(1 + \frac{0.87}{Q}\right)\right], \tag{2.16}$$

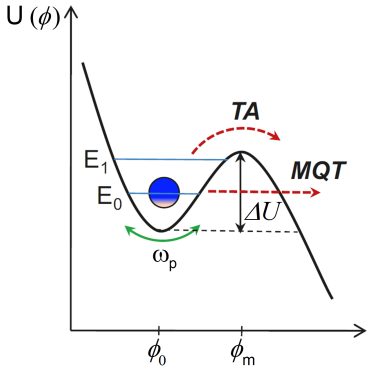

Figure 2.3: Tilted Josephson potential $U(\phi)$. The phase-particle is trapped in the potential well and it oscillates with $\omega_{\rm p}$. The red arrows indicate two escape processes: thermal activation over the barrier (TA) and quantum tunneling through the barrier (MQT).

where the prefactor $a_{\rm q}$ depends of the damping and $Q = \omega_{\rm p} RC$ is the quality factor at high frequency. Note that in both Eq. (2.15) and Eq. (2.16), the damping is assumed to be not vanishing, in such a way that equilibrium is present for each value of γ. The crossover temperature $T^\star$ that separates the thermal ($T > T^\star$) from the quantum tunneling ($T < T^\star$) regime can be estimated from the condition $\Gamma_{\rm t} = \Gamma_{\rm q}$, that in the approximation $Q \gg 1$ leads to

$$T^\star = \frac{\hbar \omega_{\rm p}(\gamma)}{7.2 k_{\rm B}}. \tag{2.17}$$

Experimentally the escape process of the Josephson phase is studied by measuring the switching current distribution of the JJ. To this purpose, the bias current is ramped up with a constant rate $\dot{I}$ and the current at which the junction switches to the voltage state is recorded. Due to the presence of fluctuations, the switching current is statistically distributed. Thus, by collecting a large amount of measurements, one can generate a histogram and determine the escape rate from [49]

$$\Gamma(I_k) = \frac{\dot{I}}{\Delta I} \ln \frac{\sum_{j=k}^{M} P(I_j)}{\sum_{j=k+1}^{M} P(I_j)}, \tag{2.18}$$

with M the total number of bins of size ΔI of the probability distribution $P(I)$. If the measurements are repeated at different temperatures T, one can observe the transition from the TA to the MQT regime by plotting the width σ of the histograms *vs* T. In the classical limit, σ reduces as the temperature is lowered, due to the decrease of the thermal energy $k_{\mathrm{B}}T$. Theory predicts $\sigma_{\mathrm{t}}(T) \propto T^{2/3}$ [49, 55]. In the quantum limit, the switching current distribution does not depend on the temperature and $\sigma_{\mathrm{q}}(T) = \text{const}$. In the experiment, the intersection of σ_{t} and σ_{q} gives the crossover temperature $T^{\star}$.

3 Unconventional Josephson junctions

3.1 The current phase relation

The first Josephson relation introduced in Chapter 1 is fundamental and determines all the main properties of a JJ. The sinusoidal-like function of Eq. (2.2) holds for most type of experimentally available junctions. However, one can write down a more general expression [2]:

$$I_{\rm s}(\phi) = \sum_{n=1}^{\infty} I_{\rm cn} \sin(n\phi) \tag{3.1}$$

The equation above satisfies the following general properties, which are independent from the junction geometry and the material used:

(i) The current-phase relation (CPR) is 2π-periodic
$I_{\rm s}(\phi) = I_{\rm s}(\phi + 2\pi)$;

(ii) The supercurrent is time-reversal symmetric
$I_{\rm s}(-\phi) = -I_{\rm s}(\phi)$;

(iii) No supercurrent flows if the phase difference is a multiple of π
$I_{\rm s}(n\pi) = 0, \qquad n = 0, \pm 1, \pm 2, ...$

A review on different types of CPRs is given in [2]. In this Chapter I will describe three kinds of novel JJs, whose CPR deviates from the one in Eq. (2.2).

3.2 π Josephson junction

Conventionally, the critical current of a JJ is positive, $I_{\rm c} > 0$, and the energy, calculated as the integral in ϕ of the CPR, has a minimum at $\phi = 0$ (see Fig. 3.1(a) and (b)). However, the case $I_{\rm c} < 0$ may also occur (Fig. 3.1(c)). A negative critical current corresponds to a phase shift of π in the ground state of the junction, thus the CPR and the energy can be written as:

$$I_{\rm s}(\phi) = |I_{\rm c}| \sin(\phi + \pi), \tag{3.2}$$

$$U(\phi) = E_{\rm J}[1 - \cos(\phi + \pi)], \tag{3.3}$$

with $E_J = |I_c|\Phi_0/2\pi$. As shown in Fig. 3.1(d), in this case the minimum of the energy is located at $\phi = \pi$, from which the name of π JJs derives.

There is a lot of interest in π JJs. They can be used in classical and quantum circuits as phase batteries [22–24]. When closed into a superconducting loop, the π JJ may lead to the spontaneous generation of a supercurrent, that can be used to feed external circuits. The main advantage of such a battery is that it is never discharging (as long as the temperature is kept below the critical value T_c) and it allows to eliminate feeding lines into the circuit, thus it can substantially reduce thermal dissipation of the whole circuit. In the quantum limit, using a phase bias instead of an applied magnetic field may provide a better decoupling from the environment.

π JJs were first predicted by Bulaevskiĭ *et al.* in 1977 [5] for SIS junctions with magnetic impurities in the barrier [6]. Some 20 years later, the π state was suggested and/or demonstrated in JJs realized with different technologies, *e.g.*, JJs with ferromagnetic layers [7–12], nano-constriction-type JJs (so-called "geometric" *d*-wave JJs) [56], d-wave/s-wave based JJs [13–15], grain boundary JJs in *d*-wave superconductors [16–18], SNS JJs with a non-equilibrium distribution of the electrons in the barrier [19] and quantum dot based JJs [20, 21].

3.3 φ_0 Josephson junctions

It has been suggested that the CPR may show a phase shift different from 0 and π in JJs involving unconventional superconductors [57, 58], non-centrosymmetric normal metal barriers [25], nonaligned geometries [26], current injectors [59] or asymmetric dc SQUIDs [60]. These types of junctions are generally called φ_0 JJs and their CPR and energy read as

$$I(\phi) = I_c \sin(\phi + \varphi_0), \tag{3.4}$$

$$U(\phi) = E_J[1 - \cos(\phi + \varphi_0)]. \tag{3.5}$$

A plot is shown in Fig. 3.1(e) and (f). Contrary to other junctions, φ_0 JJs do not satisfy conditions (ii) and (iii) of Section 3.1, that is time-reversal symmetry is not preserved and the current is not zero at $\phi = 0$. A φ_0 ground state phase can be revealed if the junction is connected to a superconducting loop. In such a system, a circulating current should be detected with no bias or magnetic flux applied.

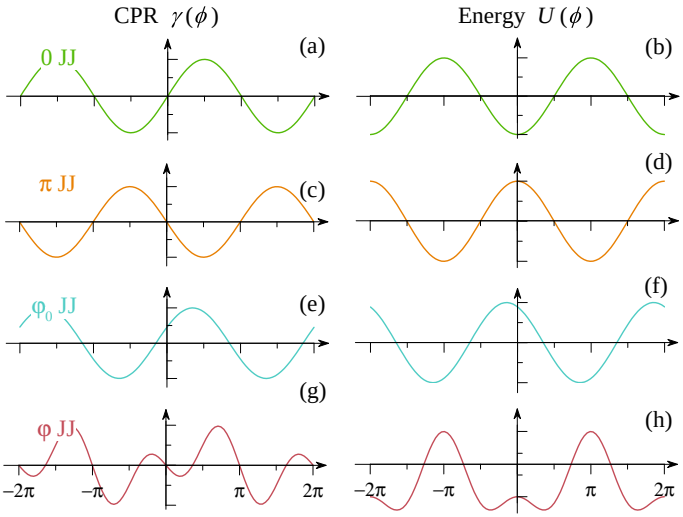

Figure 3.1: Normalized current phase relation $\gamma(\phi) = I_s/I_{c1}$ and energy profile $U(\phi)/E_J$ for a 0 JJ (a)-(b), a π JJ (c)-(d), a φ_0 JJ (e)-(f) and a φ JJ (g)-(h).

Only recently, a φ_0 JJ has been demonstrated in a junction realized with a quantum dot [28].

3.4 φ Josephson junctions

From the combination of a 0 and a π JJ, one can obtain a so-called φ JJ. The φ JJ has a doubly degenerate ground state at $\phi = \pm\varphi$ with $0 < \varphi < \pi$ [29, 61]. In terms of energy, this corresponds to an energy profile that looks like a 2π-periodic double well. The simplest CPR that results in such a $U(\phi)$ is a CPR with a negative second harmonic $I_{c2} < 0$ (*cf.* Eq. (3.1)):

$$I_s(\phi) = I_{c1}\sin(\phi) + I_{c2}\sin(2\phi). \tag{3.6}$$

The potential has two degenerate wells if $I_{c2} < -|I_{c1}|/2$, *i.e.* it results in a φ JJ [30]. The energy profile derived from Eq. (3.6) is:

$$U(\phi) = E_J\left[1 - \cos(\phi) + \frac{I_{c2}}{2I_{c1}}\cos(2\phi)\right] \quad \text{where} \quad E_J = \frac{I_{c1}\Phi_0}{2\pi}. \tag{3.7}$$

A plot of the supercurrent and of the energy for $|I_{c2}| = 1.2I_{c1}$ is displayed in Fig. 3.1(g) and (h).

φ JJs are very interesting devices showing unusual physics, *e.g.*, a magnetically tunable CPR [32], chaotic dynamics of the phase for low damping [35, 62] and splintered vortices [30, 63, 64]. They have high potential for many applications, like arbitrary phase batteries, memories [31] and ratchets [65]. The phase dynamics and the ratchet operation of a φ JJ are the subject of two of my publications, that I summarize in the next chapters.

3.5 Methods for the realization of a φ JJ

Grain boundary JJs. It was theoretically proposed that a JJ made with d-wave superconductors may lead to the φ state for certain orientations of the crystal axis and below some temperature T^* [57, 58]. The key ingredient here is the formation of zero-energy states (ZES's) around the surface of the d-wave superconductor if the pair potential of the quasiparticles involved into the Andreev reflections has opposite sign depending on the electronic trajectory. For $T < T^*$, the ZES's lead to a negative and strongly suppressed first harmonic of the CPR, thus the second harmonic becomes important. Some indications of the φ JJ-like CPR (temperature dependence of I_c and degenerate ground state) were given by different groups in 45° YBCO grain boundaries (GB) junctions [66, 67].

Long arrays of 0 and π JJs. A long JJ with a critical current density randomly alternating between positive and negative values was proposed as a possible setup to realize a φ JJ by Mints [61], having in mind real GBs of d-wave superconductors. Later, Buzdin [29] came to the same result considering a similar setup composed of a periodic array of 0 and π facets, realized using JJs with ferromagnetic barrier. In their work, the authors show that an *effective* CPR with a second harmonic can be derived by spatially averaging the total phase of the array. The CPR gives an energy with doubly degenerate ground states when the mismatch between the 0 and the π facets is small. Experimentally, such structures were realized with long GB JJs, and evidence of a nontrivial CPR were demonstrated by detecting nonquantized (splintered) vortices [64]. Nevertheless a full characterization of the system was not carried out, probably due to a poor control over the junction parameters and a high damping.

Asymmetric 0-π JJ. The theoretical arguments in [29, 61] for the chain of 0 and π JJs, were later used by Goldobin *et al.* [32] to demonstrate a φ JJ based on a single 0-π period of such a chain. The junction was considered to be asymmetric in the length of the two segments, *i.e.* $L_0 \neq L_\pi$. The same calculation has been later generalized by Lipman *et al.* [33] to the case of a junction with $j_{c0} \neq j_{c\pi}$. An asymmetric 0-π JJ resulting in a φ JJ behavior was shown by Sickinger *et al.* in 2012 using a ferromagnetic junction [34]. Currently, this is the only experiment showing the existence of two critical currents [30] and manipulation of the two phase states.

In the following, I will dedicate separated and more detailed sections to the theoretical model and to the experiments on the φ JJ realized with this technology, since the first part of my thesis shows works performed on such junctions.

A constriction-type JJ with a d-wave superconductor. φ JJs were proposed also by Gumann *et al.* [56] for a JJ patterned from a thin film of a d-wave superconductor narrowed down from one side by a wedge-shaped incision. The orientation of the d-wave order parameter is considered as $\alpha = 45°$ relative to the constriction. The model shows that the phase of the junction exhibits a 0-π transition depending on the width w of the constriction. The transition is marked by a critical width w_c that is a function of temperature. For $w > w_c$, the phase is zero, while for $w < w_c$ the phase is π. When $T < T_c$, due to a larger contribution of the second harmonic of the CPR, the φ state appears in the vicinity of the 0-π crossover. As the temperature decreases, the φ domain widens. The φ JJ is possible also for $\alpha \neq 45°$, in the limit that $\alpha > 22.5°$.

s-wave/$s_\pm$ superconductor based JJs. A φ JJ has been also suggested based on a junction fabricated using a conventional superconductor (s-wave) and an iron pnictide ($s_\pm$ state) [68]. According to several theoretical works, superconductivity in iron pnictides is mediated by spin fluctuations giving order parameters with opposite signs in the electron and hole bands ($s_\pm$ state) [69–73]. When an s-wave and an $s_\pm$ superconductor are brought closely together to create a JJ, the Josephson energy is expressed as the sum of two terms, $E_{J1} > 0$ and $E_{J2} < 0$, given by the alignment of the order parameters with the $s_\pm$ states. In the limit of $|E_{J1}| \approx |E_{J2}|$, higher harmonics must be taken into account in the calcula-

tion of the total energy of the system. If the second harmonic is negative, a junction with a degenerate double well potential is realized.

Normal/ferromagnet JJs. An SFS JJ lying on top of a normal metal (N) has been suggested as a possible candidate for the realization of a φ JJ [39, 74]. In this system a negative second harmonic in the CPR is obtained combining the properties of an SNS and an SFS junction. For some ranges of length and thickness of the F- and N-layer, in the SNS JJ, at low temperature, the first harmonic I_{c1}^{N} is positive and the second I_{c2}^{N} is large and negative; in the SFS JJ, I_{c1}^{F} can become negative with decreasing temperature, minimizing the total amplitude of the first harmonic.

Asymmetric dc SQUID. Recently Goldobin *et al.* [60] have shown that an asymmetric dc SQUID (Superconducting QUantum Interference Device) with non-vanishing inductance can effectively behave as a system having two degenerate ground states. A dc SQUID is a superconducting ring interrupted by two JJs. If the two junctions have different ground state phases and critical currents, *i.e.* one is a 0 JJ with I_c^1 and the other a π JJ with $|I_c^2| < I_c^1$, then the energy potential of the system develops two wells, if $\alpha_c < |\alpha| < 1$. The parameter $\alpha = I_c^2/I_c^1$ defines the asymmetry of the two critical currents. The parameter α_c is the value of asymmetry for which the CPR becomes φ JJ-like and it depends on the inductance of the SQUID.

3.6 A φ JJ based on an asymmetric 0-π JJ

Consider a JJ with a 0 and a π segment as sketched in Fig. 3.2. The critical current density profile is then written as [32, 33]:

$$j_c(x) = \begin{cases} j_{c0}, & 0 \le x \le L_0, \\ -j_{c\pi}, & -L_\pi \le x < 0, \end{cases} \tag{3.8}$$

with $j_{c0}, j_{c\pi} > 0$.
More conveniently, one can write $j_c(x)$ as follows [61]:

$$j_c(x) = \langle j_c(x) \rangle [1 + g(x)], \tag{3.9}$$

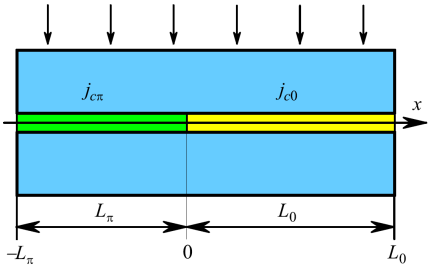

Figure 3.2: Schematic of a 0-π JJ with $L_0 \neq L_\pi$ and $j_{c0} \neq j_{c\pi}$. From [33]. © 2014 American Physical Society.

with the average $\langle j_c(x)\rangle$ and $g(x)$ defined by

$$\langle j_c(x)\rangle = \frac{1}{L}\int_{-L_\pi}^{L_0} j_c(x)dx = \frac{1}{L}(j_{c0}L_0 - j_{c\pi}L_\pi), \tag{3.10}$$

$$g(x) = \frac{j_c(x)}{\langle j_c(x)\rangle} - 1, \tag{3.11}$$

where $L = L_0 + L_\pi$ is the total length of the junction and the average of the function $g(x)$ is zero.

The spatial distribution of the phase along the junction is described by the sine-Gordon equation (Eq. (2.13)). For simplicity, here the static situation ($\partial\phi/\partial t = 0$) is considered:

$$\phi'' - j_c(x)\sin\phi = -j, \tag{3.12}$$

where the prime denotes the spatial derivative and j is the bias current (not normalized). The spatial coordinate is normalized to the Josephson length λ_J defined as:

$$\lambda_J = \sqrt{\frac{\Phi_0}{2\pi\mu_0\Lambda|\langle j_c\rangle|}}. \tag{3.13}$$

Below, the normalized lengths L_0/λ_J and L_π/λ_J will be denoted with l_0 and l_π, respectively. By inserting Eq. (3.9) into Eq. (3.12) and normalizing the currents to $\langle j_c\rangle$, one gets:

$$\phi'' - \mathrm{sgn}(\langle j_c\rangle)[1 + g(x)]\sin\phi = -\gamma. \tag{3.14}$$

Short JJs. In the limit of short JJs, the CPR can be obtained from Eq. (3.14) analytically. Following the arguments of [29, 61], one can write the phase along the junction as the sum of two terms:

$$\phi(x) = \psi + \xi(x)\sin\psi. \tag{3.15}$$

The constant $\psi = \langle\phi(x)\rangle$ is the spatial average of $\phi(x)$, while $\xi(x)\sin\psi$ is an oscillating function describing the variation of the phase around ψ. The oscillation has zero spatial average ($|\langle\xi(x)\rangle| = 0$) and a small amplitude ($|\langle\xi(x)\sin\psi\rangle| \ll 1$). Plugging this ansatz in Eq. (3.14) and expanding to the first order in $\xi(x)$, one finds:

$$\xi''\sin\psi - \mathrm{sgn}(\langle j_\mathrm{c}\rangle)[1+g(x)][1+\xi(x)\cos\psi]\sin\psi = -\gamma. \tag{3.16}$$

Eq. (3.16) can be split into a system of two equations, one for the constant terms and one for the varying ones. These equations lead to the following *effective* CPR:

$$j(\psi) = \langle j_\mathrm{c}\rangle\Big[\sin\psi \pm \frac{\Gamma_0}{2}\sin(2\psi) \pm h\Gamma_\mathrm{h}\cos\psi\Big], \tag{3.17}$$

where the signs $\pm$ stands for $\langle j_\mathrm{c}\rangle > 0$ and $\langle j_\mathrm{c}\rangle < 0$, respectively, $h = 2H/H_{\mathrm{c}1}$ is the normalized applied magnetic field, and the coefficients Γ_0 and Γ_h are geometrical factors, defined as

$$\Gamma_0 = -\frac{l_0^2 l_\pi^2}{3}\frac{(j_{\mathrm{c}0}+j_{\mathrm{c}\pi})^2}{(j_{\mathrm{c}0}l_0 - j_{\mathrm{c}\pi}l_\pi)^2} \qquad \text{and} \qquad \Gamma_\mathrm{h} = \frac{l_0 l_\pi}{2}\frac{j_{\mathrm{c}0}+j_{\mathrm{c}\pi}}{j_{\mathrm{c}0}l_0 - j_{\mathrm{c}\pi}l_\pi}.$$

The energy corresponding to the CPR in Eq. (3.17) is:

$$U(\psi) = \langle j_\mathrm{c}\rangle\Big[1 - \cos\psi \pm \frac{\Gamma_0}{2}\sin^2\psi + \pm h\Gamma_\mathrm{h}\sin\psi\Big]. \tag{3.18}$$

Thus, a JJ with unequal 0 and π segments can exhibit a CPR with a negative second harmonic, resulting in a φ JJ. The value of the ground state is calculated from Eq. (3.17) with $j, h = 0$, giving:

$$\varphi = \pm\arccos\left(-\frac{1}{\Gamma_0}\right). \tag{3.19}$$

However, not all the asymmetries between the 0 and the π facets can lead to an effective φ JJ, as shown in the domain of existence of the φ state

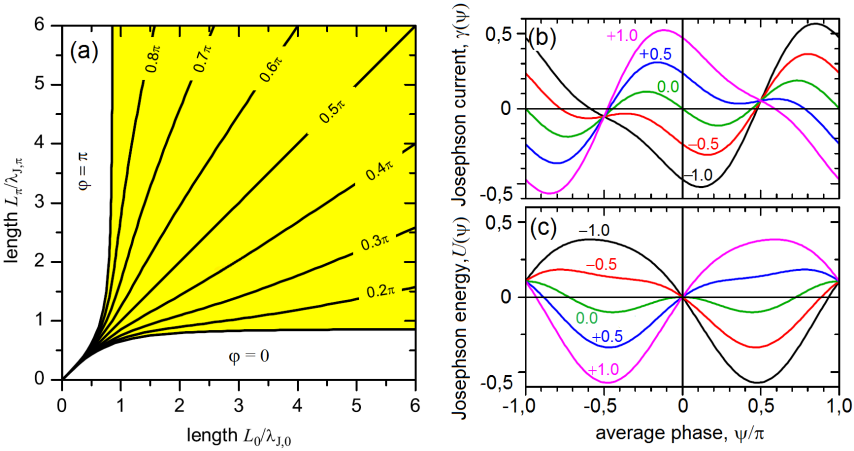

Figure 3.3: (a) The phase diagram calculated for the case $j_{c0} = j_{c\pi}$. The solid lines correspond to constant values of φ, as indicated by the numbers interrupting the lines, and they are calculated numerically from Eq. (3.16). Adapted from [33]. © 2014 American Physical Society. Effective CPR (b) and energy profile (c) of a 0-π JJ with $l_0 = 1$ and $l_\pi = 0.9$. Different colors correspond to different values of the normalized magnetic field h indicated by the numbers. One can notice that at $h = \pm 1$ the $\mp\varphi$ well is not present anymore. Adapted from [32]. © 2011 American Physical Society.

in the l_0,l_π plane in Fig. 3.3(a). Expressions for $l_0(l_\pi)$ and $l_\pi(l_0)$ can be found in [33].

What is remarkable to notice in Eq. (3.17) is that the presence of an external magnetic field contributes to an additional term in the CPR, making both the supercurrent and the energy profile tunable with h, as shown in Fig. 3.3(b) and (c).

Calculating the extrema of $j(\psi)$ (Eq. (3.17)), one can also obtain the dependence $j_c(h)$, that for small h has multiple values corresponding to the escape of the phase out of the two energy wells. The curves $j_c(h)$ for some sets of parameters l_0 and l_π with $j_{c0} = j_{c\pi}$ are plotted in Fig. 3.4. Here γ_c is the normalized critical current. In Fig. 3.4(a), the chosen l_0,l_π correspond to a value of φ deep inside the domain of existence. The dependence has a minimum at h close to zero, as expected in 0-π JJs. However, contrary to the case of a symmetric 0-π JJ, where the minimum sits exactly at $h = 0$,

in the asymmetric configuration the minimum is slightly shifted. The shift is point symmetric with respect to the polarity of the current, and its value depends on Γ_0: the smaller $|\Gamma_0|$, the larger the shift. The offset of the minimum from zero-field is a distinct feature of a φ JJ. Moreover, two critical currents ($\gamma_{c\pm}$) appear for each bias polarity for $|h| < 0.6$. The two branches correspond to the depinning of the phase from the left and the right potential well in Fig. 3.3(b). The field $|h| \approx 0.6$ at which the branches meet corresponds to the disappearance of one of the local energy minima. When the junction gets more asymmetric (see Fig. 3.4(b) and (c)), the diamond-shaped domain created by the crossing of the branches shrinks and finally it collapses. The point of collapse corresponds to the boundary of the domain of existence of the φ state.

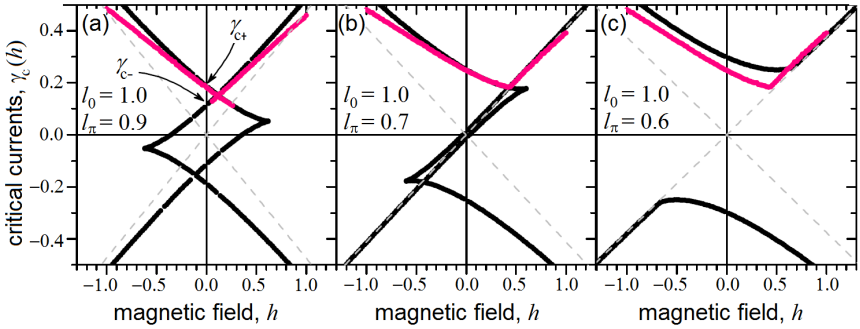

Figure 3.4: Dependence of the normalized critical current γ_c on the normalized magnetic field h for different segments lengths. The dashed lines indicate the asymptotic behavior (see [32]), while the pink curves are the result of numerical simulations of Eq. (3.16). Adapted from [32]. © 2011 American Physical Society.

Long JJs. In the limit of a long JJ, for x far away from the 0-π boundary, the spatial variation of the phase in the presence of a bias current can be approximated by

$$\phi(x) \approx \begin{cases} \pm\pi - \arcsin(j/j_{c\pi}), & x < 0, \\ \arcsin(j/j_{c0}), & x > 0. \end{cases} \tag{3.20}$$

If one takes into account the 0-π interface, in the absence of bias and

magnetic field, the phase describes a semifluxon:

$$\phi(x) \approx \begin{cases} 4\arctan\exp\left(\frac{x-x_0}{\lambda_{J0}}\right), & x < 0, \\ 4\arctan\exp\left(\frac{x-x_\pi}{\lambda_{J\pi}}\right) - \pi, & x > 0, \end{cases} \tag{3.21}$$

where $\lambda_{J0,J\pi} = \sqrt{(\Phi_0/2\pi\mu_0\Lambda j_{c0,c\pi})}$. Analytical solutions are reported in [33].

3.7 Evidence of a φ–state in a SIFS JJ

The asymmetric 0-π JJs described in Section 3.6 were investigated in 2012 by Sickinger *et al.* [34] using a SIFS structure. The junctions were fabricated using Nb|Al − Al_2O_3|$Ni_{0.6}Cu_{0.4}$|Nb heterostructures, as displayed in Fig. 3.5(a). The junctions have a length of 200 μm and a width of 10 μm. In order to realize the 0 and the π segments, the ferromagnetic layer is patterned with a step in the middle of the JJ. As a result, half of the junction has a barrier of thickness $d_{F,\pi}$ and the other half has $d_{F,0} < d_{F,\pi}$. The thicknesses are chosen in such a way that the critical current $j_{c\pi} = j_c(d_{F,\pi}) < 0$ and $j_{c0} = j_c(d_{F,0}) > 0$ are slightly different.

In the experimental characterization of such a junction, two different critical currents for each bias polarity were successfully detected at a temperature $T = 2.35\,\mathrm{K}$, as displayed in the current-voltage curve (IVC) in Fig. 3.5(b). The currents are labeled as $\pm I_{c\pm}$ where the $\pm$ in front indicates the current polarity and the $\pm$ in the subscript states for the right $(+\varphi)$and left $(-\varphi)$ well, respectively, for positive bias $I > 0$ and vice versa for $I < 0$. For $T > 3.5\,\mathrm{K}$, only one critical current (for each bias polarity) was measured, due to an increase of the damping with temperature. A further evidence of the φ state was found in the $I_c(H)$ modulation, were a minimum around $H = 0$ and four current branches were observed (Fig. 3.5(c)).

The same sample has been used by the group to demonstrate the operation of a memory bit [31]. The $\pm\varphi$ wells can be considered as the logic "0" and "1", therefore the junction can be used to store (1 bit) of information. The writing and reading procedures of such a memory are rather simple. For the writing one uses the fact that the degeneracy of the energy potential can be lifted upon application of an external magnetic field. In particular for $H > H_1$ (*cf* Fig.3.5(c)), the energy well at $\psi = +\varphi$ disappears, thus one force the phase into the $\psi = -\varphi$ well. Similarly, for $H < -H_1$, one

write the $\psi = +\varphi$ state. The read-out of the phase state, carrying the information, is executed by applying a bias current $I_{c-} < I_{RO} < I_{c+}$. The

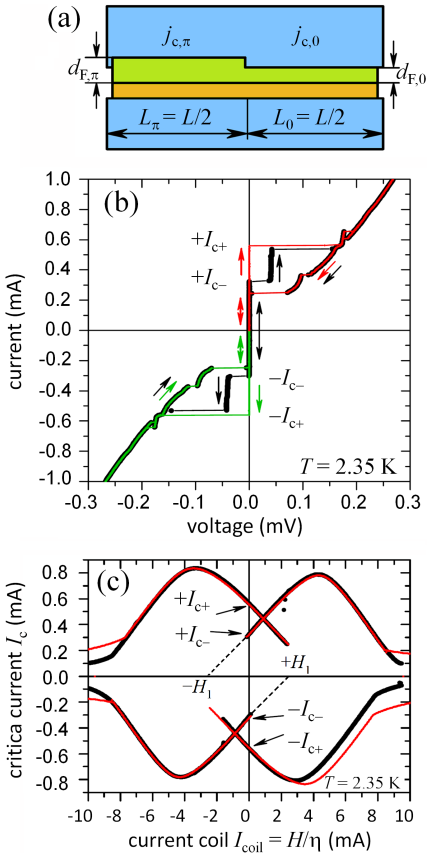

Figure 3.5: (a) Sketch of the SIFS 0-π JJ realized with a step along the ferromagnetic barrier (in green). (b) IVC measured at $T = 2.35$ K. The four critical currents $\pm I_{c\pm}$ are clearly visible. (c) Measured $I_c(H)$ dependence (black) compared to simulations (red). Here the shift of the minimum from $H = 0$ can be observed. The magnetic field H is applied by means of a coil with $H = \eta I_{coil}$ and $\eta \sim 5\,\mu$T/mA. Adapted from [34].

output will be then a finite voltage if $\psi = -\varphi$ or zero voltage if $\psi = +\varphi$.

Realization of φ JJs using the SIFS structures is quite challenging, especially in the limit of short JJs. In fact, by looking at the φ state domain in Fig. 3.3(c) it is evident that as the junction length shortens, the area of the domain shrinks significantly. In technological terms, this means that the asymmetry in the critical current of the 0 and π part has to be very small, thus the thicknesses $d_{\mathrm{F},0}$ and $d_{\mathrm{F},\pi}$ have to be controlled on the Å scale.

4 Publication 1
Phase retrapping in a φ Josephson junction: Onset of the butterfly effect

A φ JJ is defined as having an energy profile in the shape of a 2π-periodic double well potential, with minima at $\psi = \pm\varphi + 2\pi n$ (with integer n). While studying the dynamics of the phase in such a potential, a question naturally arises: in which of the two wells the phase-particle ends when it returns from the running state to the zero-voltage state? The answer to this questions is not trivial, as discussed for the case of a point-like junction in the theoretical paper of Goldobin *et al.* [35]. For a large damping α, the phase is always trapped in the $+\varphi$ well. However, as α decreases the destination well is predicted to oscillate between the two $\pm\varphi$ values. In the limit $\alpha \to 0$, the final state cannot be predicted as it strongly depends on the initial conditions of the system, in other words one deals with the butterfly effect.

In this publication, we experimentally investigate the retrapping process and compare the results to the predictions of the theory. The sample

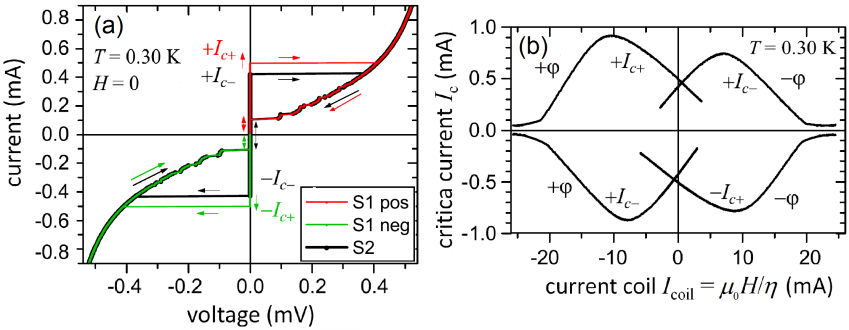

Figure 4.1: (a) IVC of the investigated SIFS φ JJ at $T = 0.3\,\mathrm{K}$. Different colors correspond to different bias sweep sequences. (b) $I_c(H)$ dependence measured by applying the field in-plane to the junction with a coil that has $\eta I_{\mathrm{coil}} = \mu_0 H$, with $\eta \sim 5\,\mu\mathrm{T/mA}$. Figure from the appended Publication 1. © 2016 American Physical Society.

we used for the measurements is the same SIFS JJ as in Ref. [34]. Basic characterization of the junction at $T = 0.3\,\mathrm{K}$ is shown in Fig. 4.1. The two critical currents $I_{c-} = 421.2\,\mu\mathrm{A}$ and $I_{c+} = 496.5\,\mu\mathrm{A}$ are clearly visible in the IVC and $I_c(H)$. The different colors in Fig. 4.1(a) indicate different sweep sequences of the bias current. We call "S1 pos(neg)" the sequence where the bias starts from $I = 0$, goes to a maximum value on the positive (negative) McCumber branch and then back to zero. The "S2 pos(neg)" sequence corresponds instead to a sweep from a maximum I on the negative (positive) McCumber branch to the same I on the positive (negative) voltage branch and then back. For the study of the retrapping dynamics

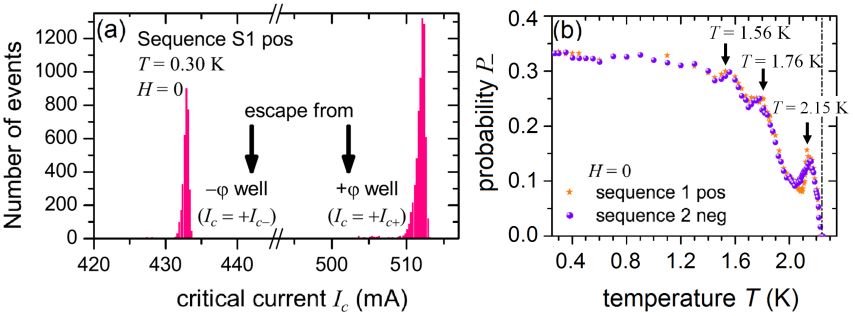

Figure 4.2: (a) A histogram built from the collected $N = 10^4$ measurements of switching current at $T = 0.3\,\mathrm{K}$ with the sweep sequence "S1 pos". Two peaks can be observed in the plot, which correspond to the escape currents from the $-\varphi$ and $+\varphi$ wells. (b) Probability of the phase to be retrapped in the $-\varphi$ well as a function of the temperature for two bias sweep sequences. Each point is extracted from the number of events populating the peak at $I_c = I_{c-}$ in (a). All the measurements are performed at zero field. Figure from the appended Publication 1. © 2016 American Physical Society.

we measured $N = 10^4$ times the switching current of the junction by ramping the bias current with a constant rate $\dot{I} = 0.1194\,\mathrm{A/s}$ and a repetition rate of 20 Hz. We performed the measurements at $H = 0$ — when the $\pm\varphi$ wells have the same depth — with different sweep sequences and for different temperatures in the range from 0.27 K to 2.30 K. The temperature is the parameter with which we can control the damping in the experiment, since $\alpha = \alpha(T)$. Hence, we change T to change α. For each T we built histograms, which show two peaks (see Fig. 4.2(a)) corresponding to the

depinning current of the phase from the $\pm\varphi$ wells. Further we calculated $P_{\pm}$ from the number of events in each peak. Obviously, the probabilities are such that the condition $P_- + P_+ = 1$ is always satisfied. In the four sweep sequences that we used, the retrapping occurs at opposite values of the bias current during the cycle, hence the probabilities are inversed, *i.e.* $P_{\pm}^{S1} = P_{\mp}^{S2}$. In Fig. 4.2(b) we show only the behavior of $P_-(T)$ for "S1 pos" and "S2 neg". The results obtained with the other sweeps is similar. In the $P_-(T)$ dependence one can distinguish three regions. (I) For $T > 2.25\,\mathrm{K}$ the probability that the phase ends into the $-\varphi$ well is zero; the retrapping dynamics is deterministic. (II) For $1.3\,\mathrm{K} < T < 2.25\,\mathrm{K}$, P_- increases and it shows some oscillations. In particular three peaks can be discerned at temperatures $T = 2.15, 1.76, 1.56\,\mathrm{K}$, where P_- is enhanced. (III) For $T < 1.3\,\mathrm{K}$, P_- saturates to ≈ 0.33. The experimental $P_-(T)$ curve agrees qualitatively with theoretical predictions [35]. However, in the experiment P_- saturates at a value smaller than the expected 0.5. We believe that the most probable reason for this discrepancy is the saturation of the damping α at low temperature. This may be caused, for instance, by leakage currents in the barrier of the junction. A dependence of the damping of our device on the temperature has been extracted by numerical fits of the IVCs using the sine-Gordon equation (see Section 2.5). The estimation of α is only qualitative, since in the simulations we consider a linear resistance

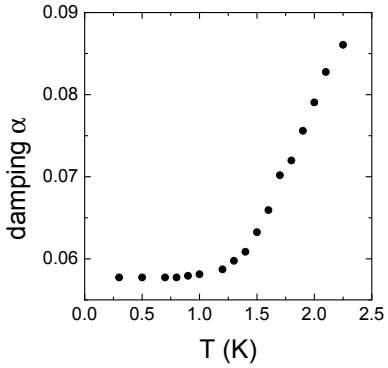

Figure 4.3: Temperature dependence of the damping α estimated from numerical simulation of the IVCs of the junction. Figure from the appended Publication 1.

(in the RCSJ fashion) which does not apply to our junction. Nevertheless, as one can see from the results plotted in Fig. 4.3, indeed the damping saturates to $\alpha_{\mathrm{sat}} \approx 0.057$ for $T < 1.2\,\mathrm{K}$, which corresponds to the temperature range where $P_{-}(T) \to 0.33$. Further simulations of the retrapping probability show a $P_{-}(T)$ comparable to the experiments, that saturates at 0.5 if the damping is lowered below α_{sat} (not shown).

In conclusion, we have investigated experimentally the phase dynamics of a φ JJ and we studied the probability of retrapping in the $\pm\varphi$ wells as a function of the temperature. The results confirm theoretical predictions: at high temperature (high damping) the process is deterministic, for decreasing temperature (lower damping) the probability of retrapping in one of the well increases and finally it saturates. Due to a saturation of the damping of the junction, just the onset to the butterfly effect with only three oscillations was observed, that is the saturation value of $P_{-}(T)$ is below the expected value of 0.5. In the future, a φ JJ built with a different technology providing smaller damping may give more insights into the topic.

Contributions to this publication

The junction used for the work reported in this publication was fabricated by M. Weides, who at that time worked in the group of Prof. H. Kohlstedt at the Forschungzentrum Jülich.
I carried out all the experiments described and evaluated the data. I also performed numerical simulations in order to extract basic parameters of the junction and to have a better understanding of the experimental results. Finally, I wrote part of the paper.
M. Žonda and T. Novotný collaborated by conducting a numerical analysis of the problem described in the Supplement of the paper.

5 Publication 2
Model I–V curves and figures of merit of underdamped deterministic Josephson ratchets

&

Publication 3
Tunable φ Josephson junction ratchet

A ratchet is a periodic system lacking reflection symmetry that can be employed to extract work out of nonequilibrium thermal fluctuations, to rectify ac signals with zero average value and to provide unidirectional motion [75–78]. Since in the framework of the RCSJ model the Josephson phase is pictured as a fictitious particle moving along the washboard potential, a JJ represents a system very close to the paradigmatic ratchet described in literature, where the driving force is an ac bias current applied to it. Nevertheless, the energy potential of a JJ is generally reflection symmetric and its profile is not controllable. In order to study the ratchet mechanism of the Josephson phase, researchers have realized complex devices based on multiple JJs [79–86]. Ratchets based on the motion of a Josephson vortex were also demonstrated [83–86]. Thus, for a long time a ratchet based on a single JJ was missing.

In these publications, first we derive a simple general model describing the current-voltage characteristic (IVC) of a Josephson ratchet and calculate some figures of merit in the presence of a counterforce to the ratchet. Second, we experimentally demonstrate an ac current to dc voltage rectifier based on a single φ JJ. As described in Section 3.6, the potential $U(\psi)$ of a φ JJ is reflection symmetric at zero magnetic field H and zero bias, but its profile is tunable with $H \neq 0$. Hence, the reflection symmetry can be easily broken. Finally, we apply the theoretical model to the φ JJ ratchet so obtained and extract useful parameters.

Model. We consider a JJ biased with a quasistatic drive $I_{\rm ac}\sin(\omega t)$ with $\omega \ll \omega_{\rm p}, \omega_{\rm J}$, where $\omega_{\rm p}, \omega_{\rm J}$ are the plasma and Josephson frequency, respectively. Moreover, we apply an additional dc current $I_{\rm dc}$ that pushes the Josephson phase in the direction opposite to the rectification. In this

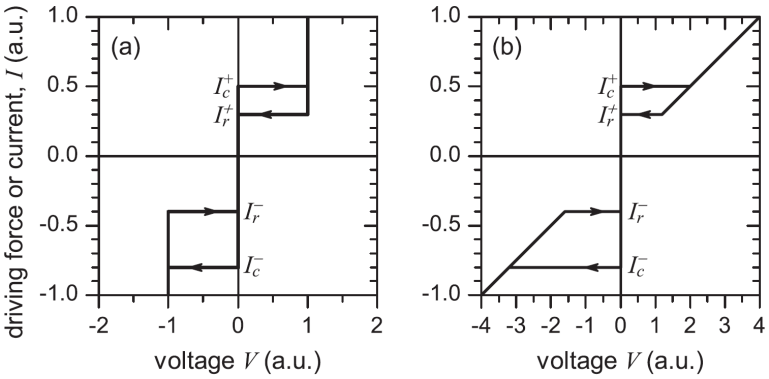

Figure 5.1: Two types of ($I_c^+ \neq |I_c^-|$) IVC used for the ratchet model. (a) IVC with a constant voltage step at $V_1 = 1$. (b) IVC with linear voltage $V = R_n I$, with $R_n = 4$. Figure from the appended Publication 2. © 2016 American Physical Society.

conditions, the ratchet is not idle — it works against the counterforce — and it produces power. The total current biasing the junction is thus:

$$I(t) = I_{dc} + I_{ac} \sin(\omega t). \tag{5.1}$$

The drive is rectified into a mean dc voltage, that can be obtained by integrating the $V(I)$ curve over one period $T = 2\pi/\omega$:

$$\overline{V} = \frac{1}{T} \int_0^T V[I(t)]dt. \tag{5.2}$$

In the paper, we treat the case of two types of asymmetric and hysteretic IVCs, namely the IVC with a constant voltage step and the IVC with a linear branch, see Fig. 5.1. In the case of $I_{dc} = 0$, we denote the positive and negative critical current of the junction as I_c^+ and I_c^-, and the positive and negative currents at which the JJ returns from the voltage to the zero-voltage state as I_r^+ and I_r^-. A finite dc current I_{dc} shifts the IVC by I_{dc}. Thus, we define the new values of the currents by

$$J_c^\pm = I_c^\pm \mp I_{dc} \qquad \text{and} \qquad J_r^\pm = I_r^\pm \mp I_{dc}. \tag{5.3}$$

The sign of the mean voltage $\overline{V}$ depends on the ratio of I_c^+ and I_c^-: if $I_c^+ < I_c^-$ ($I_c^+ > I_c^-$), then $\overline{V} \geq 0$ ($\overline{V} \leq 0$), and the counterforce must be $I_{dc} < 0$ ($I_{dc} > 0$).

Since the case of IVC with a constant voltage (*cf.* Fig. 5.1(a)) does not apply to the experiment shown later, and since the main results are qualitatively the same, below I will report only on the linear voltage model. Here, the voltage is defined as $V(I) = R_n I$, where R_n is the normal resistance. The rectification curve $\overline{V}(I_{ac})$ is calculated by using Eq. (5.2) and it is displayed in Fig. 5.2(a) for different values of I_{dc}. Here we can distinguish three different regimes. (i) For $I_{ac} < J_c^+$, the rectified voltage is zero (pinning regime). (ii) For $J_c^+ < I_{ac} < J_c^-$, the rectification is strong, because $\overline{V} > 0$ in the positive semiperiod of the drive and $\overline{V} = 0$ in the negative one. We call this region "rectification window". Notice here that the abrupt jump of $\overline{V}$ at $I_{ac} = J_c^+$ is due to the hysteresis in the IVC (underdamped JJ). In an overdamped junction, the output voltage increases smoothly. (iii) For $I_{ac} > J_c^-$, $\overline{V}$ decreases, since the voltage in the negative semiperiod is now finite and negative. In this region, the Josephson phase goes back and forth and does not produce any appreciable power (Sisyphus regime). By looking at the different curves in Fig. 5.2(a), we notice also that the rectification window shrinks as the amplitude of I_{dc} increases. In particular, it closes completely at

$$I_{dc}^{off} = (I_c^+ - I_c^-)/2, \tag{5.4}$$

indicating that the ratchet stopped.

The efficiency of the ratchet can be computed by the ratio of the mean output and input power as follows:

$$\eta = -\frac{\overline{P}_{out}}{\overline{P}_{in}} \tag{5.5}$$

and its dependence on the drive amplitude is plotted in Fig. 5.2(b) for different I_{dc}. For all the values of the counterforce, the maximum efficiency is achieved at the beginning of the rectification window, *i.e.* when $I_{ac} = J_c^+$, and it is given by

$$\eta_{max} = \frac{-2I_{dc}\left[I_{dc}\arccos\left(\frac{J_r^+}{J_c^+}\right) + \sqrt{{J_c^+}^2 - {J_r^+}^2}\right]}{{J_c^+}^2\arccos\left(\frac{J_r^+}{J_c^+}\right) + \sqrt{{J_c^+}^2 - {J_r^+}^2}(J_r^+ + 2I_{dc})}. \tag{5.6}$$

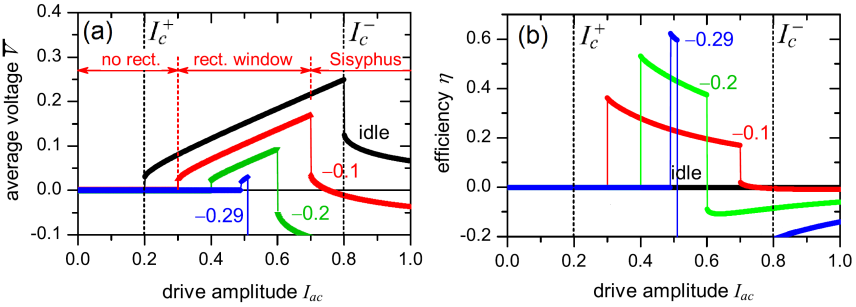

Figure 5.2: Rectification curves (a) and efficiency (b) of a JJ with a linear voltage ($R_n = 1$) for different values of the counterforce $I_{dc} = 0, -0.1, -0.2, -0.29$. Figure from the appended Publication 2. © 2016 American Physical Society.

The value of η_{max} increases as $|I_{dc}|$ increases. However, I_{dc} cannot be arbitrary large. The last value of it that makes sense is I_{dc}^{off} (see Fig. (5.4)). Hence, the ultimate maximum efficiency is calculated by inserting Eq. (5.4) in Eq. (5.6).

In the following, we apply the model to the ratchet obtained with a SIFS-based φ JJ. Although in our junction the $V(I)$ is not linear, as assumed in the theory, the formulas for some important key figures, *e.g.*, the stopping force I_{dc}^{off} and the efficiency, are still valid. These depend only on the boundaries of the rectification window, that is defined by I_c^+ and I_c^-. The non-linearity of the $V(I)$ affects only the output power and the amplitude of $\overline{V}$.

Experiment. For the experiment we used again a JJ fabricated with the SIFS technology, as in Publication 1. The measurements were conducted below $T = 2.35\,\mathrm{K}$, where the probability of detecting the escape current from the $-\varphi$ well is non-zero.

In Fig. 5.3(a) the magnetic modulation of the critical current is shown for $T = 1.70\,\mathrm{K}$. We chose this as the working temperature for this study, because here the ratchet operation is strong and the rectification curves are free from extra structures, due to resonance on the IVC, *e.g.*, half-integer zero field steps (see Fig. 4 of [34]). We label the critical currents as $I_{c,L}^{\pm}$ and $I_{cR}^{\pm}$, where the superscripts $\pm$ indicate the polarity of the applied bias

current, and the subscripts L, R refer to the left $(-\varphi)$ and right $(+\varphi)$ well.

In the first part of the experiment, we prove that the junction works as a ratchet and that its operation can be tuned by the magnetic field H. To this purpose, we measured the rectification curves $\overline{V}(I_{\mathrm{ac}})$ at the values of H indicated by the vertical lines in Fig. 5.3(a). We chose as drive a sinusoidal

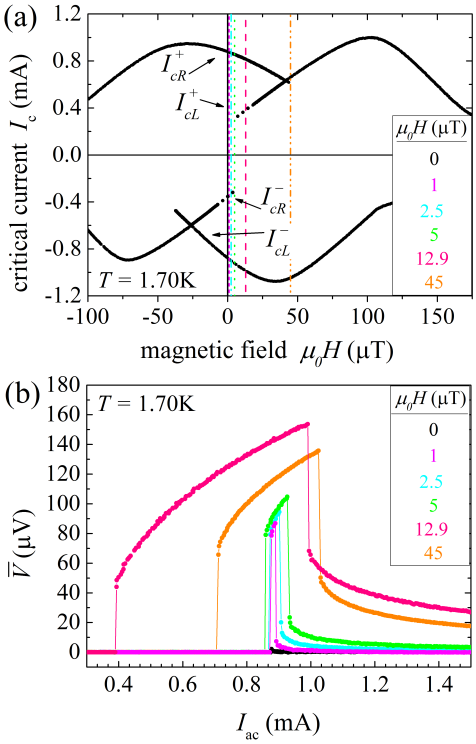

Figure 5.3: In (a) the dependence of the critical current on the magnetic field, that is applied through a coil, at $T = 1.70\,\mathrm{K}$ is shown. Two branches of critical currents for each polarity of the bias I are visible. The dots on the I_{cL}^{+} and I_{cR}^{-} branch indicate that these currents are semistable, thus they do not always appear. The vertical lines correspond to the magnetic fields at which we measured the rectification windows in (b). Figure from the appended Publication 3.

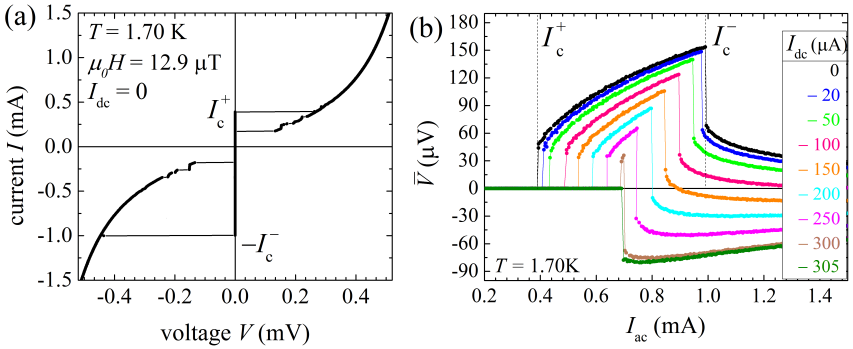

Figure 5.4: IVC (a) and rectification curves (b) for $\mu_0 H = 12.9\,\mu$T. In (b) each curve corresponds to a different amplitude of the dc current $I_{\rm dc}$ (counterforce). Figure from the appended Publication 3. © 2016 American Physical Society.

ac current $I(t) = I_{\rm ac}\sin(2\pi f t)$, with $f = 10\,$Hz (period $T = 100\,$ms) synthesized by a DAC with an update rate of 10000 points/s. The mean rectified voltage is obtained by recording and averaging the voltage across the junction 1000 times during one period, for each amplitude $I_{\rm ac}$. The results are displayed in Fig. 5.3(b). As expected, for $H = 0$ we detected no rectification ($\overline{V} = 0$) for any value of $I_{\rm ac}$, since the energy potential $U(\psi)$ is reflection symmetric. For $H \neq 0$, the asymmetry is broken and rectification occurs. The profile of the $\overline{V}(I_{\rm ac})$ curves obtained at $H \neq 0$ is similar to the ones in Fig. 5.2(a). The width of the rectification window changes with the magnetic field. This is explained by keeping in mind that by varying the field we change the asymmetry of the potential. For some values of H — *e.g.*, $\mu_0 H = 12.9\,\mu$T (magenta curve in Fig. 5.3(b)) — the asymmetry is larger than for others.

In the second part of the paper, we study the ratchet in the presence of the counterforce $I_{\rm dc}$. We carried out this experiment at the value of field $\mu_0 H = 12.9\,\mu$T, because here the rectification window is largest. The IVC of the junction at this field, in the absence of the counterforce, is shown in Fig. 5.4(a). The relevant currents are $I_{\rm c}^{+} = I_{\rm cL}^{+} = 389\,\mu$A and $I_{\rm c}^{-} = I_{\rm cL}^{-} = 997\,\mu$A. Further, we applied the dc current and measured the rectification curve at different amplitudes $I_{\rm dc}$, see Fig. 5.4(b). As expected from our theoretical model, the rectification window narrows as $|I_{\rm dc}|$ in-

creases, and at $I_{\rm dc}^{\rm off} = -305\,\mu$A it vanishes completely. The theoretical value $I_{\rm dc}^{\rm off}$ can be calculated from Eq. (5.4), which gives $I_{\rm dc}^{\rm off,th} = -304\,\mu$A, that perfectly matches the experimental value. Finally, we estimated the maximum efficiency of our ratchet system. This is a function of $I_{\rm dc}$ and it reaches its highest value at $I_{\rm dc}^{\rm off}$. Using Eq. (5.6), we have estimated $\eta_{\rm max} = 48\,\%$, that is a rather good result if compared to other kind of specifically designed ratchets [86].

In conclusion, we have theoretically and experimentally investigated a ratchet based on a φ JJ. We have demonstrated that its performance can be tuned with the magnetic field and calculated its maximum efficiency in the presence of a counterforce.

Contributions to this publication

I contributed to Publication 2 by taking part in the scientific discussion preceding the writing of the paper. Moreover, I supplied ideas and useful comments, aimed at the improvement of the manuscript and at a straightening of its main claims. Finally I reviewed the paper.
For Publication 3, I conducted all the experiments presented and analyzed the results. Furthermore, I wrote part of the paper.
M. Weides fabricated the sample.

6 Publication 4
Observation of 0-π transition in SIsFS Josephson junctions

In a Josephson junction with a ferromagnetic (F) barrier, the phase drop ϕ across the junction depends of the thickness d_F of the F-layer and it can be either 0 or π [87]. The 0-to-π phase transition as a function of d_F and temperature has been intensively studied and experimentally proven in the last fifteen years in SFS [7, 9, 88] and SIFS junctions [8, 10, 89] (S: superconductor, I: insulator). Since the ground state phase depends on d_F, the patterning of a step in the ferromagnetic barrier gives the possibility to create 0-π JJs, where half of the junction would have $\phi = 0$ and the other half would have $\phi = \pi$ [90, 91]. Using the SIFS technology with a step-like thickness of the F-layer to create an asymmetric 0-π JJ, we fabricated a φ JJ with two degenerate phase ground states [34].

Ferromagnetic junctions are generally characterized by very low values of the characteristic voltage $V_c = I_c R_n$, with I_c being the critical current and R_n the normal resistance of the junction, and low critical current densities j_c. The former lowers the switching frequency of the junction, limiting integration of such structures in superconducting logic circuits. The latter reduces the classical-to-quantum crossover temperature $T^\star$ (that scales as $\propto j_c$) and coherence times.

Driven by the necessity to increase j_c in the SIFS-based φ JJs in order to study their quantum properties, we realized SIsFS JJs, where s is a thin superconducting interlayer. Recent studies showed that the s-layer helps to recover superconductivity, leading to an enhancement of j_c to values typical of conventional SIS JJs [36–40].

In this paper we present our experimental investigation of the 0-π phase transition in $Nb|AlO_x|Nb|Ni_{60}Cu_{40}|Nb$ structures by varying the thickness of the ferromagnet d_F and of the s-layer d_s. To this purpose we fabricated two sets of samples. In the first one (F-wedge), the ferromagnetic layer is deposited as a wedge, while d_s is kept constant. In the second one (s-wedge) the s-interlayer forms a wedge, while d_F is constant. An additional difference in the wafers is the thickness of the insulating barrier. For all the F-wedge JJs, the barrier was oxidized in order to obtain reference SIS JJs with $j_c = 7\,\mathrm{kA/cm^2}$. The s-wedge JJs have $j_c = 1.2\,\mathrm{kA/cm^2}$.

F-wedge JJs. The current-voltage characteristic (IVC) and the mod-

ulation of the critical current with the magnetic field $I_c(H)$ was measured for several samples with different d_F and d_s. For each junction we recorded the maximum value of j_c and plotted it in the $j_c(d_F)$ dependences shown

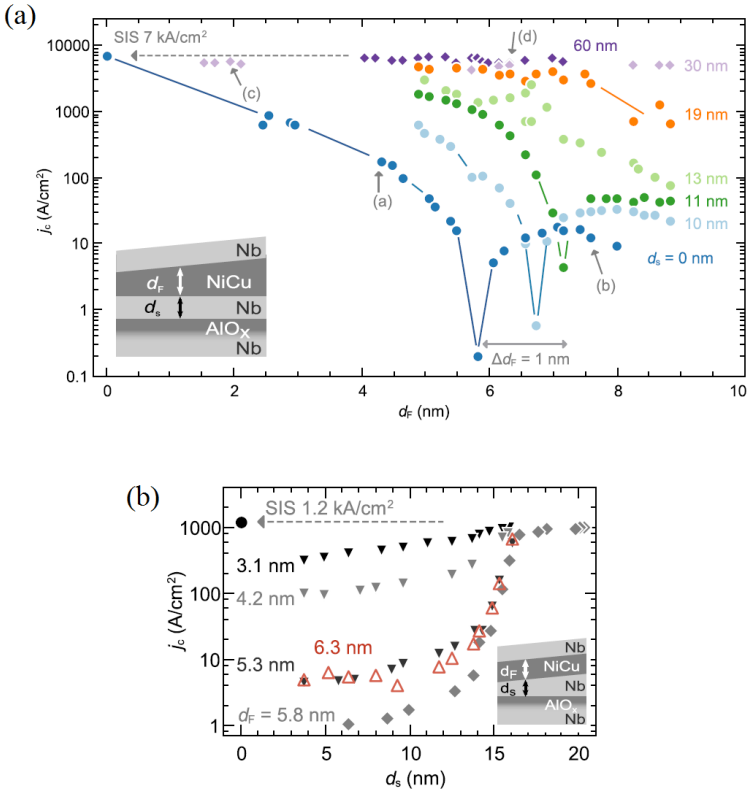

Figure 6.1: Dependence of the critical current density j_c as a function of the ferromagnetic layer thickness d_F for F-wedge SIsFS JJs (a) and as a function of the superconducting interlayer thickness d_s for s-wedge SIsFS JJs (b). The arrows in (a) indicate the junctions whose IVC and $I_c(H)$ characteristics are shown in Fig. 6.2. The insets in (a) and (b) show a schematic of the SIsFS structure. Figures from the appended Publication 4.

in Fig. 6.1(a). As the s-layer becomes thicker, one observes a general tendency of the critical current density to increase, confirming the recovery of superconductivity. Additionally, the profile of the curves changes significantly. For $d_s < 11\,\mathrm{nm}$, the $j_c(d_F)$ dependence exhibits a well distinct minimum, that is a strong indication of the transition of the phase ground state from 0 to π. The crossover thickness $d_F^{0-\pi}$ moves gradually from 5.8 nm for $d_s = 0$ (SIFS JJ) toward 7.1 nm for $d_s = 11\,\mathrm{nm}$. For

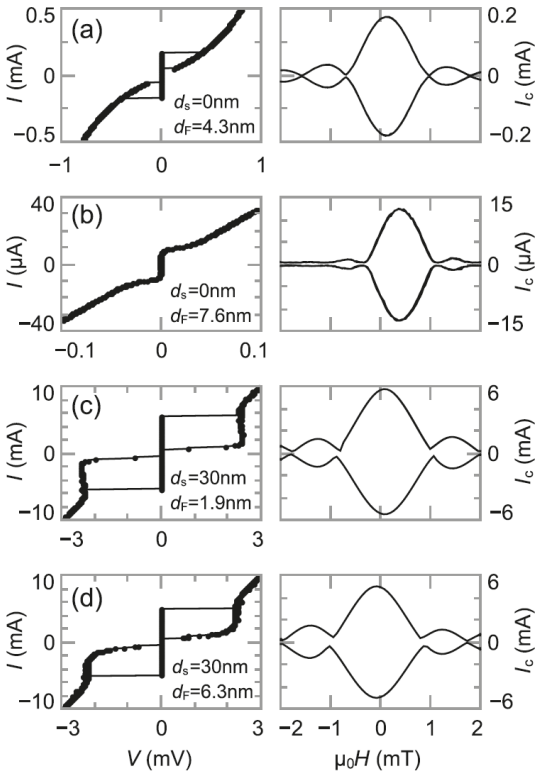

Figure 6.2: Current-voltage characteristics and magnetic modulation of the critical current for the SIsFS junctions marked by the letters (a)-(d) in Fig. 6.1(a). Figure from the appended Publication 4. © 2015 American Institute of Physics.

$d_s = 13\,\text{nm}$ and $d_s = 19\,\text{nm}$, the junctions showed extreme sensitivity to the magnetic history and no 0-π transition can be observed (or resolved). For $d_s > 30\,\text{nm}$, j_c does not depend on d_F any longer and it reaches the value of $7\,\text{kA/cm}^2$ of the reference SIS JJ. Again, no 0-π transition is visible. The measured curves match rather well the expectations from the theory [38, 40, 92]. A thin s-layer in the SIsFs stack behaves like a normal metal and shifts $d_F^{0-\pi}$ to higher values. On the other hand, if the s-layer is thick, with d_s comparable to or larger than the niobium coherence length $\xi_s = 38\,\text{nm}$, the SIsFS JJ behaves as a SIs JJ connected in series with a sFS JJ, where the physics is dominated by the junction with smaller j_c (*i.e.* the SIs one). A few selected IVC and $I_c(H)$ corresponding to different d_s and d_F (indicated by the arrows in Fig. 6.1(a)) are shown in Fig. 6.2. What can be notice here is that the IVC is more and more SIS-like as d_s becomes thicker. At $d_s = 30\,\text{nm}$ (*cf.* Fig. 6.2(c) and (d)), the only effect of the F-layer is to increase the subgap resistance. Finally, the junctions were always overdamped in the π region for $d_s < 11\,\text{nm}$ (see Fig. 6.2(b)).

s-wedge. The same set of measurements was repeated for the s-wedge samples. The results are displayed in Fig. 6.1(b). Again, we see an enhancement of j_c with increasing d_s. All the curves, corresponding to different values of d_F, saturate for very large s-layer thicknesses to the reference value of $1.2\,\text{kA/cm}^2$. By looking at both Fig. 6.1(a) and (b) one can easily deduce that a 0-π JJ can be obtained by introducing a step in the F-layer. Theoretically, it has been suggested that a 0-π transition may also be induced by temperature for $d_F \approx d_F^{0-\pi}$ [40]. Unfortunately, we were not able to observe this in our samples.

In conclusion, we have experimentally observed a 0-π phase transition in SIsFS JJs induced by the ferromagnetic layer, for several thickness of the superconducting interlayer. The latter leads, as expected, to an increase of the critical current density of 2-3 orders of magnitude. However, in the range of $d_s < 11\,\text{nm}$ where the 0-π crossover was actually observed, the maximum obtained j_c in the π-region was of the order of only $60\,\text{A/cm}^2$ at 4.2 K, that is not a significant improvement with respect to the previous SIFS technology.

Contributions to this publication

The junctions used for the work reported in this publication were fabricated by N. Ruppelt, who at that time was a Ph.D student in the group of Prof. H. Kohlstedt at the University of Kiel. He also wrote the paper. H. Sickinger and me performed the experimental characterization of the JJs at $T = 4.2\,\mathrm{K}$ and evaluated the data. Additionally, we reviewed the paper.

7 Manuscript in preparation
An artificial φ Josephson junction: Evidence of macroscopic quantum tunneling from both ground states

A first draft of a paper we are preparing is given in this chapter.

Authors: **R. Menditto**, M. Merker, M. Siegel, D. Koelle, R. Kleiner and E. Goldobin

φ Josephson junctions (JJs) are fascinating devices, since they show unique physics [30, 35, 62] and a potential for applications in superconducting electronics, *e.g.*, phase batteries, memories and ratchets [22, 23, 31, 65]. Furthermore, in the quantum domain, such junctions can be seen as a macroscopic two-level system, thus macroscopic quantum effects (MQE) can be investigated. Our group realized the first φ JJ out of 0-π JJ based on a SIFS heterostructure with a tailored ferromagnetic barrier [34]. The experiment follows the theoretical prediction that a 0-π JJ with unequal 0 and π segments ($L_0 \neq L_\pi$ or $j_{c0} \neq j_{c\pi}$) results in a φ JJ, if parameters are carefully chosen [32, 33, 93]. In our SIFS sample, the existence of two phase states was successfully demonstrated by detecting two critical currents: I_{c+} and I_{c-}, corresponding to the escape of the phase from the $\pm\varphi$ wells of the potential. Further theoretical and experimental investigation of the SIFS-based φ JJs was carried out and reported by our group in several works [31, 35, 62, 65]. However, the quantum properties of a φ JJ remain uninvestigated. Only in one work known to us [94] the macroscopic quantum tunneling (MQT) in grain boundary biepitaxial JJs was investigated. In such JJs a strong second harmonic in the current-phase relation (CPR) appears at low temperatures and, therefore, one deals with a double-well potential. Although an MQT-like saturation of the histogram peak width with an unusual temperature dependence was demonstrated [94], the evidence for the presence of two critical currents expected in this

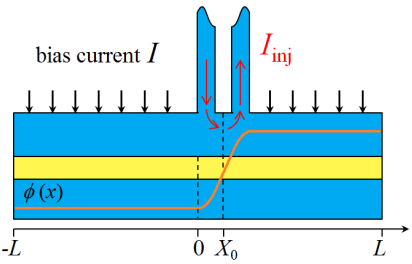

Figure 7.1: Sketch of the investigated Josephson junction with two current injector leads attached on the top electrode. The orange line represents the spatial variation of phase along the junction length.

case is missing.

In this work, we realize a φ JJ based on conventional SIS technology and investigate the phase escape from *both* potential wells of the energy $U(\phi)$, giving evidence of macroscopic quantum tunneling. Our sample consists of a 0 JJ where the 0-π phase discontinuity is artificially created by means of two tiny current injectors placed on top of the junction, at a position slightly away from its center. The injectors have a width W_{inj} and are separated by a distance W_{d}. In order to have an ideal discontinuity, injectors dimensions are chosen in such a way that $2W_{\mathrm{inj}} + W_{\mathrm{d}} \ll \lambda_J$, where λ_J is the Josephson penetration depth. The current flowing through the injectors I_{inj} twists the phase ϕ, consequently ϕ changes from 0 to κ between the injector leads. The value of κ is proportional to I_{inj}, thus a κ, *e.g.*, π, discontinuity can be created by applying the proper I_{inj} [41].

The injector concept was implemented in the past to realize symmetric 0-π, or more generally 0-κ, JJs aimed to the investigation of integer [85, 86, 95, 96] and fractional vortices [41, 42, 97, 98]. Now, we demonstrate that a similar device can be used to built a junction that can be turned from a 0 into a φ JJ by simply controlling the current applied to the injectors [59]. The tunability of the phase discontinuity is a powerful tool for measurements in the quantum domain, since it allows us to rule out effects due to parasitic noise in our system.

In the following, we introduce the model used to describe and numerically simulate a JJ with an artificially induced phase discontinuity. Results are compatible with the ones obtained from the effective model

for a point-like JJ with δ-injectors presented in [59]. However, here, we take into account the finite size of the junction and of the injectors leads. We show simulations of the energy of the junction as a function of various parameters and discuss the results. Further, we present characterization in the classical regime and statistics of *both* switching currents of our φ JJ in the quantum limit. The dependence of the widths $\sigma_{\pm}$ of both histograms *vs* temperature and injector current, together with calculation of the escape rate, is shown and proofs of MQT are provided.

The model. We consider a 1D JJ of normalized length $l = L/\lambda_J$ equipped with a pair of current injectors of width $w_{\rm inj} = W_{\rm inj}/\lambda_J$ and distance $w_{\rm d} = W_{\rm d}/\lambda_J$ from each other, that are connected on top of the junction at a position $x_0 = X_0/\lambda_J \neq 0$. A sketch of the investigated device is shown in Fig. 7.1. In this work, we will describe the case $x_0 > 0$; the opposite configuration ($x_0 < 0$) is analogous. In such a system, the dynamics of the Josephson phase $\phi(x,t)$ can be modeled by the 1D sine-Gordon equation

$$\phi_{xx} - \phi_{tt} - \sin\phi = \alpha\phi_t - \gamma - \gamma_{\rm inj}(x) \tag{7.1}$$

where $\alpha = 1/\sqrt{\beta_{\rm c}}$ is the damping parameter, $\gamma = j/j_{\rm c}$ is the bias current density normalized to the critical current density of the junction and $\gamma_{\rm inj}(x)$ is the injector current density. In Eq. (7.1), the spatial coordinate x is normalized to λ_J and the time t is normalized to the inverse of the plasma frequency ω_p^{-1}. The injector current density distribution is considered as

$$\gamma_{\rm inj} = \begin{cases} \frac{\kappa}{w_{\rm inj}(w_{\rm inj}+w_{\rm d})} & x_0 - (w_{\rm inj} + \frac{w_{\rm d}}{2}) < x < x_0 - \frac{w_{\rm d}}{2}, \\ 0 & x_0 - \frac{w_{\rm d}}{2} < x < x_0 + \frac{w_{\rm d}}{2}, \\ -\frac{\kappa}{w_{\rm inj}(w_{\rm inj}+w_{\rm d})} & x_0 + \frac{w_{\rm d}}{2} < x < x_0 + (w_{\rm inj} + \frac{w_{\rm d}}{2}). \end{cases} \tag{7.2}$$

The phase profile in the injector area $\phi_{\rm inj}(x)$ is derived by doubly integrating Eq. (7.2) and it is depicted in Fig. 7.1. For the numerical solution of Eq. (7.1), we introduce the phase $\mu(x,t) = \phi(x,t) + \phi_{\rm inj}(x) + 2\pi\varphi_{\rm ext}x$, where φ_{ext} is the externally applied magnetic flux Φ, normalized to the flux quantum Φ_0. Eq. (7.1) can be rewritten in terms of $\mu(x,t)$ as:

$$\mu_{xx} - \phi_{tt} - \sin[\mu - \phi_{\rm inj}(x) + 2\pi\varphi_{\rm ext}x] = \alpha\mu_t - \gamma \tag{7.3}$$

Next, we describe the physics of the device in Fig. 7.1 by showing simulations of the effective energy potential $U(\psi)$, with $\psi = \langle\mu(x)\rangle$ the

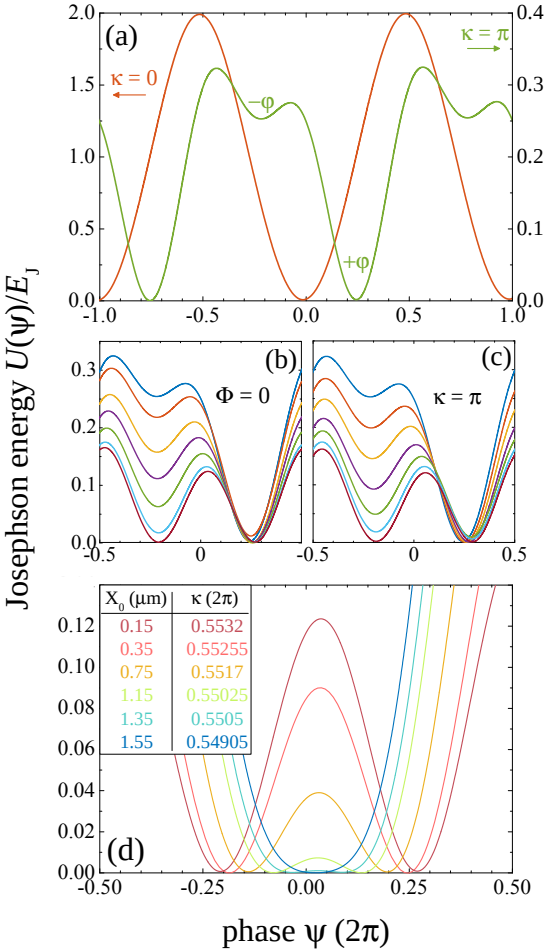

Figure 7.2: Simulated potential $U(\psi)$ for $L = 10\,\mu$m, $W_{\rm inj} = W_{\rm d} = 1\,\mu$m, $X_0 = 0.15\,\mu$m and $\lambda_{\rm J} = 5\,\mu$m. (a) Josephson potential for $\kappa = 0$ and $\kappa = \pi$. Tunability of the Josephson energy with $\kappa/2\pi$ (b) and Φ/Φ_0 (c). In panel (b), $\kappa/2\pi$ varies from 0.5 (blue curve) to 0.5532 (red curve), while Φ/Φ_0 is constant and equal to zero. In panel (c), Φ/Φ_0 varies from 0 (blue curve) to -0.094 (red curve), while $\kappa/2\pi$ is constant and equal to 0.5. (d) Josephson energy as a function of the injector distance from the center of the junction. The value of κ is adjusted to keep the potential symmetric. No magnetic field is applied.

average phase, as a function of different parameters. For this purpose, we considered $l = 2$, $w_{\rm inj} = w_{\rm d} = 0.2$ and $x_0 = 0.03$, close to the experimental values. In Fig. 7.2(a), the potential $U(\psi)$ normalized to the Josephson energy $E_{\rm J} = I_{\rm c}\Phi_0/2\pi$ for $\kappa = 0, \pi$ is displayed. When $\kappa = 0$, the JJ is in the 0 state and the potential changes as $\sim \cos(\psi)$ with minima at $\psi = 2\pi n$, with n an integer. As κ approaches π, two minima develop within every 2π-period in the potential at $\psi = \pm\varphi$. The value of φ depends on the geometry of the junction. This result confirms previous theoretical predictions, made for a point-like JJ with δ-injectors [59]. However, in our case of finite injectors, an asymmetry in the potential at $\kappa = \pi$ appears, *i.e.* the two energy wells have different depths. We associate this asymmetry to the presence of an effective field component due to the finite size of the junction and of the injector leads. The field component can be compensated by either varying κ slightly from π or by applying a small magnetic flux Φ to the junction, see Fig. 7.2(b) and (c). For a finer tuning of the potential, κ and Φ can be changed simultaneously (not shown). Furthermore, the height of the energy barrier U_0 separating the $\pm\varphi$ wells decreases as the injectors move away from the center of the junction, as shown in Fig. 7.2(c). Here we observe that by varying the injector position, together with κ to retain the symmetry of the potential, the two wells become more and more shallow with increasing distance x_0. Eventually, for $x_0 > x_{\rm c}$, U_0 disappears completely and one returns to the case of a single minimum. However, the minimum is shifted from zero, *i.e.* we obtain a φ_0 JJ. The value of $x_{\rm c}$ strongly depends on the length of the junction — the shorter l, the smaller $x_{\rm c}$ — as already pointed out in previous works [29, 32, 33, 59]. Below we use this model to numerically fit the experimental results. Possible discrepancies are to be explained considering that the theory describes the simple geometry of a 1D junction with 1D injectors, while in real samples, we have 3D objects and the distribution of the currents applied to the junction and to the injectors may flow in a more complex way.

Experiment. We fabricated Nb-AlO_x-Nb JJs with two injectors connected on the top electrode of the junction. The JJs have moderate length $L \sim 1.25...2.5\lambda_{\rm J}$ and different width $W_{\rm inj} = 1, 1.5\,\mu$m and position $X_0 \sim 0...9\,\mu$m of the injectors [99]. In all our samples, $W_{\rm d} \simeq W_{\rm inj}$. A picture of one of the JJ is shown in Fig. 7.3. We have measured several junctions. The data presented in this letter were obtained on a junction with $L = 40\,\mu$m, width $W = 0.8\,\mu$m, $W_{\rm inj} = 1.5\,\mu$m and $X_0 \sim 0.125\,\mu$m.

The junction has a perfect SIS JJ current-voltage (I–V) characteristic and $I_c(H)$ dependence (both not shown), with critical current $I_c = 667\,\mu$A at $T = 4.2\,$K and $I_c = 727\,\mu$A at $T = 20\,$mK (estimated from single I–V measurement). This corresponds to $j_c \approx 2.8\,$kA/cm^2 and $\lambda_J \approx 16\,\mu$m (calculated from a numerical fit of $I_c(H)$) at $T = 4.2\,$K. Thus, our JJ has a normalized length $l = 2.5\lambda_J$ and normalized injectors size $w_{\rm inj} \sim 0.09$.

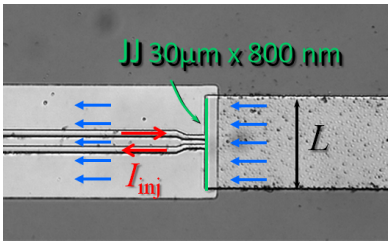

Figure 7.3: Optical image in false colors of one of the investigated JJ with current injectors. The junction is nominally equal to the one used for the experiments shown here.

Classical domain. In order to understand which value of the current $I_{\rm inj}$ we need to apply to have a phase discontinuity $\kappa = \pi$, we use the fact that $\kappa \propto I_{\rm inj}$. Therefore we measure the $I_c(I_{\rm inj})$ dependence, also referred to as "injectors calibration curve". We know from [42] that for a perfectly symmetric JJ ($X_0 = 0$) and no self-field effect, $\kappa = \pi$ corresponds to the first minimum of the $I_c(I_{\rm inj})$ curve, which is symmetric for positive and negative bias. For a JJ with $X_0 \neq 0$, the first minimum of the $|I_c(I_{\rm inj})|$ curves occur at different values of $I_{\rm inj}$. The injector current corresponding to $\kappa = \pi$ is centered between these values. The experimental calibration curve of our junction is shown in Fig. 7.4(a) and (b). The first thing to notice here is that four critical currents (two for each bias polarity) appear around the first minimum of the curve. In addition, if we zoom in and inspect more carefully, we observe a tiny asymmetry between the positive and negative bias curves (see Fig. 7.4(b)). These two features prove our φ JJ. The dotted line in Fig. 7.4(b) indicates the value of $I_{\rm inj}$ corresponding to the middle point between the crossing of the four current branches, where the Josephson potential has symmetric wells, that is $I_{\rm inj}^{\rm sym} = 3.67\,$mA. From the comparison with the simulated curve, *cf.* Fig. 7.4(b), we can notice that $I_{\rm inj}^{\rm sym}$ corresponds to a $\kappa = 1.02\pi$ slightly different from π,

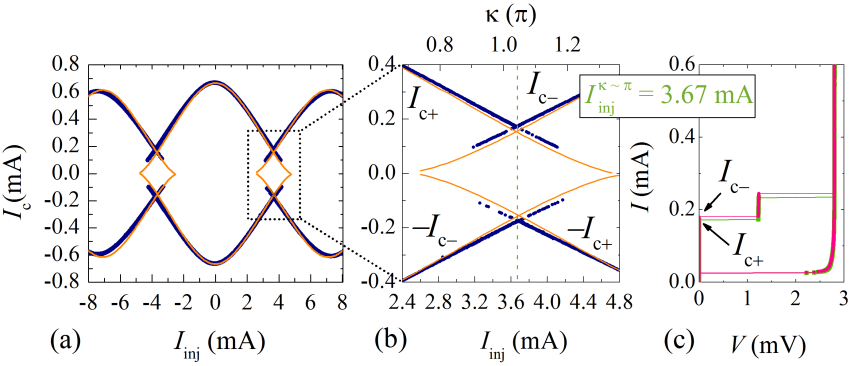

Figure 7.4: (a) Experimental (blue line) and simulated (orange line) calibration of the injectors of a 40 μm long JJ with 1.5 μm wide injectors located at $X_0 = 0.125\,\mu$m at $T = 4.2$ K and $H = 0$. In (b) a zoom around the first minimum is displayed. The dotted line indicates the value of κ (or $I_{\rm inj}$) for which the potential has symmetric $\pm\varphi$ wells. (c) The I–V curve at $I_{\rm inj}^{\rm sym} = 3.67$ mA showing two distinct critical currents is plotted.

as expected, due to the finite size of the junction and of the injectors. The value of $I_{\rm inj}^{\rm sym}$ changes slightly with temperature; at $T = 20$ mK we measured $I_{\rm inj}^{\rm sym} = 3.71$ mA.

Fig. 7.4 shows the I–V curve measured for $I_{\rm inj}^{\rm sym} = 3.67$ mA. By applying the bias current using special sweep sequences, we were able to detect the two critical currents I_{c-} and I_{c+}. The two currents are also observable in the $I_c(H)$ dependence, where a characteristic minimum around $H = 0$ appears (not shown), as we know from [32]. In our previous work, where we used the SIFS-based φ JJ, the high damping prevented us to observe two critical currents at $T = 4.2$ K. In the present junctions, instead, the damping is very low and two critical currents are measurable in a wide range of temperatures.

Quantum domain. Further we investigated the phase escape from the double well potential of the φ JJ. For this, we have cooled down our sample in a dilution refrigerator and performed measurements in a temperature range from 20 mK to 600 mK. We have collected statistics of critical currents at $I_{\rm inj}^{\rm sym} = 3.71$ mA by sweeping the bias current with a constant

ramp rate $\dot{I} = 79.6\,\mathrm{mA/s}$, recording the exact value of the switching current during each sweep. By repeating such measurements $N = 5000$ times, we were able to plot histograms of critical current distributions. Since at low damping the initial state ($-\varphi$ or $+\varphi$) is random [35, 62], we obtain histograms containing two peaks corresponding to I_{c-} and I_{c+}, as shown in Fig. 7.5(a). As the temperature decreases, each peak shifts towards the noise-free critical current $I_{c0\pm}$ and the width of the histogram decreases. The dependence of the width $\sigma_\pm(T)$ of each peak is extracted from the experimental data and presented in Fig. 7.5(b). One clearly sees that both $\sigma_\pm(T)$ saturate at $T < T^\star \approx 260\,\mathrm{mK}$ at values $\sigma_+^{\mathrm{sat}} \approx 137\,\mathrm{nA}$ and $\sigma_-^{\mathrm{sat}} \approx 142\,\mathrm{nA}$. Such a saturation of the escape peak width is an evidence of the crossover from the thermal escape to the macroscopic quantum tunneling of the phase out of the $-\varphi$ or $+\varphi$ well.

However, one should be extremely careful with such conclusions, since the saturation might be caused (a) by the parasitic heating of the sample to a temperature above the bath temperature due to temporary switching to the resistive state or (b) by some background noise in our experimental setup, which has little to do with MQT. There can be several types of such noise: (i) constant background noise picked up from the environment because some wires work as an antenna; (ii) noise in the bias current circuit with $\sigma_b = c_0 + c_1 I$; (iii) the noise in the injector circuit with $\sigma_{\mathrm{inj}} \propto I_{\mathrm{inj}}$.

To rule out overheating, we have repeated our measurements using different duty cycles and different ramp rates and observed no qualitative difference.

The standard technique to exclude the saturation due to electronic noise is to demonstrate that in the used setup one can measure σ values, which are below $\sigma_\pm^{\mathrm{sat}}$, possibly in the same experiment and with the same sample. Already from Fig. 7.5(b) one can conclude that σ_-^{sat} is *not* due to the background noise because we have measured a smaller value of σ_+^{sat} at the same I_{inj}. Nevertheless, if the noise is $\propto I$, one can easily observe such σ_-^{sat} as $I_{c-} > I_{c+}$. An analysis of the $\sigma(I_c)$ dependence suggests that this is not the case in our measurements, since $\sigma_\pm(I_c)$ stays approximatively constant when I_c is modulated by the injector current, see Fig. 7.6. Moreover, we can exclude significant contribution of random noise in the bias circuit as, for $T < T^\star$, the dependences of the skewness (S) and kurtosis (K) of escape histograms on I_c are constant and they tend to the universal values of $S = -1$ and $K = 5$ [100].

In MQT experiments with conventional small JJs, one usually changes

some parameter, *e.g.*, one applies a magnetic field, in order to decrease the effective I_c and, accordingly [101], the histogram width $\sigma \propto I_c^{3/5}$. In our system the tuning parameter is κ, therefore we have measured $\sigma_{\pm}^{\mathrm{sat}}(I_{\mathrm{inj}})$ at $T = 20\,\mathrm{mK}$, see Fig. 7.6. The dependence is almost symmetric with

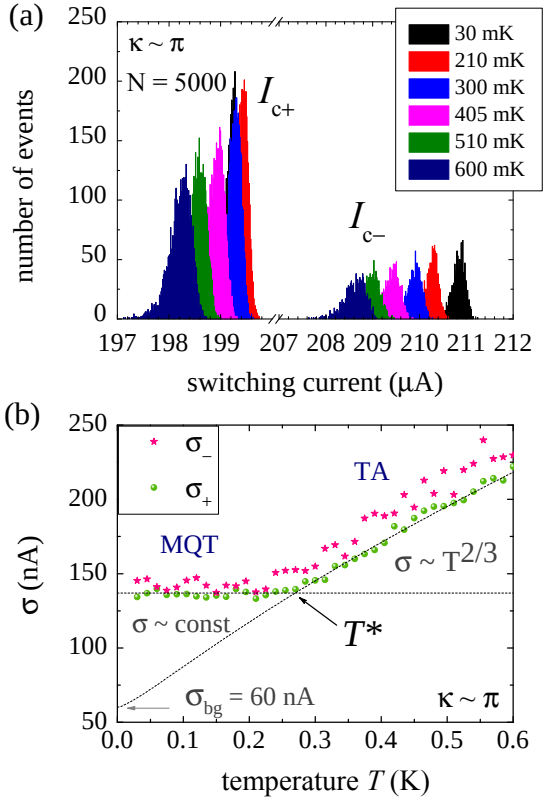

Figure 7.5: (a) Several switching current histograms taken at $I_{\mathrm{inj}}^{\mathrm{sym}} = 3.71\,\mathrm{mA}$ ($\kappa \sim \pi$) and at different temperatures. Each histogram has two peaks corresponding to the escape from the $-\varphi$ and the $+\varphi$ well. Each peak is somewhat below I_{c0+} and I_{c0-}, the fluctuation-free critical currents of the φ JJ. (b) The widths $\sigma_{\pm}$ of the I_{c-} and I_{c+} peaks in (a) as a function of temperature T is shown.

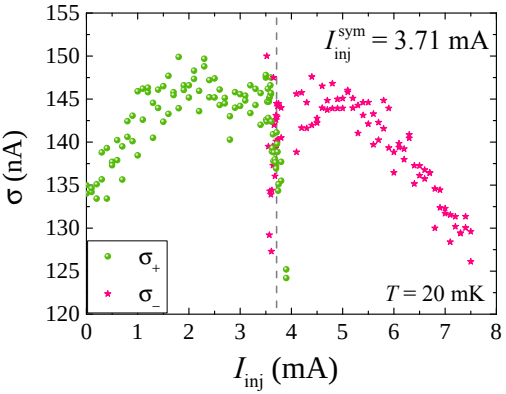

Figure 7.6: The dependences $\sigma_{\pm}(\kappa)$ at $T = 20\,\mathrm{mK}$. The dotted line indicates the symmetry point occuring at $I_{\mathrm{inj}}^{\mathrm{sym}} = 3.71\,\mathrm{mA}$.

respect to the value $I_{\mathrm{inj}}^{\mathrm{sym}} = 3.71\,\mathrm{mA}$. One can see that both $\sigma_{+}^{\mathrm{sat}}$ and $\sigma_{-}^{\mathrm{sat}}$ have a maximum at $\kappa \approx \pi$ and that our setup is able to measure values of σ as low as 130 nA. The presence of points (κ values) where $\sigma_{\pm} < \sigma_{\pm}^{\mathrm{sat}}$ automatically means that at all other values of κ, where $\sigma_{\pm}$ is larger, we *do not* observe saturation due to noise. Also, if the noise would be caused by I_{inj}, one would observe its monotonous increase as $\kappa \propto I_{\mathrm{inj}}$ grows. Fig. 7.6 clearly shows that this is *not* the case. The higher moments $S(I_{\mathrm{inj}}) \approx -1$ and $K(I_{\mathrm{inj}}) \approx 5$ confirm also absence of white noise contributions. We conclude that we indeed observe MQT.

The presence of some background noise of non-thermal origin is nevertheless obvious. One can see that the extrapolation of the $\sigma_{\pm}(T) \sim T^{2/3}$ dependence, shown in Fig. 7.5(b), from the thermal escape region towards $T \to 0$, results in $\sigma_{\mathrm{bg}} \approx 60\,\mathrm{nA}$, which can be taken as a reasonable estimate of the parasitic noise level in our system.

Additional indications of the quantum behavior of the phase in our φ JJ can be found in the analysis of the escape rate Γ as a function of the bias current. For the computation of the experimental Γ for both switching current peaks in Fig. 7.5(a) we have used the formula [49]

$$\Gamma_{\pm}(I_k) = \frac{\dot{I}}{\Delta I} \ln \frac{\sum_{j=k}^{M} P(I_j)}{\sum_{j=k+1}^{M} P(I_j)}, \tag{7.4}$$

where M is the number of bins of width ΔI of the built histogram and $P(I_j)$ is the discretized probability distribution of the switching current. The results are compared to the theoretical expectations for the thermal activation (TA) and the MQT regime, which, in the low-to-moderate damping limit, are respectively given by [50, 54]

$$\Gamma_t(I) = a_t \frac{\omega_p}{2\pi} \exp\left(- \frac{\Delta U}{k_B T} \right), \tag{7.5}$$

$$\Gamma_q(I) = a_q \frac{\omega_p}{2\pi} \exp\left(- 7.2 \frac{\Delta U}{\hbar \omega_p} \right), \tag{7.6}$$

where a_t and a_q are damping-dependent prefactors, $\omega_p(I) = P_{\omega_0}(1 - I/I_{c0})^{1/4}$ is the plasma frequency and $\Delta U = P_{\Delta U}(1 - I/I_{c0})^{3/2}$ is the energy barrier. P_{ω_0} and $P_{\Delta U}$ are the plasma frequency and the energy barrier prefactors for a JJ with two degenerate ground states. The expression and the theoretical study of such parameters are given in [59]. By explicating the current dependence of all parameters in the exponent of Eq. (7.5) and Eq. (7.6), one obtains $\Gamma_t, \Gamma_q \sim \exp[(1 - I/I_{c0})^m]$, where $m = 3/2$ in the thermal regime and $m = 5/4$ in the quantum regime.

To perform the comparison, we first plotted the quantity $[\ln(\omega_p/2\pi\Gamma_\pm)]^{1/m}$ versus the switching current I for a few temperatures in the range from 600 to 30 mK. In such a way, one gets a linear function and the noise-free current $I_{c0\pm}$ can be extrapolated from the intercept with the current axis. We iteratively fitted the experimental data with a weighted linear least-square fit in order to have a precise estimation of $I_{c0\pm}$. For the sake of simplicity, in our procedure we adopted $a_t, a_q = 1$. Subsequently, we graphed the double logarithm of the normalized inversed escape rate $\omega_p/2\pi\Gamma_\pm$ as a function of $\ln(1 - I/I_{c0})$, that is again a linear function. The choice of the double-log plot has been made in order to highlight the difference in the slopes m of the thermal and quantum formulas. Our results are displayed in Fig. 7.7 for both the right and left peak of Fig. 7.5(a). In Fig. 7.7(a) and (c), we fitted the data using the thermal formula for the escape rate (Eq. (7.5)), while in (b) and (d) we used the quantum expression (Eq. (7.6)). What is evident here is that, for both peaks, Γ_t matches the experimental points perfectly for $T > T^\star$, but it deviates significantly for $T < T^\star$. The experimental escape below $T^\star$ is fitted very well by Γ_q, which in turn fails for higher temperature. This analysis lends further support to the claim that below the crossover temperature the escape mechanism in

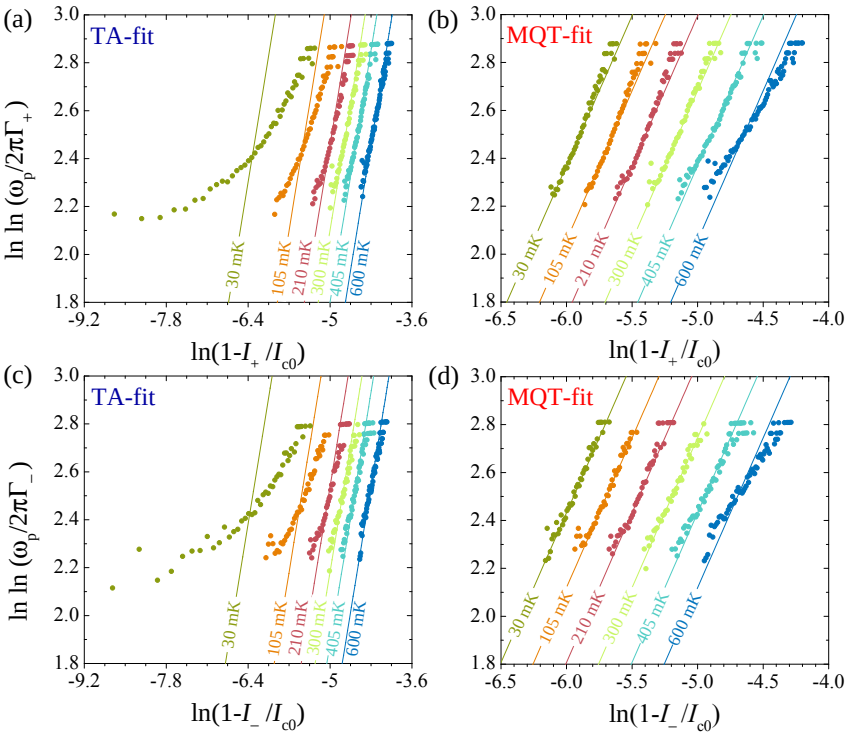

Figure 7.7: Double logarithm of the normalized inverse escape rate $\ln\ln(\omega_p/2\pi\Gamma)$ for different temperatures in the range $600\,\mathrm{mK} < T < 30\,\mathrm{mK}$ for the right peak of Fig. 7.5(a) (panels (a) and (b)) and for the left peak of Fig. 7.5(a) (panels (c) and (d)). In the graphs, the points represent the experimental data and the lines the fits obtained by using the equations Eq. (7.5) (TA-fit) and Eq. (7.6) (MQT-fit). One can clearly observe that for both peaks (both energy wells $\pm\varphi$) the TA-formula fits very well the experimental points above $T^\star$, but it does not below $T^\star$. The opposite occurs for the MQT-formula, proving quantum tunneling below the crossover, where the standard deviations $\sigma_\pm$ saturate. In panels (b) and (d), the curves where manually shifted by -0.5 to display them better. Since there is no dependence on temperature in Γ_q, the curves sit almost at the same position in the diagram.

our junction is dominated by quantum tunneling of the phase. Note that the assumption of $a_t = 1$ and $a_q = 1$ does not affect latter result, since the prefactors logarithmically enter into the escape rate computation.

In conclusion, we have demonstrated a φ JJ realized with an artificial phase discontinuity κ created in a SIS JJ by two tiny current injectors of finite size and investigated the quantum properties of the phase. We have described the system theoretically and have shown simulations of the Josephson energy potential taking into account the finite size of the junction and of the injectors. We have proven experimentally that such a junction can be turned from a 0 JJ to a φ JJ by simply varying the amplitude of the current applied to the injector I_{inj}. To adjust possible asymmetries of the potential, one can fine-tune the injector current or apply an external magnetic flux. Simulations show that by changing the position of the injectors along the length of the junction, the energy barrier U_0 between the $\pm\varphi$ wells decreases down to values of the order of $10^{-5}E_J$, which is interesting if one wants to perform measurements to study macroscopic quantum coherence between the $-\varphi$ and $+\varphi$ states. However, the technology is not ideal for such an operation. In order to have very shallow and symmetrical wells, the position of the injectors and the values of the applied I_{inj} have to be controlled with high precision [29, 32, 33, 59]. In the future, one can think about more advanced technological designs of our junction, for instance one could implement more than one injector pair, to be able to fully control the energy profile electronically, without moving the injectors.

Finally, we have performed quantum mechanical experiments of the Josephson phase escape and provided evidence of macroscopic quantum tunneling of the average phase ψ from *both* minima of the Josephson potential. The thermal to MQT crossover temperature occurring at $T^\star \approx 260\,\mathrm{mK}$ is indicated by the saturation of the width $\sigma_\pm$ of the histograms of the switching currents $I_{\mathrm{c}-}$ and $I_{\mathrm{c}+}$. We exclude the possible influence of background noise in our system, since we could measure values of σ lower than σ^{sat} by sweeping the injector current. Further proofs of MQT are given by the calculated escape rate from both wells. Fits of the experimental data with the formulas present in literature clearly show that thermal activation is the dominant escape process above $T^\star$, while quantum tunneling prevails below $T^\star$.

Contributions to this publication

For this publication, I performed all the simulations and the experiments presented and analyzed the results. Moreover, I wrote the paper.
M. Merker is a Ph.D student in the group of Prof. M. Siegel. He fabricated the sample, according to design parameters given by me.

8 Summary

The focus of my thesis is the experimental investigation of φ Josephson junctions (JJs) in the classical and in the quantum limit.

A φ JJ is a bi-stable system exhibiting a degenerate ground state at phases $\pm\varphi$, with $0 < \varphi < \pi$ [29, 30, 32, 61]. In terms of the Josephson energy $U(\psi)$, this corresponds to a double well potential with a periodicity of 2π. The special profile of $U(\psi)$ originates from an unconventional current-phase relation (CPR) that has a non-zero and negative second harmonic. The supercurrent $I_s(\psi)$ and the energy $U(\psi)$ are tunable with an externally applied magnetic field.

φ JJs are fascinating devices showing unique physics, *e.g.*, non-quantized Josephson vortices [30, 63, 64] and a nontrivial phase dynamics [35, 62]. Additionally, in the quantum limit, the junction can be pictured as a quantum-mechanical two-level system, thus it represents an ideal tool to study quantum coherence. The properties of a φ JJ are of huge interest for many applications [31, 65]. The most attracting one is definitively the realization of an arbitrary (never discharging) phase battery, providing a current to be used to feed other circuits.

Several systems have been suggested as possible candidates for the realization of a φ JJ [29, 39, 56, 58, 60, 61, 68, 74]. However, the simplest setup is a single JJ with asymmetric 0 and π segments [32]. Experimentally, an asymmetric 0-π JJ has been realized using **S**uperconductor-**I**nsulator-**F**erromagnet-**I**nsulator (SIFS) JJs, where the φ was state successfully proven [34].

In the first part of my thesis we used these SIFS JJs to investigate the retrapping dynamics of the Josephson phase [62]. Since two possible final states of the phase exist, it is not obvious where the phase-particle ends when returning from the running ($V \neq 0$) to the trapped state ($V = 0$). In particular, we have measured switching current distributions and estimated the probability P of retrapping the phase in the "unnatural well", that is $-\varphi$ ($+\varphi$) for a positive (negative) bias. We have collected measurements at several temperatures below $T = 2.30\,\mathrm{K}$ and plotted the $P_-(T)$ dependence. From this curve we could demonstrate that the retrapping process is deterministic for high temperature (*i.e.* high damping), while it is unpredictable for low temperature (*i.e.* low damping), confirming theoretical predictions [35]. However, due to a saturation of the damping of our junctions, we could not penetrate the regime of extremely low damping

and observe the predicted butterfly effect. Here a probability $P_- = 50\%$ is expected, while we observed $P_- \approx 33\%$.

In the future, we plan to realize a φ JJ using a discrete device, *i.e.* an 0-π asymmetric dc SQUID [60] or a three JJs SQUID, where the damping is expected to be very low, since the junction are fabricated with standard SIS technology. Such systems offer many advantages over the continuous ones, like a wider φ domain and less geometrical constrictions. One could take also a 0-0 SQUID with asymmetric junctions, which can turn from an effective 0 JJ to a φ_0 or even a $\varphi_0 \pm \varphi$ upon application of half flux quantum $\Phi = \Phi_0/2$, provided proper values of the junctions critical currents and inductance of the SQUID.

The same SIFS samples have been used to demonstrate a deterministic and tunable ratchet [65]. A ratchet can be realized only if the energy of the system has no reflection symmetry. In conventional JJs this condition is not fulfilled, therefore for a long time a Josephson phase ratchet based on a single JJ was missing. The advent of φ JJ allows to fill this gap. In fact, in a φ JJ, the symmetry of the energy potential can be broken if an external magnetic field is applied. In our work, we theoretically describe and experimentally demonstrate the rectification operation of a SIFS φ JJ, and show its tunability with H. Furthermore, we estimate its efficiency by opposing the rectification with a counterforce. Our sample was not optimized for such an application — one could think of a better design with a stronger asymmetry between the 0 and π facets of the junction — nevertheless it appears rather efficient with $\eta_{\max} = 48\%$.

In the second part of my thesis we searched for evidence of macroscopic quantum tunneling (MQT) in a φ JJ. This study was carried out on a junction fabricated with a new technology, involving no ferromagnetic layer. The junction is realized with a conventional Nb|AlO_x|Nb trilayer and the 0-π phase discontinuity is artificially induced by a pair of current injectors connected to one of the electrodes [59]. A new setup was necessary for investigations in the quantum limit, since the SIFS junctions show an unaccessible low thermal-to-quantum crossover temperature $T^\star$ of only few mK. As shown in the thesis, the insertion of an additional thin superconducting interlayer in the stack, giving rise to SIsFS JJs, was not enough to reach higher $T^\star$ (*i.e.* larger j_c).

In our measurements on the injector JJs, the fingerprint of MQT is evident in the saturation of the width $\sigma_\pm$ of the switching current distribution $P(I_{c\pm})$ for $T < T^* \approx 260\,\mathrm{mK}$. Stronger proofs of quantum tunneling are

given by fitting the experimental escape rate with theoretical predictions. The formula for the thermal escape rate does not match the data below the crossover temperature, while the quantum formula perfectly fits them.

In the future, it is our intention to continue experimenting with these types of SIS junctions to prove energy level quantization in the wells. To this purpose we are going to excite the junction with a microwave signal and then measure the $P(I)$ distribution by varying the power at fixed microwave frequencies. If tunneling from excited levels occurs, two or more peaks appear in $P(I)$.

9 Outlook

A φ JJ is an ideal tool for the investigation of macroscopic quantum effects (MQE), since it naturally has two degenerate ground states, hence it can be pictured as a quantum-mechanical two-level system. In particular, it would be ideal to have a junction in which the energy barrier U_0 separating the local minima at $\pm\varphi$ can be ramped up and down. In this way, one can study not only quantum coherence between the quantized energy level in the single wells, but also between the $\pm\varphi$ states. As mentioned in my manuscript in preparation, this tunability of the Josephson energy can be achieved in JJ equipped with a single injector pair. However, this kind of setup it is not ideal. First, the energy barrier U_0 can be varied only by physically changing the position of the injectors along the junction, therefore the ramping up/down process is not feasible in the same junction. Second, the control over the barrier is very poor, because for very small

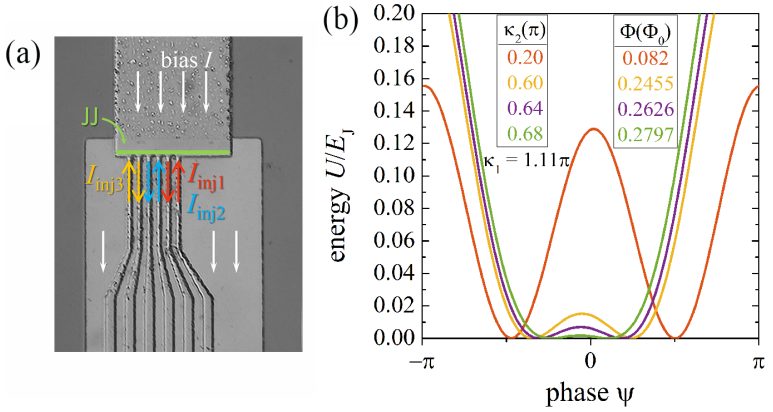

Figure 9.1: (a) Optical image in false colors of a JJ with multi-injectors. The arrows indicate how the bias current I and the injector currents $I_{\rm inj1}, I_{\rm inj2}$ and $I_{\rm inj3}$ flow. The junction area is colored in green. (b) Simulated Josephson energy potential $U(\psi)$ for a JJ with three current injector pairs with normalized length $l = L/\lambda_{\rm J} = 2$ and normalized injector size and spacing $w_{\rm inj} = w_{\rm d} = 0.2$. The first pair, positioned symmetrically along the junction, creates the $\kappa_1 \sim \pi$ phase discontinuity. The additional pairs, with $\kappa_2 = -\kappa_3$, together with the magnetic flux Φ tune electronically the energy profile.

values of U_0, *i.e.* $U_0 < 10^{-5}E_J$, the energy barrier height is extremely sensitive to the amplitude of the applied injector current and to geometrical dimensions.

A more flexible device can be obtained if we introduce additional injector pairs along the junction, as shown in Fig. 9.1(a). Simulations of the dynamics of the JJ using the sine-Gordon equation reveal that a JJ with electronically tunable energy profile is realized with three pairs of injectors. The pair located in the center of the JJ is to be used to produce the $\kappa_1 \sim \pi$ phase discontinuity, while the other two serve to control the Josephson potential. The ramping up/down process is performed by locking the values of the secondary injector current, with $\kappa_2 = -\kappa_3$, with the externally magnetic flux Φ, as shown in Fig. 9.1(b).

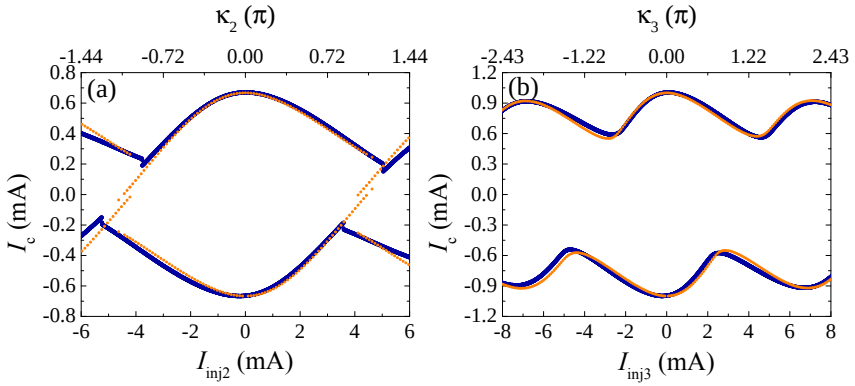

Figure 9.2: Calibration of the secondary injectors (blue curve), fitted by numerical simulations (orange curve), at $T = 4.2\,\mathrm{K}$.

I have already started some basic measurements with such devices as the characterization of the junction and of the injectors. The JJ under investigation has a length $L = 40\,\mu\mathrm{m} = 2.5\lambda_J$ and injectors size and spacing $W_{inj} = W_d = 1.5\,\mu\mathrm{m}$. The modulation of the critical current with the injector pair 1 is similar to the one shown in Fig. 7.4(a), while the modulation with the injectors pair 2 and 3 is displayed in Fig. 9.2. The curves differ from each other, due to the dissimilar position of the injectors along the junction. As these depart from the center of the JJ, the depth of the modulation diminishes and the minimum becomes smoother, following

the predictions of Ref. [59]. The plots show also fits with numerical simulations. The mismatch between the theory and the experiment can be explained considering that the theory describes the injectors and the junction as one-dimensional objects, while in reality we have three-dimensional devices and the currents can flow in a different way. Additionally, in simulations we consider the injectors to have all the same geometrical dimension. This is however an ideal assumption, since technological variations may cause slightly different width and spacing of the injector leads.

In Fig. 9.3, I show the preliminary calibration of the secondary injectors with the magnetic field H, that is applied through a coil with $I_{\mathrm{coil}} = H/\eta$ and $\eta = 5\,\mu\mathrm{T/mA}$. Here, $I_{\mathrm{inj1}} = 3.67\,\mathrm{mA}$, that creates the $\kappa_1 \sim \pi$ discontinuity. The $I_{\mathrm{c}}(I_{\mathrm{coil}})$ dependence is measured for different values of $\kappa_2 = -\kappa_3$. In this way, I can understand which values of the coil current (*i.e.* the magnetic field) $I_{\mathrm{coil}}^{\mathrm{sym}}$ I have to apply to get a symmetric potential for a given $\kappa_2(\kappa_3)$. This corresponds to the middle point between the central minima of the $\pm I_{\mathrm{c}}(I_{\mathrm{coil}})$ curves, where the critical currents are symmetric, *i.e.* $+I_{\mathrm{c}\pm} = |-I_{\mathrm{c}\pm}|$. As one can observe in Fig. 9.3(b), the dependence $I_{\mathrm{coil}}^{\mathrm{sym}}(\kappa_2)$ is almost linear at the beginning, then it turns

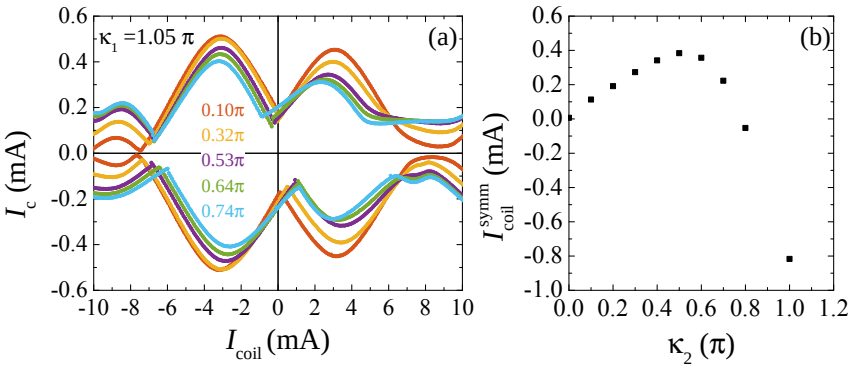

Figure 9.3: (a) Calibration of the secondary injectors $\kappa_{2,3}$ with the magnetic field H, that is applied by means of a coil with $I_{\mathrm{coil}} = H/\eta$ and $\eta = 5\,\mu\mathrm{T/mA}$. By varying $\kappa_{2,3}$, the value of coil current at which the Josephson potential is symmetric changes. This value, labeled $I_{\mathrm{coil}}^{\mathrm{sym}}$, lies in the middle between the two minima near $I_{\mathrm{coil}} = 0$. For each $\kappa_{2,3}$, I recorded the corresponding $I_{\mathrm{coil}}^{\mathrm{sym}}$ and plotted it *vs* $\kappa_{2,3}$ (b).

down at $\kappa_2 \approx 0.5\pi$ where the energy barrier U_0 disappears. I expect the dependence to be 2π-periodic, thus I suppose that the curve will turn upwards again around $\kappa_2 \sim \pi$ and reach approximatively $I_{\mathrm{coil}}^{\mathrm{sym}}(\kappa_2 = 0)$ at $\kappa_2 = 2\pi$. Further measurements are needed to confirm this assumption.

In the future, these results will be used to perform energy level and time resolved spectroscopy, and to probe the coherence of the Josephson phase in the double well potential of the φ JJ.

Bibliography

[1] B. D. Josephson. Possible new effects in superconductive tunneling. *Phys. Lett.*, 1:251, 1962.

[2] A. A. Golubov, M. Y. Kupriyanov, and E. Il'ichev. The current-phase relation in Josephson junctions. *Rev. Mod. Phys.*, 76:411, 2004.

[3] A. Bauer, J. Bentner, M. Aprili, M. L. Della Rocca, M. Reinwald, W. Wegscheider, and C. Strunk. Spontaneous supercurrent induced by ferromagnetic π junctions. *Phys. Rev. Lett.*, 92:217001, 2004.

[4] H. J. H. Smilde, Ariando, D. H. A. Blank, H. Hilgenkamp, and H. Rogalla. π-SQUIDs based on Josephson contacts between high-T_c and low-T_c superconductors. *Phys. Rev. B*, 70:024519, 2004.

[5] L. N. Bulaevskiĭ, V. V. Kuziĭ, and A. A. Sobyanin. Superconducting system with weak coupling to the current in the ground state. *JEPT Lett.*, 25:290, 1977.

[6] O. Vávra, S. Gaži, D. S. Golubović, I. Vávra, J. Dérer, J. Verbeeck, G. Van Tendeloo, and V. V. Moshchalkov. 0 and π phase Josephson coupling through an insulating barrier with magnetic impurities. *Phys. Rev. B*, 74:020502, 2006.

[7] V. V. Ryazanov, V. A. Oboznov, A. Yu. Rusanov, A. V. Veretennikov, A. A. Golubov, and J. Aarts. Coupling of two superconductors through a ferromagnet: Evidence for a π junction. *Phys. Rev. Lett.*, 86:2427, 2001.

[8] T. Kontos, M. Aprili, J. Lesueur, F. Genêt, B. Stephanidis, and R. Boursier. Josephson junction through a thin ferromagnetic layer: Negative coupling. *Phys. Rev. Lett.*, 89:137007, 2002.

[9] J. W. A. Robinson, S. Piano, G. Burnell, C. Bell, and M. G. Blamire. Critical current oscillations in strong ferromagnetic π junctions. *Phys. Rev. Lett.*, 97:177003, 2006.

[10] M. Weides, M. Kemmler, E. Goldobin, D. Koelle, R. Kleiner, H. Kohlstedt, and A. Buzdin. High quality ferromagnetic 0 and π Josephson tunnel junctions. *Appl. Phys. Lett.*, 89:122511, 2006.

[11] N. Ruppelt, H. Sickinger, R. Menditto, E. Goldobin, D. Koelle, R. Kleiner, O. Vavra, and H. Kohlstedt. Observation of 0-π transition in SIsFS Josephson junctions. *Appl. Phys. Lett.*, 106:022602, 2015.

[12] E. C. Gingrich, B. M. Niedzielski, J. A. Glick, Y. Wang, D. L. Miller, R. Loloee, W. P. Pratt Jr, and N. O. Birge. Controllable 0-π Josephson junctions containing a ferromagnetic spin valve. *Nature Physics*, 12:564, 2016.

[13] D. A. Wollman, D. J. Van Harlingen, J. Giapintzakis, and D. M. Ginsberg. Evidence for $d_{x^2-y^2}$ pairing from the magnetic field modulation of $YBa_2Cu_3O_7$/Nb Josephson junctions. *Phys. Rev. Lett.*, 74:797, 1995.

[14] D. A. Brawner and H. R. Ott. Evidence for a non-s-wave superconducting order parameter in $YBa_2Cu_3O_6.6$ with $T_c = 60$ K. *Phys. Rev. B*, 53:8249, 1996.

[15] H. J. H. Smilde, Ariando, D. H. A. Blank, G. J. Gerritgma, H. Hilgenkamp, and Rogalla. H. d-wave-induced Josephson current counterflow in $YBa_2Cu_3O_7$/Nb zigzag junctions. *Phys. Rev. Lett.*, 88:057004, 2002.

[16] C. C. Tsuei, J. R. Kirtley, C. C. Chi, Lock See Yu-Jahnes, A. Gupta, T. Shaw, J. Z. Sun, and M. B. Ketchen. Pairing symmetry and flux quantization in a tricrystal superconducting ring of $YBa_2Cu_3O_{7-\delta}$. *Phys. Rev. Lett.*, 73:593, 1994.

[17] J. R. Kirtley, C. C. Tsuei, J. Z. Sun, C. C. Chi, L. S. Yu-Jahnes, A. Gupta, M. Rupp, and B. Ketchen. Symmetry of the order parameter in the high-T_c superconductor $YBa_2Cu_3O_{7-\delta}$. *Nature*, 373: 225, 1995.

[18] Yu. S. Barash, H. Burkhardt, and D. Rainer. Low-temperature anomaly in the Josephson critical current of junctions in d-wave superconductors. *Phys. Rev. Lett.*, 77:4070, 1996.

[19] J. J. A. Baselmans, A. F. Morpurgo, B. J. Van Wees, and T. M. Klapwijk. Reversing the direction of the supercurrent in a controllable Josephson junction. *Nature*, 397:43, 1999.

[20] J. A. van Dam, Y. V. Nazarov, E. P. A. M. Bakkers, S. De Franceschi, and L. P. Kouwenhoven. Supercurrent reversal in quantum dots. *Nature*, 442:667, 2006.

[21] H. I. Jørgensen, T. Novotný, K. Grove-Rasmussen, K. Flensberg, and P. E. Lindelof. Critical current 0-π transition in designed Josephson quantum dot junctions. *Nano Lett.*, 7:2441, 2007.

[22] T. Ortlepp, Ariando, O. Mielke, C. J. M. Verwijs, K. F. K. Foo, H. Rogalla, F. H. Uhlmann, and H. Hilgenkamp. Flip-flopping fractional flux quanta. *Science*, 312:1495, 2006.

[23] A. K. Feofanov, V. A. Oboznov, V. V. Bol'ginov, J. Lisenfeld, S. Poletto, V. V. Ryazanov, A. N. Rossolenko, M. Khabipov, D. Balashov, A. B. Zorin, P. N. Dmitriev, V. P. Koshelets, and A. V. Ustinov. Implementation of superconductor/ferromagnet/superconductor π-shifters in superconducting digital and quantum circuits. *Nature Physics*, 6:593, 2010.

[24] M. I. Khabipov, D. V. Balashov, F. Maibaum, A. B. Zorin, V. V. Oboznov, V. A. Bolginov, A. N. Rossolenko, and V. V. Ryazanov. A single flux quantum circuit with a ferromagnet-based Josephson π-junction. *Supercond. Sci. Technol.*, 23:045032, 2010.

[25] A. Buzdin. Direct coupling between magnetism and superconducting current in the Josephson φ_0 junction. *Phys. Rev. Lett.*, 101:107005, 2008.

[26] M. Alidoust and J. Linder. φ-state and inverted Fraunhofer pattern in nonaligned Josephson junctions. *Phys. Rev. B*, 87(6):060503, 2013.

[27] F. S. Bergeret and I. V. Tokatly. Theory of diffusive φ_0 Josephson junctions in the presence of spin-orbit coupling. *EPL*, 110(5):57005, 2015.

[28] D. B. Szombati, S. Nadj-Perge, D. Car, S. R. Plissard, E. P. A. M. Bakkers, and L. P. Kouwenhoven. Josephson φ_0-junction in nanowire quantum dots. *Nature Physics*, 12:568, 2016.

[29] A. Buzdin and A. E. Koshelev. Periodic alternating 0- and π-junction structures as realization of φ-Josephson junctions. *Phys. Rev. B*, 67: 220504, 2003.

[30] E. Goldobin, D. Koelle, R. Kleiner, and A. Buzdin. Josephson junctions with second harmonic in the current-phase relation: Properties of φ junctions. *Phys. Rev. B*, 76:224523, 2007.

[31] E. Goldobin, H. Sickinger, M. Weides, N. Ruppelt, H. Kohlstedt, R. Kleiner, and D. Koelle. Memory cell based on a φ Josephson junction. *Appl. Phys. Lett.*, 102:242602, 2013.

[32] E. Goldobin, D. Koelle, R. Kleiner, and R. G. Mints. Josephson junction with a magnetic-field tunable ground state. *Phys. Rev. Lett.*, 107:227001, 2011.

[33] A. Lipman, R. G. Mints, R. Kleiner, D. Koelle, and E. Goldobin. Josephson junctions with tunable current-phase relation. *Phys. Rev. B*, 90:184502, 2014.

[34] H. Sickinger, A. Lipman, M. Weides, R. G. Mints, H. Kohlstedt, D. Koelle, R. Kleiner, and E. Goldobin. Experimental evidence of a φ Josephson junction. *Phys. Rev. Lett.*, 109:107002, 2012.

[35] E. Goldobin, D. Koelle, R. Kleiner, and R. G. Mints. Phase retrapping in a pointlike φ Josephson junction: The butterfly effect. *Phys. Rev. Lett.*, 111:057004, 2013.

[36] V. V. Ryazanov, V. V. Bol'ginov, D. S. Sobanin, I. V. Vernik, S. K. Tolpygo, A. M. Kadin, and O. A. Mukhanov. Magnetic Josephson junction technology for digital and memory applications. *Physics Procedia*, 36:35, 2012.

[37] T. I. Larkin, V. V. Bol'ginov, V. S. Stolyarov, V. V. Ryazanov, I. V. Vernik, S. K. Tolpygo, and O. A. Mukhanov. Ferromagnetic Josephson switching device with high characteristic voltage. *Appl. Phys. Lett.*, 100:222601, 2012.

[38] I. V. Vernik, V. V. Bol'ginov, S. V. Bakurskiy, A. A. Golubov, M. Y. Kupriyanov, Ryazanov, and O. A. Mukhanov. Magnetic Josephson junctions with superconducting interlayer for cryogenic memory. *IEEE Transactions on Applied Superconductivity*, 23:1701208, 2013.

[39] S. V. Bakurskiy, N. V. Klenov, I. I. Soloviev, V. V. Bol'ginov, V. V. Ryazanov, I. V. Vernik, O. A. Mukhanov, M. Yu. Kupriyanov, and

A. A. Golubov. Theoretical model of superconducting spintronic SIsFS devices. *Appl. Phys. Lett.*, 102:192603, 2013.

[40] S. V. Bakurskiy, N. V. Klenov, I. I. Soloviev, M. Yu. Kupriyanov, and A. A. Golubov. Theory of supercurrent transport in SIsFS Josephson junctions. *Phys. Rev. B*, 88:144519, 2013.

[41] E. Goldobin, A. Sterck, T. Gaber, D. Koelle, and R. Kleiner. Dynamics of semifluxons in Nb long Josephson 0-π junctions. *Phys. Rev. Lett.*, 92:057005, 2004.

[42] T. Gaber, E. Goldobin, A. Sterck, R. Kleiner, D. Koelle, M. Siegel, and M. Neuhaus. Non-ideal artificial phase discontinuity and fractional vortex dynamics in long Josephson 0-κ junctions. *Phys. Rev. B*, 72:054527, 2005.

[43] H. Kamerlingh-Onnes. The superconductivity of mercury. *Comm. Phys. Lab. Univ. Leiden*, 122:124, 1911.

[44] W. Meissner and R. Ochsenfeld. Ein neuer Effekt bei Eintritt der Supraleitfähigkeit. *Naturwissenschaften*, 21:787, 1933.

[45] J. Bardeen, L. N. Cooper, and J. R. Schrieffer. Theory of superconductivity. *Phys. Rev.*, 108:1175, 1957.

[46] V. L. Ginzburg and L. D. Landau. On the theory of superconductivity. *Zh. Eksp. Teor. Fiz.*, 20:1064, 1950.

[47] W. C. Stewart. Current-voltage characteristics of Josephson junctions. *Appl. Phys. Lett.*, 12:277, 1968.

[48] D. E. McCumber. Effect of ac impedance on dc voltage-current characteristics of superconductor weak-link junctions. *J. Appl. Phys.*, 39: 3113, 1968.

[49] T. A. Fulton and L. N. Dunkleberger. Lifetime of the zero-voltage state in Josephson tunnel junctions. *Phys. Rev. B*, 9:4760, 1974.

[50] H. A. Kramers. Brownian motion in a field of force and the diffusion model of chemical reactions. *Physica (Utrecht)*, 79:284, 1940.

[51] M. Büttiker, E. P. Harris, and R. Landauer. Thermal activation in extremely underdamped Josephson-junction circuits. *Phys. Rev. B*, 28:1268, 1983.

[52] B. Ruggiero, C. Granata, V. G. Palmieri, A. Esposito, M. Russo, and P. Silvestri. Supercurrent decay in extremely underdamped Josephson junctions. *Phys. Rev. B*, 57:134, 1998.

[53] D. Vion, A. A. Götz, P. Joyez, D. Esteve, and M. Devoret. Thermal activation above a dissipation barrier: Switching of a small Josephson junction. *Phys. Rev. Lett.*, 77:3435, 1996.

[54] A. O. Caldeira and A. J. Leggett. Quantum tunneling in a dissipative system. *Ann. Phys.*, 149:374, 1983.

[55] L. D. Jackel, J. P. Gordon, E. L. Hu, R. E. Howard, L. A. Fetter, D. M. Tennant, R. W. Epworth, and J. Kurkijärvi. Decay of the zero-voltage state in small-area, high-current-density Josephson junctions. *Phys. Rev. Lett.*, 47:697, 1981.

[56] A. Gumann and N. Schopohl. Phase diagram of geometric d-wave superconductor Josephson junctions. *Phys. Rev. B*, 79:144505, 2009.

[57] Y. Tanaka and S. Kashiwaya. Theory of Josephson effects in d-wave superconductors. *Phys. Rev. B*, 53:R11957, 1996.

[58] Y. Tanaka and S. Kashiwaya. Theory of Josephson effects in anisotropic superconductors. *Phys. Rev. B*, 56:892, 1997.

[59] E. Goldobin, S. Mironov, A. Buzdin, R. G. Mints, D. Koelle, and R. Kleiner. Effective model for a short Josephson junction with a phase discontinuity. *Phys. Rev. B*, 93:134514, 2016.

[60] E. Goldobin, D. Koelle, and R. Kleiner. Tunable $\pm\varphi$, φ_0 and $\varphi_0 \pm \varphi$ Josephson junction. *Phys. Rev. B*, 91:214511, 2015.

[61] R. G. Mints. Self-generated flux in Josephson junctions with alternating critical current density. *Phys. Rev. B*, 57:R3221, 1998.

[62] R. Menditto, H. Sickinger, M. Weides, H. Kohlstedt, M. Žonda, T. Novotný, D. Koelle, R. Kleiner, and E. Goldobin. Phase retrapping in a φ Josephson junction: Onset of the butterfly effect. *Phys. Rev. B*, 93:174506, 2016.

[63] R. G. Mints and I. Papiashvili. Josephson vortices with fractional flux quanta at $YBa_2Cu_3O_{7-x}$ grain boundaries. *Phys. Rev. B*, 64: 134501, 2001.

[64] R. G. Mints, I. Papiashvili, J. R. Kirtley, H. Hilgenkamp, G. Hammerl, and J. Mannhart. Observation of splintered Josephson vortices at grain boundaries in $YBa_2Cu_3O_{7-\delta}$. *Phys. Rev. Lett.*, 89:067004, 2002.

[65] R. Menditto, H. Sickinger, M. Weides, H. Kohlstedt, D. Koelle, R. Kleiner, and E. Goldobin. Tunable φ Josephson junction ratchet. *Phys. Rev. E*, 94:042202, 2016.

[66] E. Il'ichev, M. Grajcar, R. Hlubina, R. P. J. IJsselsteijn, H. E. Hoenig, H.-G. Meyer, A. Golubov, M. H. S. Amin, A. M. Zagoskin, A. N. Omelyanchouk, and M. Yu. Kupriyanov. Degenerate ground state in a mesoscopic $YBa_2Cu_3O_{7-x}$ grain boundary Josephson junction. *Phys. Rev. Lett.*, 86:5369, 2001.

[67] G. Testa, E. Sarnelli, A. Monaco, E. Esposito, M. Ejrnaes, D.-J. Kang, S. H. Mennema, E. J. Tarte, and M. G. Blamire. Evidence of midgap-state-mediated transport in 45° symmetric [001] tilt $YBa_2Cu_3O_{7-x}$ bicrystal grain-boundary junctions. *Phys. Rev. B*, 71:134520, 2005.

[68] A. E. Koshelev. Phase diagram of Josephson junction between s and $s_{\pm}$ superconductors in the dirty limit. *Supercond. Sci. Technol.*, 26: 015005, 2013.

[69] I. I. Mazin, D. J. Singh, M. D. Johannes, and M. H. Du. Unconventional superconductivity with a sign reversal in the order parameter of $LaFeAsO_{1-x}F_x$. *Phys. Rev. Lett.*, 101:057003, 2008.

[70] K. Kuroki, S. Onari, R. Arita, H. Usui, Y. Tanaka, H.i Kontani, and H. Aoki. Unconventional pairing originating from the disconnected Fermi surfaces of superconducting $LaFeAsO_{1-x}F_x$. *Phys. Rev. Lett.*, 101:087004, 2008.

[71] K. Seo, B. A. Bernevig, and J. Hu. Pairing symmetry in a two-orbital exchange coupling model of oxypnictides. *Phys. Rev. Lett.*, 101:206404, 2008.

[72] S. Graser, T. A. Maier, P. J. Hirschfeld, and D. J. Scalapino. Near-degeneracy of several pairing channels in multiorbital models for the Fe pnictides. *New J. Phys.*, 11:025016, 2009.

[73] V. Cvetkovic and Z. Tesanovic. Multiband magnetism and superconductivity in Fe-based compounds. *Europhys. Lett.*, 85:37002, 2009.

[74] D. M. Heim, N. G. Pugach, M. Yu Kupriyanov, E. Goldobin, D. Koelle, and R. Kleiner. Ferromagnetic planar Josephson junction with transparent interfaces: a φ junction proposal. *J. Phys.: Condens. Matter*, 25:215701, 2013.

[75] P. Reimann. Brownian motors: Noisy transport far from equilibrium. *Phys. Rep.*, 361:57, 2002.

[76] H. Linke. Ratches and Brownian motors: Basics, experiments and applications. *Appl. Phys. A*, 75:167, 2002.

[77] P. Hänggi, F. Marchesoni, and F. Nori. Brownian motors. *Ann. Phys.*, 14:51, 2005.

[78] P. Hänggi and F. Marchesoni. Artificial Brownian motors: Controlling transport on the nanoscale. *Rev. Mod. Phys.*, 81:387, 2009.

[79] A. Sterck, S. Weiss, and D. Koelle. SQUID ratchets: basics and experiments. *Appl. Phys. A*, 75:25, 2002.

[80] A. Sterck, R. Kleiner, and D. Koelle. Three-junction SQUID rocking ratchet. *Phys. Rev. Lett.*, 95:177006, 2005.

[81] A. Sterck, D. Koelle, and R. Kleiner. Rectification in a stochastically driven three-junction SQUID rocking ratchet. *Phys. Rev. Lett.*, 103: 047001, 2009.

[82] J. Spiechowicz, P. Hänggi, and J. Łuczka. Josephson junction ratchet: The impact of finite capacitances. *Phys. Rev. B*, 90:054520, 2014.

[83] E. Trías, J. J. Mazo, F. Falo, and T. P. Orlando. Depinning of kinks in a Josephson-junction ratchet array. *Phys. Rev. E*, 61:2257, 2000.

[84] G. Carapella and G. Costabile. Ratchet effect: Demonstration of a relativistic fluxon diode. *Phys. Rev. Lett.*, 87:077002, 2001.

[85] M. Beck, E. Goldobin, M. Neuhaus, M. Siegel, R. Kleiner, and D. Koelle. High-efficiency deterministic Josephson vortex ratchet. *Phys. Rev. Lett.*, 95:090603, 2005.

[86] M. Knufinke, K. Ilin, M. Siegel, D. Koelle, R. Kleiner, and E. Goldobin. Deterministic Josephson vortex ratchet with a load. *Phys. Rev. E*, 85:011122, 2012.

[87] A. I. Buzdin, L. N. Bulaevskii, and S. V. Panyukov. Current oscillations as a function of the exchange field and thickness of the ferromagnetic metal (f) in an S-F-S Josephson junction. *JEPT Lett.*, 36: 235, 1982.

[88] V. A. Oboznov, V. V. Bol'ginov, A. K. Feofanov, V. V. Ryazanov, and A. I. Buzdin. Thickness dependence of the Josephson ground states of superconductor-ferromagnet-superconductor junctions. *Phys. Rev. Lett.*, 96:197003, 2006.

[89] A. S. Vasenko, S. Kawabata, A. A. Golubov, M. Yu. Kupriyanov, C. Lacroix, F. S. Bergeret, and F. W. J. Hekking. Current-voltage characteristics of tunnel Josephson junctions with a ferromagnetic interlayer. *Phys. Rev. B*, 84:024524, 2011.

[90] M. Weides, M. Kemmler, H. Kohlstedt E. Goldobin, R. Waser, D. Koelle, and R. Kleiner. 0-π Josephson tunnel junctions with ferromagnetic barrier. *Phys. Rev. Lett.*, 97:247001, 2006.

[91] M. Weides, H. Kohlstedt, R. Waser, M. Kemmler, J. Pfeiffer, D. Koelle, R. Kleiner, and E. Goldobin. Ferromagnetic 0-π Josephson junctions. *Appl. Phys. A*, 89:613, 2007.

[92] D. M. Heim, N. G. Pugach, M. Yu. Kupriyanov, E. Goldobin, D. Koelle, and R. Kleiner. The effect of normal and insulating layers on 0-π transitions in Josephson junctions with a ferromagnetic barrier. *New J. Phys.*, 17:113022, 2015.

[93] N. G. Pugach, E. Goldobin, R. Kleiner, and D. Koelle. Method for reliable realization of a φ Josephson junction. *Phys. Rev. B*, 81: 104513, 2010.

[94] T. Bauch, F. Lombardi, F. Tafuri, A. Barone, G. Rotoli, P. Delsing, and T. Claeson. Macroscopic quantum tunneling in d-wave $YBa_2Cu_3O_{7-\delta}$ Josephson junctions. *Phys. Rev. Lett.*, 94:087003, 2005.

[95] A. V. Ustinov. Fluxon insertion into annular Josephson junctions. *Appl. Phys. Lett.*, 80(17):3153, 2002.

[96] B. A. Malomed and A. V. Ustinov. Creation of classical and quantum fluxons by a current dipole in a long Josephson junction. *Phys. Rev. B*, 69:064502, 2004.

[97] K. Buckenmaier, T. Gaber, M. Siegel, D. Koelle, R. Kleiner, and E. Goldobin. Spectroscopy of the fractional vortex eigenfrequency in a long Josephson 0-κ junction. *Phys. Rev. Lett.*, 98:117006, 2007.

[98] A. Dewes, T. Gaber, D. Koelle, R. Kleiner, and E. Goldobin. Semifluxon molecule under control. *Phys. Rev. Lett.*, 101:247001, 2008.

[99] J. M. Meckbach, M. Merker, S. J. Buehler, K. Ilin, B. Neumeier, U. Kienzle, E. Goldobin, R. Kleiner, D. Koelle, and M. Siegel. Sub-μm Josephson junctions for superconducting quantum devices. *IEEE Trans. Appl. Supercond.*, 23:1100504, 2013.

[100] A. Murphy, P. Weinberg, T. Aref, C. Coskun, V. Vakaryuk, A. Levchenko, and A. Bezryadin. Universal features of counting statistics of thermal and quantum phase slips in nanosize superconducting circuits. *Phys. Rev. Lett.*, 110:247001, 2013.

[101] A. Garg. Escape-field distribution for escape from a metastable potential well subject to a steadily increasing bias field. *Phys. Rev. B*, 51:15592, 1995.

10 Appended publications

Publication 1

Phase retrapping in a φ Josephson junction: Onset of the butterfly effect

R. Menditto,[1] H. Sickinger,[2] M. Weides,[3,*] H. Kohlstedt,[4] M. Žonda,[5] T. Novotný,[5] D. Koelle,[2] R. Kleiner,[2] and E. Goldobin[2]

[1]*Physikalisches Institut and Center for Quantum Science in* LISA$^+$*, Universität Tübingen, Auf der Morgenstelle 14, D-72076 Tübingen, Germany*

[2]*Physikalisches Institut and Center for Collective Quantum Phenomena in* LISA$^+$*, Universität Tübingen, Auf der Morgenstelle 14, D-72076 Tübingen, Germany*

[3]*Peter Grünberg Institute and JARA-Fundamentals of Future Information Technology, Forschungszentrum Jülich GmbH, 52425 Jülich, Germany*

[4]*Nanoelektronik, Technische Fakultät, Christian-Albrechts-Universität zu Kiel, D-24143 Kiel, Germany*

[5]*Department of Condensed Matter Physics, Faculty of Mathematics and Physics, Charles University in Prague, Ke Karlovu 5, 121 16 Praha 2, Czech Republic*

(Received 22 June 2015; revised manuscript received 26 December 2015; published 12 May 2016)

We investigate experimentally the retrapping of the phase in a φ Josephson junction upon return of the junction to the zero-voltage state. Since the Josephson energy profile $U_0(\psi)$ in φ JJ is a 2π periodic double-well potential with minima at $\psi = \pm\varphi \bmod 2\pi$, the question is at which of the two minima $-\varphi$ or $+\varphi$ the phase will be trapped upon return from a finite voltage state during quasistatic decrease of the bias current (tilt of the potential). By measuring the relative population of two peaks in escape histograms, we determine the probability of phase trapping in the $\pm\varphi$ wells for different temperatures. Our experimental results agree qualitatively with theoretical predictions. In particular, we observe an onset of the butterfly effect with an oscillating probability of trapping. Unexpectedly, this probability saturates at a value different from 50% at low temperatures.

DOI: 10.1103/PhysRevB.93.174506

I. INTRODUCTION

The *butterfly effect* occurs in deterministic nonlinear systems, and, in essence, it refers to the extreme sensitivity of the final state of the system to initial conditions [1,2]. The effect puts a clear distinction between determinism and predictability. A canonical example [3] is the weather, which cannot be predicted reliably for more than 3–5 days in advance, although computing power allows us to make simulations much farther ahead. Deterministic chaotic systems must exhibit the butterfly effect. However, deterministic continuous systems (also known as flows in nonlinear physics) with dimensionality less than 3 cannot exhibit chaos [2], but they can exhibit the butterfly effect. Below we investigate experimentally one such system based on a Josephson φ junction.

Josephson φ junctions (φ JJs) have attracted a lot of interest in the past few years, both theoretically [4–14] and experimentally [15–19], due to the peculiar physics and their properties. In general, a JJ can be thought of as a system in which a particle with coordinate ψ (Josephson phase) moves along a one-dimensional (1D) potential $U_0(\psi)$. In the φ JJ, the potential $U_0(\psi)$ has the form of a 2π periodic double-well profile with degenerate minima at $\psi = \pm\varphi + 2\pi n$, where $0 < \varphi < \pi$ depends on the parameters and n is an integer.

In the ground state (no current applied), the phase is trapped in one of two wells of $U_0(\psi)$. Upon application of the bias current I, the potential will be tilted as $U(\psi) = U_0(\psi) - \psi I \Phi_0/(2\pi)$, where $\Phi_0 \approx 2.067$ fWb is the magnetic flux quantum. At some critical value of the bias current (tilt), the phase escapes from the corresponding well and starts sliding down the potential. Therefore, in an experiment one can observe two critical currents I_{c-} and I_{c+}, each corresponding to the escape of the phase from different wells [9,18]. In general, $I_{c+} \neq I_{c-}$. Thus, the measurement of the critical current (I_{c-} or I_{c+}) can be used as a simple way to read out an unknown state ($-\varphi$ or $+\varphi$) of the φ JJ [18,19].

It is also interesting to understand in which of the two wells the phase is retrapped when the bias current (tilt) is decreased. In a previous experiment [18], we noticed that the retrapping process depends strongly on temperature: for $T \gtrsim 2.4$ K, the destination well (state) is always $+\varphi$ (if the JJ returns to a zero-voltage state from positive currents and voltages), while for low temperatures, $T \sim 300$ mK, the destination well is random. Theoretical analysis [13] of a simplified deterministic model shows that the destination well is indeed $+\varphi$ at large damping α. However, it changes between $+\varphi$ and $-\varphi$ back and forth as α decreases. Actually, the intervals of α corresponding to the trapping in a particular well get shorter and shorter as $\alpha \to 0$. This, in fact, results in a butterfly effect in the limit $\alpha \to 0$, i.e., any tiny change (fluctuation) of the bias current or the damping will change the destination well. In the presence of noise (electronic or thermal), we expect [13] that the probability $P(\alpha)$ to be trapped in a particular well should exhibit smeared oscillations and should saturate at 0.5 for $\alpha \to 0$.

In this work, we present measurements of the probabilities of phase retrapping in the $\pm\varphi$ wells as a function of temperature, and we compare them with theoretical predictions. We note that the model [13] represents a simplified version of the real system, resulting from several approximations: (a) an effective (spatially averaged) model was used, which works well only for very short JJs and reduces an infinite-dimensional system to a 2D one (without chaos); (b) only "slow" (in comparison with the retrapping time) noise was treated [13]; (c) a linear damping was assumed [13]. Therefore,

*Present address: Physikalisches Institut, Karlsruher Institut für Technologie, 76131 Karlsruhe, Germany.

it is necessary to check the predictions of the model [13] experimentally.

Our results demonstrate a crossover from the deterministic behavior of the probability to be trapped in the $-\varphi$ well $P_-(T) = 0$ at high temperature $T > T^*$ to an oscillating probability $P_-(T)$ at the onset of the butterfly effect at $T < T^*$. However, at even lower temperatures $P_-(T)$ saturates at about 0.33 instead of 0.5 predicted theoretically. Possible reasons for this are discussed.

II. EXPERIMENTAL RESULTS

For our investigations, we have used a superconductor-insulator-ferromagnet-superconductor (SIFS) JJ with a stepwise thickness of the F layer (see Fig. 1), i.e., a JJ with one half behaving like a conventional 0 JJ and the other half behaving like a π JJ (also called 0-π JJ). This JJ is short in the x direction (the length L is smaller than or of the order of the Josephson length λ_J) and much smaller in the y direction ($w \ll L$). Treating this JJ as a pointlike device with the properties averaged along its length L, we obtain a φ JJ with an effective (averaged) Josephson energy profile $U_0(\psi)$ looking like a 2π periodic double well. Here ψ is the average phase across the device. The sample described here was used in our previous works before [18,19].

The current-voltage characteristic (IVC) at $H = 0$ and the critical current dependence on the applied magnetic field $I_c(H)$ at $T = 0.30$ K are shown in Figs. 2(a) and 2(b). Here one can observe the presence of the two critical currents I_{c-} and I_{c+} in each direction of the bias.[1]

In our experiment, we measured the probability to trap the phase in one of the two wells for different values of the temperature in the range $0.27 < T < 2.30$ K. Note that the damping α is a function of the temperature T in our tunnel-like φ JJ. So we change T to change α. We sweep the bias current $N = 10^4$ times with a constant rate $\dot{I} = 0.1194$ A/s at $H = 0$ and obtain a histogram such as the one shown in Fig. 2(c). In general, it consists of two peaks: one situated just below the fluctuation-free I_{c-} and another one below I_{c+}. The probability $P_\pm = N_\pm/N$ that the phase was trapped and then escapes from the $\pm\varphi$ well is proportional to the number of events $N_\pm$ in the corresponding peak in the histogram.

We performed the escape measurements using two different sweep sequences; refer to Fig. 2(a).

[1] Another main feature of the φ JJ is visible in the $I_c(H)$ curve [Fig. 2(b)], which has cusplike minima that are point symmetrically shifted from $H = 0$.

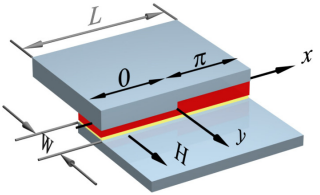

FIG. 1. Sketch of the sample under investigation—a (from bottom to top) Nb|AlO|CuNi|Nb JJ of length $L = 200\ \mu\text{m} \sim \lambda_J$ and width $w = 10\ \mu\text{m} \ll L$. The critical temperature of the device $T_c \sim 9$ K. The magnetic field H is applied along the y direction.

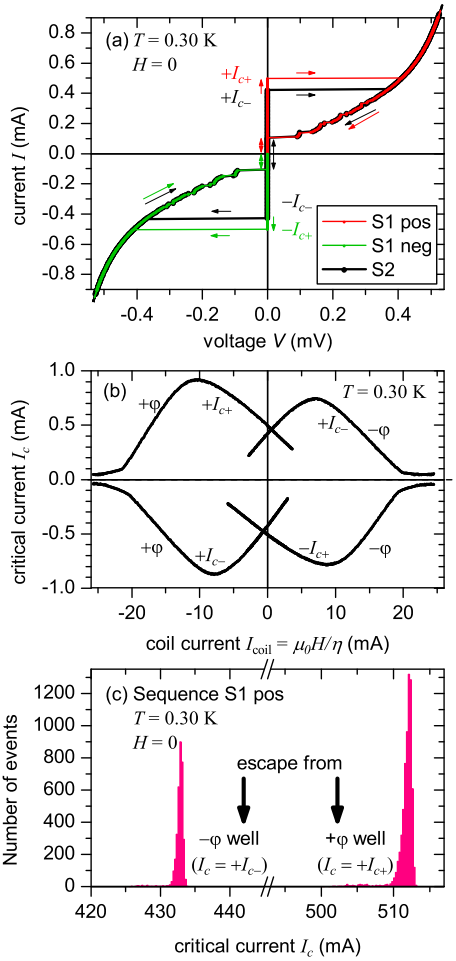

FIG. 2. Current-voltage characteristic (a), critical current dependence on the magnetic field (b), and escape histogram (c) at $T = 0.30$ K. In (a), different colors correspond to different sweep sequences of the bias current I. In (b), the magnetic field is applied in-plane of the junction by means of a coil with $\mu_0 H = \eta I_{\text{coil}}$ with the coil factor $\eta \sim 5\ \mu$ T/mA. The histogram in (c), measured by using sequence S1 pos, shows two peaks corresponding to the two critical currents $I_{c\pm}$.

S1. In the sequence "S1 pos(neg)" we sweep the current I from zero (zero voltage) to a maximum positive (negative) value with $V > 0$ ($V < 0$) at the McCumber branch. During this forward sweep, we read out the value of the critical current and add this to the statistics to produce a histogram later on. Then we sweep back to $I = 0$. During this sweep, the phase is retrapped in one of the wells, $-\varphi$ or $+\varphi$, when the voltage jumps back to $V = 0$. The value of the phase ($-\varphi$ or $+\varphi$) will be read out during the next cycle.

S2. In the sequence "S2 pos(neg)" the sweep starts from the negative (positive) voltage state at the McCumber branch. Then the current I is swept to a positive (negative) value up to the resistive branch. During this sweep, the phase is retrapped when the current approaches $I = 0$, but it is still negative (positive), and then the critical current is read out (and added to statistics) when the voltage jumps from $V = 0$ to $V > 0$ ($V < 0$). Finally, we sweep I back to the initial value.

Note that the probabilities $P_{\pm}$ to be trapped in the $\pm\varphi$ wells (populations of histogram peaks) obtained using S1 and S2 are expected to be inverse, provided the potential $U_0(\psi)$ is symmetric, i.e., $P_{\pm}^{S1} = P_{\mp}^{S2}$, because the trapping during S1 and S2 takes place at opposite values of the bias current (tilt). Also, the results of "pos" and "neg" sequences are opposite. Obviously, for any sequence, $P_- + P_+ = 1$. Therefore, below, we discuss only $P_-(T)$ for "S1 pos," and the other $P(T)$ that are supposed to be the same (P_+^{S1neg}, P_+^{S2pos}, and P_-^{S2neg}) may be plotted in addition (see Fig. 3 below).

We have already seen [18] that for high damping, the retrapping process is deterministic and we can predict the destination well of the Josephson phase. Namely, at $T > 2.3$ K the phase is always trapped in the $+\varphi$ well, i.e., $P_- = 0$. However, as the damping decreases, the destination well cannot be predicted and it depends on α and noise (thermal or electronic) [13]. In our experiment, the damping should depend on temperature quite strongly as in any tunnel junction. Therefore, we study $P_-(T)$ instead of the $P_-(\alpha)$ in experiment.

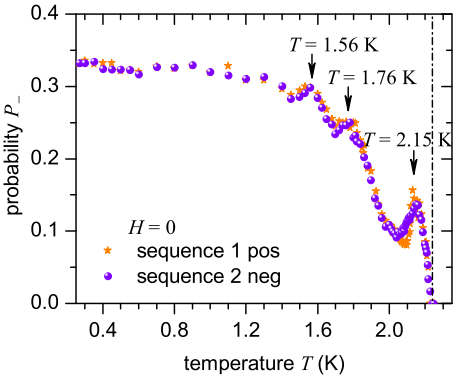

FIG. 3. Retrapping probability P_- of the phase in the $-\varphi$ of the Josephson potential $U(\psi)$ for different temperatures T at zero applied magnetic field H. The two sets of data correspond to two different sweep sequences of the bias current I.

Also, the noise is most probably dominated by electronic noise in the setup rather than by the thermal fluctuations in the JJ itself. Thus, it does not depend strongly on T.

In Fig. 3, we present the experimentally determined probability $P_-(T)$. The vertical line in the figure indicates the temperature $T^* \approx 2.25$ K, where the boundary between deterministic and nondeterministic retrapping is situated. For $T < T^*$, we observe an increase and several oscillations of the probability $P_-(T)$, qualitatively similar to the theoretical prediction [13]. Three peaks at $T = 2.15$, 1.76, and $T = 1.56$ K indicate an enhanced probability to be trapped in the "unnatural" $-\varphi$ well. Those peaks are the smeared traces of the regions where the phase is trapped in the $-\varphi$ well in the noiseless case. For $T < 1.3$ K, the $P_-(T)$ saturates similar to the theoretical prediction [13]. However, the asymptotic value of P_- in this region is $\approx$0.33 rather than 0.5 as expected from the theory.

Retrapping measurements with the other possible sweep sequences show similar results ("S2 neg" is shown in Fig. 3, "S1 neg" and "S2 pos" are not shown). The results also do not depend strongly on the ramp rate $\dot{I}$. Very similar results can be obtained by just moving the bias point along IVC with an unknown ramp rate defined by measurement electronics.

III. DISCUSSION

Here we discuss several possible reasons that can lead to the saturation value of $P_-(T)$ different from 0.5.

A. Asymmetric $U_0(\psi)$

First, one of the possible reasons can be an asymmetry of the potential $U_0(\psi)$. The limit $\alpha \to 0$ implies that the retrapping current $I_R \to 0$. Therefore, in this limit, the potential is untilted and, in the case of a symmetric potential, one expects equal probabilities of trapping for both wells. If, however, the potential is asymmetric, $P_-(\alpha \to 0) \neq 0.5$.

Of course, the potential $U_0(\psi)$ in our φ JJ can be somewhat asymmetric, in particular because of nonuniformities along the JJ or because of a remnant magnetic field. However, an asymmetric potential will result in asymmetric critical currents $\pm I_{c+}$ and $\pm I_{c-}$. In our experiment, we can affect the asymmetry of the potential by applying an external magnetic field H. We have repeated the measurements shown in Fig. 3 applying a small [$|I_{\rm coil}| < 1$ mA; see Fig. 2(b)] magnetic field such that the measurements always take place at symmetric critical currents. We have found that such a technique changes the $P_-(T)$ curve in the vicinity of the peaks, however the saturation value remains almost unchanged.

One can further argue that the symmetry of the critical currents does not guarantee the symmetry of the potential, as the measurements of the critical currents are the measurements of the maximum slopes of the potential rather than the whole potential. However, such a coincidence is very improbable. Nevertheless, we have generalized the deterministic model [13] to the case of an *asymmetric* potential and *weak noise* (quasideterministic limit), i.e., the noise energy is smaller than the depth of each potential well, measured relative to the potential barrier separating the wells. Qualitatively, one can say that at $\alpha \to 0$, the particle experiences several dephasings

during the relaxation process and arrives at the decision point (last pass over the barrier separating the well) with a small, but random energy (velocity). Then one can conjecture that $P_{\pm} \propto Q_{\pm}$—the heat dissipated by the particle starting with zero velocity at the barrier during the "left and back" (along $-\varphi$ well) or "right and back" (along $+\varphi$ well) semiperiods. That is, the more energy that is lost during traveling along a particular well, the larger is the probability to be trapped in this well. In the perturbation theory limit [13] ($\alpha \to 0$),

$$Q_{\pm} = \pm 2\alpha \int_{\psi_0}^{\pm\psi(U_{\rm bar})} \sqrt{2[U_{\rm bar} - U_0(\psi)]}\, d\psi, \qquad (1)$$

where ψ_0 is the phase corresponding to the "small" maximum of the potential $U_0(\psi)$ between the wells, i.e., the barrier, $U_{\rm bar} = U_0(\psi_0)$. The phases $\pm\psi(U_{\rm bar})$ are the phases at the left and right slopes of the double-well potential where $U_0(\psi) = U_{\rm bar}$. The final normalized expression for the probabilities is

$$P_{\pm} = \frac{Q_{\pm}}{Q_+ + Q_-}, \qquad (2)$$

which is independent of α.

To check our conjecture, we have performed direct numerical simulations of a particle falling into a double-well potential subject to a weak noise, which confirms the prediction given by Eq. (2); see the Supplemental Material [20].

Then, we tried different asymmetric potentials, having the same symmetric $\pm I_{c+}$ and $\pm I_{c-}$ critical currents, and we estimated P_- using Eq. (2). It turns out that one can find some asymmetric profiles $U_0(\psi)$ that give $P_- \approx 0.33$; see the supplemental material [20]. However, for such profiles the dependence of $\pm I_{c\pm}(H)$ is not point symmetric as in experiment. Of course, one can further argue that the magnetic field H also has an asymmetric effect on $U_0(\psi)$, rather than just adding an odd function. The reason for this can be the same as the reason for the asymmetry of $U_0(\psi)$ without a magnetic field. This special asymmetry can make $\pm I_{c\pm}(H)$ symmetric, as in experiment. However, again, such a coincidence is highly unlikely. Thus, to explain $P_- \approx 0.33$ with the help of an asymmetric potential, we have to make two improbable assumptions.

Finally, the strongest argument in favor of a symmetric potential is the fact that the dependences $P_-(T)$ obtained using S1 and $P_+(T)$ obtained using S2 almost coincide; see Fig. 3.

B. Saturation of damping $\alpha(T)$

Actually, the simplest and most probable reason for our observation is the saturation of damping $\alpha(T)$ at low temperatures caused, e.g., by leakage currents in the barrier. If the damping $\alpha(T)$ does not decrease further with $T \to 0$, but saturates below $T_{\rm sat}$ at the value $\alpha_{\rm sat}$, then in the $P_-(\alpha)$ plot we are able to go only down to $\alpha_{\rm sat}$, where $P_-(\alpha)$ is not saturated yet but still performs decaying oscillations. So, what we see in the limit $T \to 0$ is then just $P_-(\alpha_{\rm sat})$, which happens to be 0.33 in our system.

To check this, we determine $\alpha(T)$ from IVCs taken at different temperatures. The pitfall here is that our SIFS JJ is not RSJ-like, i.e., the resistance is voltage-dependent and, strictly speaking, α is not defined. However, our task is not to determine the exact value of α, but rather to see whether

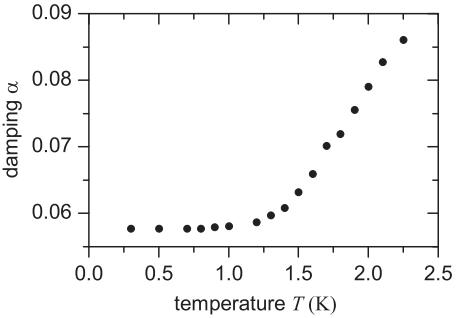

FIG. 4. Plot of $\alpha(T)$ obtained by means of fitting IVCs as described in the text.

it saturates or not, and at which T. For this purpose, we have performed a fitting of the low-voltage part of experimental IVCs by solving the 1D perturbed sine-Gordon equation for a 0-π JJ with constant (x-independent) damping α; see Fig. 1. Before doing these fits, we estimated the other key parameters of our JJ, such as its Josephson length λ_J, and critical current densities j_{c0} and $j_{c\pi}$ of the 0 and the π parts, respectively, by fitting the numerically obtained $I_c(H)$ dependence to the experimentally measured one. The dependence $\alpha(T)$ is then obtained from fitting IVCs at different temperatures and is shown in Fig. 4. One sees that at $T < T_{\rm sat} \approx 1.2$ K, the damping $\alpha(T)$ saturates, presumably due to leakage. Self-heating at $T \sim 1$ K is still a minor effect.

Knowing the $\alpha(T)$ dependence, we have also performed simulations of the retrapping probability for different values of T. Since our 0-π JJ is not extremely short, the model of a pointlike JJ with a biharmonic averaged current-phase relation is valid only qualitatively. Therefore, for simulations we again used a 0-π JJ of finite length to be as close as possible to the experiment. The thermal noise term was taken as $\propto T$. The results show a behavior of $P_-(T)$ qualitatively similar to the experimental one in Fig. 3, i.e., $P_-(T)$ makes a few oscillations and saturates at a value different from 0.5 (e.g., 0.21) as T decreases (not shown). The discrepancy between the experimentally and numerically obtained saturation value of $P_-(T \to 0)$ can be caused by some fine details, such as nonlinearity of the damping in experiment or x-dependent damping in the sample (different damping in 0 and π parts).

Nevertheless, we have checked that in our simulations $P_- \to 0.5$ when the damping becomes much smaller than $\alpha_{\rm sat} = 0.057$—the saturation value in Fig. 4. During this simulation, the noise was kept constant and corresponding to a value $T = 300$ mK (constant noise amplitude independent of α). These results support our claim that the saturation of the damping $\alpha(T)$ leads to $P_-(T \to 0) \neq 0.5$.

Finally, we would like to estimate whether the peak width in the $P_-(T)$ plot in Fig. 3 is in agreement with the noise level. The noise amplitude in our setup $\sqrt{\langle \delta I^2 \rangle} \sim 1$ μA. In normalized units, $\sqrt{\langle \delta\gamma^2 \rangle} \sim 0.002$. This translates into the "noise" in α as $\sqrt{\langle \delta\alpha^2 \rangle} = \sqrt{\langle \delta\gamma^2 \rangle}/I(\Gamma_0)$, where [13] $I(\Gamma_0) \sim 1$.

Using the $\alpha(T)$ plot in Fig. 4, one can measure that above 1.5 K the slope $\partial\alpha/\partial T \approx 1/(60\ \mathrm{K})$. This gives

$$\sqrt{\langle\delta T^2\rangle} \sim \sqrt{\langle\delta\alpha^2\rangle}\frac{\partial T}{\partial\alpha} \sim 0.002 \times 60\ \mathrm{K} = 0.12\ \mathrm{K},$$

in good agreement with Fig. 3. Note, however, that at $T <$ 1 K, where the $\alpha(T)$ dependence saturates, the slope $\partial\alpha/\partial T$ vanishes, which leads to $\sqrt{\langle\delta T^2\rangle} \to \infty$. In this sense, a weakly pronounced maximum at $T \sim 1$ K can be yet another stretched oscillation.

IV. CONCLUSIONS

We have performed measurements of the phase escape and retrapping from/in two distinct states $\pm\varphi$ of a Josephson φ junction in a temperature range from 0.3 to 3 K. We have seen that retrapping is deterministic above some damping (temperature) α^* (T^*). At $\alpha < \alpha^*$ ($T < T^*$), the probability of trapping in the unnatural well $P_-[\alpha(T)]$ grows and oscillates, demonstrating the onset of the butterfly effect as predicted earlier [13]. However, we observe that the probability $P_-(T)$ saturates at a level different from 0.5 most probably because $\alpha(T)$ saturates at its minimum value α_{sat} for $T < T_{\mathrm{sat}}$. Thus, we were not able to penetrate deep into the region of the butterfly effect. Further experiments with the φ JJs showing lower damping, e.g., an effective φ JJ based on dc SQUID [21], may help us to move further in this direction.

ACKNOWLEDGMENTS

R.M. gratefully acknowledges support by the Carl Zeiss Stiftung. This work was supported by the Deutsche Forschungsgemeinschaft (DFG) via Project No. GO-1106/5, via project A5 within SFB/TRR-21, and by the EU-FP6-COST action MP1201. This work is also supported by the National Science Centre (Poland) under Contract No. DEC-2014/13/B/ST3/04451 (T.N.) and by the Czech Science Foundation via Project No. 16-19640S (M.Z.).

[1] A. Scott, *Encyclopedia of Nonlinear Science* (Taylor & Francis, New York, 2005).
[2] J. Sprott, *Chaos and Time-Series Analysis* (Oxford University Press, Oxford, 2003).
[3] E. N. Lorenz, J. Atmos. Sci. **20**, 130 (1963).
[4] R. G. Mints, Phys. Rev. B **57**, R3221(R) (1998).
[5] A. Buzdin and A. E. Koshelev, Phys. Rev. B **67**, 220504(R) (2003).
[6] Y. Tanaka and S. Kashiwaya, Phys. Rev. B **56**, 892 (1997).
[7] A. Gumann and N. Schopohl, Phys. Rev. B **79**, 144505 (2009).
[8] N. G. Pugach, E. Goldobin, R. Kleiner, and D. Koelle, Phys. Rev. B **81**, 104513 (2010).
[9] E. Goldobin, D. Koelle, R. Kleiner, and A. Buzdin, Phys. Rev. B **76**, 224523 (2007).
[10] E. Goldobin, D. Koelle, R. Kleiner, and R. G. Mints, Phys. Rev. Lett. **107**, 227001 (2011).
[11] S. V. Bakurskiy, N. V. Klenov, T. Y. Karminskaya, M. Y. Kupriyanov, and A. A. Golubov, Supercond. Sci. Technol. **26**, 015005 (2013).
[12] D. M. Heim, N. G. Pugach, M. Y. Kupriyanov, E. Goldobin, D. Koelle, and R. Kleiner, J. Phys.: Condens. Matter **25**, 215701 (2013).
[13] E. Goldobin, R. Kleiner, D. Koelle, and R. G. Mints, Phys. Rev. Lett. **111**, 057004 (2013).
[14] A. Lipman, R. G. Mints, R. Kleiner, D. Koelle, and E. Goldobin, Phys. Rev. B **90**, 184502 (2014).
[15] E. Il'ichev, M. Grajcar, R. Hlubina, R. P. J. IJsselsteijn, H. E. Hoenig, H.-G. Meyer, A. Golubov, M. H. S. Amin, A. M. Zagoskin, A. N. Omelyanchouk, and M. Yu. Kupriyanov, Phys. Rev. Lett. **86**, 5369 (2001).
[16] G. Testa, E. Sarnelli, A. Monaco, E. Esposito, M. Ejrnaes, D.-J. Kang, S. H. Mennema, E. J. Tarte, and M. G. Blamire, Phys. Rev. B **71**, 134520 (2005).
[17] R. G. Mints, I. Papiashvili, J. R. Kirtley, H. Hilgenkamp, G. Hammerl, and J. Mannhart, Phys. Rev. Lett. **89**, 067004 (2002).
[18] H. Sickinger, A. Lipman, M. Weides, R. G. Mints, H. Kohlstedt, D. Koelle, R. Kleiner, and E. Goldobin, Phys. Rev. Lett. **109**, 107002 (2012).
[19] E. Goldobin, H. Sickinger, M. Weides, N. Ruppelt, H. Kohlstedt, R. Kleiner, and D. Koelle, Appl. Phys. Lett. **102**, 242602 (2013).
[20] See Supplemental Material at http://link.aps.org/supplemental/10.1103/PhysRevB.93.174506 for theoretical analysis of a particle trapping in an asymmetric double-well potential in the limit of a small damping and a weak noise.
[21] E. Goldobin, D. Koelle, and R. Kleiner, Phys. Rev. B **91**, 214511 (2015).

Publication 2

Model I–V curves and figures of merit of underdamped deterministic Josephson ratchets

E. Goldobin, R. Menditto, D. Koelle, and R. Kleiner
Physikalisches Institut and Center for Quantum Science in LISA⁺, Universität Tübingen, Auf der Morgenstelle 14, D-72076 Tübingen, Germany
(Received 28 June 2016; published 7 September 2016)

We propose simple models for the current-voltage characteristics of typical Josephson ratchets. We consider the case of a ratchet working against a constant applied counter force and derive analytical expressions for the key characteristics of such a ratchet: rectification curve, stopping force, input and output powers, and rectification efficiency. Optimization of the ratchet performance is discussed.

DOI: 10.1103/PhysRevE.94.032203

I. INTRODUCTION

The discovery of Brownian motion suggests the idea of extracting useful work out of random motion. As Richard Feynman *et al.* demonstrated [1], drawing energy from equilibrium thermal fluctuations (white noise) is forbidden by the second law of thermodynamics. The extraction of work out of *nonequilibrium* or time-correlated noise (colored noise) is possible using ratchet systems [2–5]. As an extreme case of correlated input signal one can consider a deterministic signal with zero time average, which will be rectified by the ratchet into a dc output signal. Such *deterministic ratchets* find many applications as rectifiers, sorters, *etc.* Deterministic and stochastic ratchets have been the focus of attention during the past two decades in various implementations. In particular, Josephson systems based on the motion of Josephson vortices [6–15] or the Josephson phase [16–21] have been suggested and tested experimentally.

Josephson ratchets have some advantages over other ratchet systems: (I) directed motion results in an average dc voltage, which makes ratchet operation easily accessible in experiment; (II) Josephson junctions are very fast devices, i.e., they can be operated in a broad frequency range from dc up to 100 GHz, which allows them to capture a lot of spectral energy; (III) both underdamped and overdamped systems can be investigated by proper junction design and the variation of the bath temperature.

It turns out that regardless of the underlying physics (vortex motion or Josephson phase motion) the I–V characteristic (IVC) looks rather universal. Therefore, in this paper, we do not discuss *how* such an asymmetric IVC can be obtained. Instead, we assume some specific typical IVC, parametrize it, and calculate the most important figures of merit. The model presented here is an extension of a simpler model presented earlier [22] in two aspects. First, the present model takes into account possible hysteresis in the IVC and, therefore, allows us to analyze underdamped as well as overdamped ratchets. Second, it includes two specific types of the IVC: the constant voltage step and the linear voltage branch. Within the framework of this new model we obtain rectification curves, stopping force, input and output powers, and rectification efficiency.

The paper is organized as follows. In Sec. II we describe the model IVCs. In Sec. III the expressions for mean voltage, stopping force, input and output power, and efficiency are derived. In Sec. IV we discuss the obtained results and the optimization of the ratchet. Section V concludes this work.

II. MODEL

Since the typical frequencies of the Josephson devices are very high (from a few GHz up to a few THz) we consider the most simple case of the quasistatic drive $I_{ac}\sin(\omega t)$, when $\omega \ll (\omega_p,\omega_c)$. Here ω_p is the plasma frequency and ω_c is the characteristic frequency of the Josephson junction. To derive our results in the most general form from the very beginning, we assume an additional dc current (counter force) $I_{\rm dc}$, which is applied to the ratchet trying to stop it. This allows us to study the loading capabilities of the ratchet and, thus, to calculate its output power and efficiency. The total applied driving current (force) can be written as

$$I(t) = I_{\rm dc} + I_{\rm ac}\sin(\omega t). \tag{1}$$

Taking into account the smallness of ω, the rectified (mean) voltage can be obtained just by integrating a dc current-voltage characteristic $V(I)$ (most frequently measured in experiment) as

$$\overline{V} = \frac{1}{T}\int_0^T V[I(t)]\,dt, \tag{2}$$

where $T = 2\pi/\omega$ is the period of the ac drive. Note, that $V(I)$ is, in general, a hysteretic (multivalued) function, which depends on the prehistory of the biasing.

In this work we discuss two types of IVCs shown in Figs. 1(a) and 1(b). The first is an IVC with a constant voltage step, see Fig. 1(a), typical for relativistic motion of the phase or vortex in a Josephson device. The second is an IVC with a linear branch, see Fig. 1(b), typical for nonrelativistic motion.

The hysteresis is included in the IVC as follows. In the simplest case of only one hysteretic branch, see Figs. 1(a) and 1(b), we assume that when the current is increased from $I = 0$, the voltage $V(I) = 0$ up to $I = I_c^+$, see Fig. 1. Then the voltage is given by some function $\mathcal{V}(I)$ specified below. However, if the current is then decreased, the voltage is given by $\mathcal{V}(I)$ down to the "return current" $I_r^+ \leqslant I_c^+$ and $V = 0$ for lower currents. If one sweeps the current I in the negative direction, the corresponding critical and return currents are $-I_c^- < 0$ and $-I_r^- < 0$, so that $0 \leqslant I_r^- \leqslant I_c^-$.

An additional bias current (counter force) $I_{\rm dc}$, if any, shifts the origin of the ac drive from the point $I = 0$ to the point $I = I_{\rm dc}$. Alternatively, one can also treat this as an ac drive with the origin at $I = 0$, but the values of $I_c^\pm$ and $I_r^\pm$ are

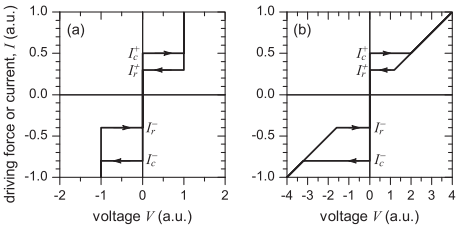

FIG. 1. Model IVCs for the two studied cases: (a) constant voltage step, (b) linear branch. The parameters used for plotting are: $I_c^+ = 0.5$, $I_c^- = 0.8$, $I_r^+ = 0.3$, $I_r^- = 0.4$, $V_1 = 1$, and $R_n = 4$.

shifted by $I_{\rm dc}$ to the new values, $J_c^\pm$ and $J_r^\pm$ given by

$$J_c^+ = I_c^+ - I_{\rm dc}, \quad J_r^+ = I_r^+ - I_{\rm dc},$$
$$J_c^- = I_c^- + I_{\rm dc}, \quad J_r^- = I_r^- + I_{\rm dc}. \tag{3}$$

For the sake of simplicity, below we assume that $I_c^+ < I_c^-$. Then the rectified voltage $\overline{V} \geqslant 0$ and the counter force $I_{\rm dc} < 0$.

III. RESULTS

A. Output (rectified) voltage

It is convenient to calculate the *average voltage* $\overline{V}$ as a sum of average voltages over the positive and the negative periods of the drive, i.e.,

$$\overline{V} = \overline{V}_+ + \overline{V}_-, \tag{4}$$

where

$$\overline{V}_\pm(I_{\rm ac}) = \begin{cases} 0, & \text{if } I_{\rm ac} < J_c^\pm \\ \overline{\mathcal{V}}_\pm(I_{\rm ac}), & \text{if } I_{\rm ac} > J_c^\pm \end{cases}. \tag{5}$$

The functions $\overline{\mathcal{V}}_\pm(I_{\rm ac})$ will be calculated below for a particular model as follows:

$$\overline{\mathcal{V}}_\pm \overset{(2)}{=} \frac{\omega}{2\pi}\int_{t_1^\pm}^{t_2^\pm} \mathcal{V}[I_{\rm dc} + I_{\rm ac}\sin(\omega t)]dt,$$
$$= \pm\frac{1}{2\pi}\int_{\phi_1^\pm}^{\phi_2^\pm} \mathcal{V}[I_{\rm dc} + I_{\rm ac}\sin(\phi)]d\phi, \tag{6}$$

where $\phi_1^\pm$ and $\phi_2^\pm$ define the phases ($t_1^\pm$ and $t_2^\pm$ define times) when the system switches to and from the voltage state, i.e., the instant value of current $I(t)$ exceeds $I_c^\pm$ or falls below $I_r^\pm$, i.e., $I_{\rm ac}\sin(\omega t)$ exceeds $J_c^\pm$ or falls below $J_r^\pm$. They are given by

$$\omega t_1^+ \equiv \phi_1^+ = +\arcsin(J_c^+/I_{\rm ac}), \tag{7a}$$
$$\omega t_2^+ \equiv \phi_2^+ = \pi - \arcsin(J_r^+/I_{\rm ac}), \tag{7b}$$
$$\omega t_1^- \equiv \phi_1^- = \pi + \arcsin(J_c^-/I_{\rm ac}), \tag{7c}$$
$$\omega t_2^- \equiv \phi_2^- = 2\pi - \arcsin(J_r^-/I_{\rm ac}). \tag{7d}$$

1. Constant voltage model

For a constant voltage model [22], see Fig. 1(a),

$$\mathcal{V}(I) = V_1\,\mathrm{sgn}(I), \tag{8}$$

relevant for step-like behavior of the IVC, see Fig. 1(a). Here, V_1 is the voltage of the step.

Substituting Eq. (8) into Eq. (6) we obtain

$$\overline{\mathcal{V}}_\pm = \pm\frac{V_1}{2\pi}(\phi_2^\pm - \phi_1^\pm), \tag{9}$$

and using Eqs. (7) we obtain the final explicit expression:

$$\overline{\mathcal{V}}_\pm = \pm\frac{V_1}{2\pi}\left[\arccos\left(\frac{J_r^\pm}{I_{\rm ac}}\right) + \arccos\left(\frac{J_c^\pm}{I_{\rm ac}}\right)\right]. \tag{10}$$

2. Linear voltage model

For the linear voltage model, see Fig. 1(b),

$$\mathcal{V}(I) = R_n I, \tag{11}$$

relevant for IVCs obtained from the resistively and capacitively shunted junction (RCSJ) model with resistance R_n, Fig. 1(b).

Substituting Eq. (11) into Eq. (6) we obtain

$$\overline{\mathcal{V}}_\pm = \frac{R_n}{2\pi}\{I_{\rm dc}(\phi_2^\pm - \phi_1^\pm) + I_{\rm ac}[\cos(\phi_1^\pm) - \cos(\phi_2^\pm)]\}. \tag{12}$$

Using Eqs. (7) and taking into account that $\cos(\phi_1^\pm) \gtrless 0$, while $\cos(\phi_2^\pm) \lessgtr 0$ we obtain

$$\overline{\mathcal{V}}_\pm = \pm\frac{R_n}{2\pi}\left\{I_{\rm dc}\left[\arccos\left(\frac{J_r^\pm}{I_{\rm ac}}\right) + \arccos\left(\frac{J_c^\pm}{I_{\rm ac}}\right)\right]\right.$$
$$\left. + I_{\rm ac}\left[\sqrt{1-\left(\frac{J_c^\pm}{I_{\rm ac}}\right)^2} + \sqrt{1-\left(\frac{J_r^\pm}{I_{\rm ac}}\right)^2}\right]\right\}. \tag{13}$$

Note, that the first term in Eqs. (12) and (13) vanishes for $I_{\rm dc} = 0$ (idle ratchet).

B. Input power, output power, and efficiency

Without applied dc bias (counter force) the ratchet rectifies, but it is idle, i.e., it does not produce any output power. Therefore, for the analysis of power input, output, and efficiency we consider the case $I_{\rm dc} \neq 0$, i.e., the ratchet should work against an applied dc current (counter force) $I_{\rm dc}$.

A set of rectification curves for several values of $I_{\rm dc} \lessgtr 0$ is shown in Figs. 2(a) and 2(b). The general behavior of $\overline{V}(I_{\rm ac})$ follows from Eqs. (4) and (5). For small values of the drive $I_{\rm ac} < J_c^+$ the value of $\overline{V} = 0$. Then, for $J_c^+ < I_{\rm ac} < J_c^-$, we get a strong rectification because $\overline{V}_+ > 0$ while $\overline{V}_- = 0$. Finally, at $I_{\rm ac} > J_c^-$, both $\overline{V}_+ > 0$ and $\overline{V}_- < 0$ almost cancel each other.

The no-rectification regime at $I_{\rm ac} < J_c^+$ we shall call a pinning regime. We define a *rectification window* as a range of $I_{\rm ac}$ where rectified voltage is large, i.e., $J_c^+ < I_{\rm ac} < J_c^-$. The region $I_{\rm ac} > J_c^-$ we shall call a "Sisyphus" regime since the system makes a lot of useless back and forth motion, dissipating a lot of power, but not producing any appreciable mean output. We do not pay much attention to the Sisyphus region since it is not interesting for applications.

From Fig. 2 we see that the rectification window shrinks as the absolute value of the counter force $I_{\rm dc} < 0$ increases. Let us plot the beginning and the end of the rectification window, i.e., $J_c^\pm(I_{\rm dc})$ given by Eq. (3); see Fig. 3. The window shrinks linearly with $I_{\rm dc}$. The two lines $J_c^+(I_{\rm dc})$ and $J_c^-(I_{\rm dc})$ cross (and

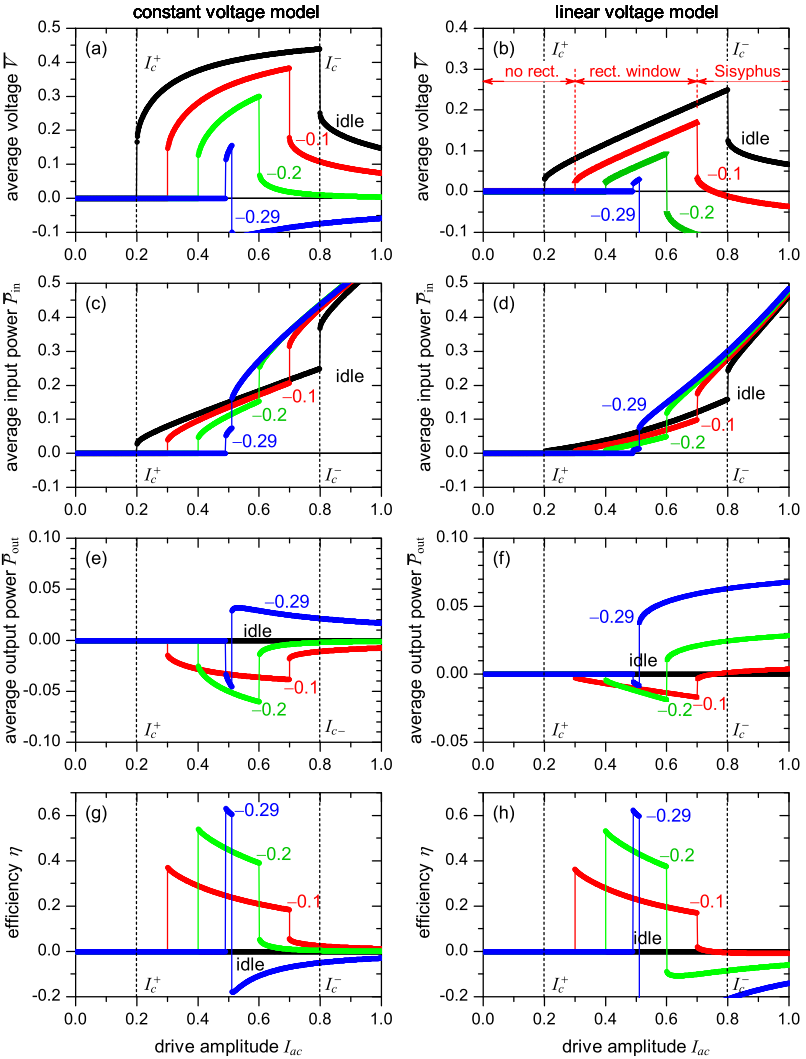

FIG. 2. A set of rectification curves $\overline{V}(I_{ac})$ (a, b), input power $P_{in}(I_{ac})$ (c, d), output power $P_{out}(I_{ac})$ (e, f), and efficiency $\eta(I_{ac})$ (g, h) calculated for different values of $I_{dc} = 0, -0.1, -0.2, -0.29$. The left column of plots, i.e. (a, c, e, g), is calculated using the constant voltage model with $V_1 = 1$. The right column, i.e. (b, d, f, h), is calculated using the linear voltage model with $R_n = 1$. The other parameters are $I_c^+ = 0.2$, $I_c^- = 0.8$, $I_r^+ = 0.1$, $I_r^- = 0.3$. In (b) the most important regions are marked for the case of a ratchet loaded by $I_{dc} = -0.10$.

the rectification window closes) at $I_{dc} = (I_c^+ - I_c^-)/2$. Just before closing, the rectification takes place only at the single value of $I_{ac} = (I_c^+ + I_c^-)/2$, i.e., just in the middle of the idle ($I_{dc} = 0$) rectification window.

The *stopping force* I_{stop} is defined as the dc counter force I_{dc} that one has to apply at fixed I_{ac} to stop the ratchet. Since we are ignoring the Sisyphus region, the stopping force is basically defined by the motion of boundaries of the

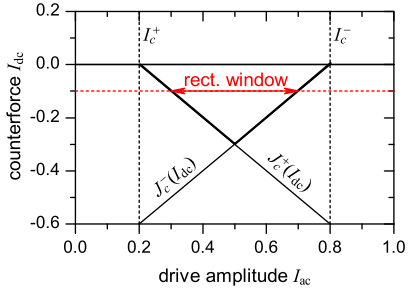

FIG. 3. The size of the rectification window at given I_{dc}. As an example the arrow shows the size of rectification window at $I_{dc} = -0.1$. Simultaneously this plot shows the stopping force I_{stop} at given drive amplitude I_{ac}.

rectification window, see Fig. 3, i.e., it is determined only by $I_c^{\pm}$ and is independent on exact details of $\mathcal{V}(I)$, provided it is point-symmetric, i.e., $\mathcal{V}(I) = -\mathcal{V}(-I)$. The stopping force is given by [23]

$$I_{stop} = \begin{cases} 0, & \text{for } I_{ac} < I_c^+; \\ I_c^+ - I_{ac}, & \text{for } I_c^+ < I_{ac} < (I_c^+ + I_c^-)/2; \\ I_{ac} - I_c^-, & \text{for } (I_c^+ + I_c^-)/2 < I_{ac} < I_c^-; \\ 0 & \text{for } I_{ac} > I_c^- \text{ (Sisyphus)} \end{cases} \quad (14)$$

The mean *input ac power* is given by

$$\overline{P}_{in} = \frac{1}{2\pi}\int_0^{2\pi} V[I_{dc} + I_{ac}\sin(\phi)]I_{ac}\sin(\phi)\,d\phi = \overline{P}_{in}^{+} + \overline{P}_{in}^{-}, \quad (15)$$

where the power during the positive and negative semiperiods are given by

$$\overline{P}_{in}^{\pm} = \begin{cases} 0, & \text{for } I_{ac} < J_c^{\pm} \\ \overline{\mathcal{P}}_{in}^{\pm} & \text{for } I_{ac} > J_c^{\pm}. \end{cases} \quad (16)$$

Here,

$$\overline{\mathcal{P}}_{in}^{\pm} = \frac{1}{2\pi}\int_{\phi_1^{\pm}}^{\phi_2^{\pm}} V[I_{dc} + I_{ac}\sin(\phi)]I_{ac}\sin(\phi)\,d\phi. \quad (17)$$

The mean *output dc power* for constant dc bias current I_{dc} is given by

$$\overline{P}_{out} = \frac{1}{2\pi}\int_0^{2\pi} V(I_{dc} + I_{ac}\sin\phi)I_{dc}\,d\phi = \overline{V}I_{dc}. \quad (18)$$

Note that for $I_c^+ < I_c^-$ the rectified voltage $\overline{V} \geqslant 0$, so that we apply a stopping current $I_{dc} < 0$. Thus, $\overline{P}_{out} < 0$, which indicates that the power is not consumed but rather given out to the dc load (dc current source). Equation (18) says that $\overline{P}_{out}(I_{dc})$ does not require any separate calculations and can be obtained from $\overline{V}(I_{ac})$ in a trivial way.

The *efficiency* is given by

$$\eta = -\overline{P}_{out}/\overline{P}_{in}. \quad (19)$$

1. Constant voltage model

For model Eq. (8), after integration of Eq. (17) we have

$$\overline{\mathcal{P}}_{in}^{\pm} = \frac{V_1 I_{ac}}{2\pi}\left[\sqrt{1-\left(\frac{J_c^{\pm}}{I_{ac}}\right)^2} + \sqrt{1-\left(\frac{J_r^{\pm}}{I_{ac}}\right)^2}\right]. \quad (20)$$

The plots $P_{in}(I_{ac})$ for different values I_{dc} are shown in Fig. 2(c), while $P_{out}(I_{ac})$ is shown in Fig. 2(e).

The efficiency $\eta(I_{ac})$ can be calculated explicitly using Eq. (19). We do not show this bulky expression here, however, we plot the result in Fig. 2(g). The efficiency has a maximum just at the beginning of the rectification window, i.e., at $I_{ac} = \min(J_c^+, J_c^-)$. Assuming that $J_c^+ < J_c^-$, which is always the case for the still open rectification window, the maximum efficiency is reached at $I_{ac} = J_c^+$ and is given by

$$\eta_{max} = \frac{-I_{dc}}{2}\frac{\arccos\left(\frac{J_r^+}{J_c^+}\right)}{\sqrt{J_c^{+2} - J_r^{+2}}}. \quad (21)$$

No hysteresis. In the case of no hysteresis ($I_r^+ \to I_c^+$, i.e., $J_r^+ \to J_c^+$) we recover the previous result [22], namely $\eta \to -I_{dc}/J_c^+ = -I_{dc}/(I_c^+ - I_{dc})$. This is a monotonically increasing function of $-I_{dc}$. However, $-I_{dc}$ cannot be made arbitrary large. At $I_{dc} \to (I_c^+ - I_c^-)/2$ the rectification window is about to close, but efficiency approaches its ultimate value given by

$$\eta_{ult} \to \frac{I_c^- - I_c^+}{I_c^- + I_c^+}. \quad (22)$$

Maximum hysteresis. In this case ($I_r^+ = 0$) we obtain the ultimate rectification at $I_{dc} \to (I_c^+ - I_c^-)/2$ (just before the rectification window closes) given by

$$\eta_{ult} \to \frac{I_c^- - I_c^+}{2\sqrt{I_c^- I_c^+}}\arccos\left(\frac{I_c^- - I_c^+}{I_c^- + I_c^+}\right). \quad (23)$$

Let us make several notes. First, when we speak about efficiency (and discuss effects of hysteresis), we focus on the rectification window only. There, only the hysteresis of the positive branch I_r^+ matters because the negative branch is not participating yet. Thus, the value of I_r^- is irrelevant, while the value of I_c^- only affects the upper edge of the rectification window. Second, to make the ratchet more efficient one has to design it with $I_c^+ \to 0$, while keeping I_c^- constant. In this limit the hysteresis of the positive part of the IVC (the value of I_r^+) becomes irrelevant too since $I_r^+ < I_c^+$, i.e., $I_r^+ = 0$.

2. Linear voltage model

For model Eq. (11), after integration of Eq. (17) we have

$$\overline{\mathcal{P}}_{in}^{\pm} = \frac{I_{ac}R_n}{4\pi}\left\{(J_c^{\pm} \pm 2I_{dc})\sqrt{1-\frac{J_c^{\pm 2}}{I_{ac}^2}} + (J_r^{\pm} \pm 2I_{dc}) \times \sqrt{1-\frac{J_r^{\pm 2}}{I_{ac}^2}} + I_{ac}\left[\arccos\left(\frac{J_c^{\pm}}{I_{ac}}\right) + \arccos\left(\frac{J_r^{\pm}}{I_{ac}}\right)\right]\right\}. \quad (24)$$

The efficiency $\eta(I_{\rm ac})$ can be calculated explicitly using Eq. (19). We do not show this bulky expression here, however, we plot the result in Fig. 2(h). The efficiency has a maximum at the beginning of the rectification window, i.e., at $I_{\rm ac} = \min(J_c^+, J_c^-)$. Assuming that $J_c^+ < J_c^-$, which is always the case for the still open rectification window, the maximum efficiency is reached at $I_{\rm ac} = J_c^+$ and is given by

$$\eta_{\rm max} = \frac{-2I_{\rm dc}\left[I_{\rm dc}\arccos\left(\frac{J_r^+}{J_c^+}\right) + \sqrt{{J_c^+}^2 - {J_r^+}^2}\right]}{{J_c^+}^2\arccos\left(\frac{J_r^+}{J_c^+}\right) + \sqrt{{J_c^+}^2 - {J_r^+}^2}(J_r^+ + 2I_{\rm dc})}. \quad (25)$$

No hysteresis. Note that in the limit of no hysteresis ($J_r^+ \to J_c^+$) we again recover the previous result [22]; see Eq. (22). This is independent on our model (linear branch or constant voltage branch) as at the beginning of the rectification window the branch is not really traced yet (only its first point).

Maximum hysteresis. In this case ($I_r^+ = 0$) we obtain the ultimate rectification at $I_{\rm dc} \to (I_c^+ - I_c^-)/2$ (just before the rectification window closes) given by

$$\eta_{\rm ult} = \frac{-2(I_c^- - I_c^+)^2\arccos\left(\frac{I_c^- - I_c^+}{I_c^- + I_c^+}\right) + 4(I_c^- - I_c^+)\sqrt{I_c^+ I_c^-}}{(I_c^+ + I_c^-)^2\arccos\left(\frac{I_c^- - I_c^+}{I_c^- + I_c^+}\right) + 2(I_c^+ - I_c^-)\sqrt{I_c^+ I_c^-}}. \quad (26)$$

IV. DISCUSSION

The plots of $\overline{P}_{\rm in}(I_{\rm dc})$ and $\overline{P}_{\rm out}(I_{\rm dc})$ as well as $\eta(I_{\rm dc})$ for both models are shown in Figs. 2(c)–2(h). From Figs. 2(c) and 2(d) we see that the input power is zero for $I_{\rm ac} < J_c^+$, increases inside the rectification window, and increases even further in the Sisyphus regime. As we apply the counter force $I_{\rm dc}$, the input power within the rectification window decreases slightly.

The behavior of $\overline{P}_{\rm out}(I_{\rm ac})$ is more complicated. First of all, for the case of the idle and unloaded ratchet ($I_{\rm dc} = 0$) $\overline{P}_{\rm out}(I_{\rm ac}) \equiv 0$ for any $I_{\rm ac}$. For the loaded ratchet ($I_{\rm dc} < 0$), the power $\overline{P}_{\rm out}(I_{\rm ac}) = 0$ in the pinning regime, and $\overline{P}_{\rm out}(I_{\rm ac})$ has its maximum value inside the rectification window. In the Sisyphus regime the power $\overline{P}_{\rm out}(I_{\rm ac})$ becomes small or even changes sign (power consumption instead of power generation). Interestingly, the maximum value $\overline{P}_{\rm out}(I_{\rm ac})$ is reached for some $I_{\rm dc}$ in the middle of the interval $(I_c^+ - I_c^-)/2 \ldots 0$.

The efficiency $\eta(I_{\rm ac})$ has a more clear behavior. It has a maximum in the beginning of the rectification window and grows as the load, i.e., $|I_{\rm dc}|$, increases.

From a practical point of view we would like to choose the parameters $I_c^\pm$, $I_r^\pm$, V_1, or R_n to optimize the following figures of merit of our Josephson ratchet. (a) The *rectification window* should be made as wide as possible and it should start at the lowest possible $I_{\rm ac}$. The stopping force and current $I_{\rm stop}$ is directly related to the rectification window size, so that a large window automatically leads to a high $|I_{\rm stop}|$. (b) The output (rectified) voltage $\overline{V}$ should be made as high as possible. (c) The output power $P_{\rm out}$ should be made as large as possible. (d) The efficiency η should be made as large as possible.

The parameters V_1 and R_n have a direct effect on $\overline{V}$ and $\overline{P}_{\rm out}$ and have no effect on the rectification window and efficiency. Therefore, to increase $\overline{V} \propto (V_1, R_n)$ and $\overline{P}_{\rm out} \propto (V_1, R_n)$, one should increase V_1 or R_n.

To enlarge the rectification window one has to make I_c^+ and I_c^- as different as possible (maximum possible asymmetry). In an ideal case, one would like to have $I_c^+ \to 0$ (which automatically means $I_r^+ \to 0$). The values of $I_r^\pm$ are not relevant for the rectification window size. Simultaneously, a large rectification window leads to large values of the stopping force up to $(I_c^+ - I_c^-)/2$. The efficiency has its maximum value in the beginning of the rectification window and also grows with increasing load current $|I_{\rm dc}|$. However, with increasing load the rectification window shrinks. At the end one has to find a compromise between efficiency and rectification window size for a particular application. If the value of $I_c^+ \neq 0$ the value of I_r^+ does not have a major effect on the rectification curves—smaller I_r^+ improves the figures of merit such as $\overline{V}$, $\overline{P}_{\rm out}$, and η somewhat. The value of I_r^- is relevant only in the Sisyphus region, which is not interesting for applications.

V. CONCLUSIONS

We have suggested two simple models of a Josephson ratchet—the linear voltage branch and the constant voltage branch—based on few experimentally relevant parameters. We have derived analytical expressions for the mean voltage $\overline{V}$, the rectification window size, the stopping force $I_{\rm stop}$, the input power $\overline{P}_{\rm in}$, the output power $\overline{P}_{\rm out}$, and efficiency η. We have demonstrated the performance of the ratchet for some typical set of parameters and discussed the optimization of different figures of merit. These results should be useful for designing the next generation of Josephson ratchets as well as for fitting already obtained results.

ACKNOWLEDGMENTS

R.M. gratefully acknowledges support by the Carl Zeiss Stiftung. This work was supported by the Deutsche Forschungsgemeinschaft (DFG) via Project No. GO-1106/5, via project A5 within SFB/TRR-21, and by the EU-FP6-COST action Grant No. MP1201.

[1] R. P. Feynman, R. B. Leighton, and M. Sands, *The Feynman Lectures on Physics* (Addison-Wesley, Reading, MA, 1966), Vol. I, Chap. 46.
[2] M. O. Magnasco, Phys. Rev. Lett. **71**, 1477 (1993).
[3] F. Jülicher, A. Ajdari, and J. Prost, Rev. Mod. Phys. **69**, 1269 (1997).
[4] P. Reimann, Phys. Rep. **361**, 57 (2002).
[5] P. Hänggi and F. Marchesoni, Rev. Mod. Phys. **81**, 387 (2009).
[6] F. Falo, P. J. Martínez, J. J. Mazo, and S. Cilla, Europhys. Lett. **45**, 700 (1999).
[7] E. Trías, J. J. Mazo, F. Falo, and T. P. Orlando, Phys. Rev. E **61**, 2257 (2000).

[8] E. Goldobin, A. Sterck, and D. Koelle, Phys. Rev. E **63**, 031111 (2001).
[9] G. Carapella, Phys. Rev. B **63**, 054515 (2001).
[10] G. Carapella and G. Costabile, Phys. Rev. Lett. **87**, 077002 (2001).
[11] G. Carapella, G. Costabile, N. Martucciello, M. Cirillo, R. Latempa, A. Polcari, and G. Filatrella, Physica C **382**, 337 (2002).
[12] J. B. Majer, J. Peguiron, M. Grifoni, M. Tusveld, and J. E. Mooij, Phys. Rev. Lett. **90**, 056802 (2003).
[13] A. V. Ustinov, C. Coqui, A. Kemp, Y. Zolotaryuk, and M. Salerno, Phys. Rev. Lett. **93**, 087001 (2004).
[14] M. Beck, E. Goldobin, M. Neuhaus, M. Siegel, R. Kleiner, and D. Koelle, Phys. Rev. Lett. **95**, 090603 (2005).
[15] H. B. Wang, B. Y. Zhu, C. Gürlich, M. Ruoff, S. Kim, T. Hatano, B. R. Zhao, Z. X. Zhao, E. Goldobin, D. Koelle, and R. Kleiner, Phys. Rev. B **80**, 224507 (2009).
[16] P. Hänggi and R. Bartussek, in *Nonlinear Physics of Complex Systems*, Lecture Notes in Physics, edited by J. Parisi, S. C. Müller, and W. Zimmermann (Springer, Berlin, 1996), Vol. 476, pp. 294–308.
[17] I. Zapata, R. Bartussek, F. Sols, and P.Hänggi, Phys. Rev. Lett. **77**, 2292 (1996).
[18] S. Weiss, D. Koelle, J. Müller, R. Gross, and K. Barthel, Europhys. Lett. **51**, 499 (2000).
[19] A. Sterck, S. Weiss, and D. Koelle, Appl. Phys. A **75**, 253 (2002).
[20] A. Sterck, R. Kleiner, and D. Koelle, Phys. Rev. Lett. **95**, 177006 (2005).
[21] A. Sterck, D. Koelle, and R. Kleiner, Phys. Rev. Lett. **103**, 047001 (2009).
[22] M. Knufinke, K. Ilin, M. Siegel, D. Koelle, R. Kleiner, and E. Goldobin, Phys. Rev. E **85**, 011122 (2012).
[23] Our previous paper [22] contains erroneous expression for $I_{\rm stop}$ for $I_{\rm ac} > (I_c^+ + I_c^-)/2$.

Publication 3

Tunable φ Josephson junction ratchet

R. Menditto,[1] H. Sickinger,[1] M. Weides,[2] H. Kohlstedt,[3] D. Koelle,[1] R. Kleiner,[1] and E. Goldobin[1,*]
[1]*Physikalisches Institut and Center for Quantum Science in LISA$^+$, Universität Tübingen, Auf der Morgenstelle 14, D-72076 Tübingen, Germany*
[2]*Physikalisches Institut, Karlsruher Institut für Technologie, D-76128 Karlsruhe, Germany*
[3]*Nanoelektronik, Technische Fakultät, Christian-Albrechts-Universität zu Kiel, D-24143 Kiel, Germany*
(Received 11 July 2016; published 3 October 2016)

We demonstrate experimentally the operation of a deterministic Josephson ratchet with tunable asymmetry. The ratchet is based on a φ Josephson junction with a ferromagnetic barrier operating in the underdamped regime. The system is probed also under the action of an additional dc current, which acts as a counterforce trying to stop the ratchet. Under these conditions the ratchet works against the counterforce, thus producing a nonzero output power. Finally, we estimate the efficiency of the φ Josephson junction ratchet.

DOI: 10.1103/PhysRevE.94.042202

I. INTRODUCTION

Ratchets or Brownian motors have attracted a lot of interest in the last few decades [1–37]. Apart from answering some fundamental questions, they can be immediately employed for the extraction of work out of nonequilibrium thermal fluctuations, for rectification of deterministic signals, or for particle separation [1–4]. Apart from the ratchets existing in nature [5], there are many artificial ratchet implementations, in particular, based on nanostructured superconductors: Josephson vortex ratchets [6–16], SQUID ratchets [17–23], and Abrikosov vortex ratchets [24,25].

A huge number of theoretical works [28–37] published more than a decade ago, were devoted to a paradigmatic system: a pointlike particle moving in a 1D periodic potential without reflection symmetry under the action of a deterministic or random force with zero time average. To create such a system using a Josephson junction (JJ), one recalls that the Josephson phase ϕ can be considered as the coordinate of a fictitious particle moving in a 2π-periodic Josephson potential energy profile $U(\phi)$. The ratchet's driving force is the bias current. However, the Josephson potential $U(\phi)$ in most types of known JJs is reflection symmetric and its shape is hardly controllable. Thus, for many years there was no possibility to create a Josephson junction ratchet, which would be as simple as the paradigmatic examples discussed in the literature and check experimentally all the predictions. Researchers, however, were able to demonstrate more complex Josephson ratchets (with more than one JJ or with extended JJ), such as asymmetric SQUID ratchets [18–21] or Josephson vortex ratchets [7,10,14,16]. The physics of such devices is more complicated and they are not as reliable as the generic ratchet.

Current progress in JJs allows us to solve this long-standing problem. Recently our group suggested [38] and demonstrated [39] a φ JJ with a magnetic-field-tunable Josephson energy profile. By definition, φ JJ is a JJ having a *nonzero* and *degenerate* phase $\psi = \pm\varphi \neq 0$ in the ground state, i.e., when no current is applied to the JJ. In particular, in the case of a φ JJ made of a short 0-π JJ (two parallel segments with 0 and π ground state), the Josephson energy can be written in a simple analytical form as [38,40]

$$U(\psi) = 1 - \cos(\psi) + \frac{\Gamma_0}{4}[1 - \cos(2\psi)] + \Gamma_h h \sin(\psi), \quad (1)$$

where $\psi = \langle\phi(x)\rangle$ is the average Josephson phase across the JJ (the averaging $\langle \ldots \rangle$ is over the JJ length L, which is assumed to be smaller than the Josephson length λ_J). This is the phase that is measured across the JJ, if it is treated as an element with two wires or electrodes coming out. The constants $\Gamma_0 < 0$ and Γ_h are related to the geometrical and electrical parameters of the JJ, and h is the normalized magnetic field [38,40]. For longer JJs, the $U(\psi)$ profile deviates from the analytical form given by Eq. (1) but can be calculated numerically. In any case, the following common behavior of the φ JJ is observed: at zero magnetic field $h = 0$ the Josephson energy $U(\psi)$ is reflection symmetric (see Fig. 1); at $h \neq 0$ it becomes asymmetric due to the presence of both $\cos(2\psi)$ and $\sin(\psi)$ terms in Eq. (1). Thus, one is able not only to construct a ratchet closely mimicking the paradigmatic example, but also tune its asymmetry during experiments by changing h, e.g., switch it on, off, reverse its sign, etc. This is an extremely useful feature from a practical point of view as it allows to compare the transport or rectification with and without asymmetry and explore and optimize the ratchet performance by tuning the asymmetry of $U(\psi)$.

The paper is organized as follows. In Sec. II we describe the sample design and present the experimental results of the ratchet operation in the underdamped regime. Section III concludes the paper.

II. EXPERIMENTAL RESULTS

We used superconductor-insulator-ferromagnet-superconductor (SIFS) Josephson junctions that are fabricated as Nb|Al-Al_2O_3|$Ni_{0.6}Cu_{0.4}$|Nb multilayers [41,42]. They consist of two segments: the first is a 0 segment of length L_0 with the thickness of the ferromagnetic layer $d_{F,0}$ and the critical current density $j_{c,0} > 0$. The second is a π segment of length L_π with the thickness of the ferromagnetic layer $d_{F,\pi}$ and $j_{c,\pi} < 0$. Such a JJ as a whole behaves [38,40] as a φ JJ with the average phase $\psi = \langle\phi(x)\rangle$ and the Josephson energy $U(\psi)$ qualitatively similar to the one given by Eq. (1). The exact $U(\psi)$ profile can be calculated only numerically [39].

*gold@uni-tuebingen.de

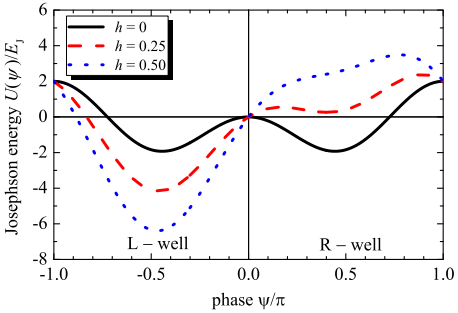

FIG. 1. Josephson energy $U(\psi)$ tuned by an applied magnetic field h, normalized in the usual way as $h = 2H/H_{c1}$, where $H_{c1} = \Phi_0/(\pi\mu_0\Lambda\lambda_J)$ is the vortex penetration field and Λ is the effective magnetic thickness of the JJ. Note that at any h the $U(\psi)$ profile remains 2π periodic.

In any case it is important that at bias current $I = 0$ and magnetic field $h = 0$, $U(\psi)$ is a reflection symmetric 2π periodic double well potential with the minima of the wells at $\psi = \pm\varphi + 2\pi n$; see Fig. 1. At $h = 0$ the wells are degenerate, while for $h \neq 0$ the degeneracy is removed [38–40].

As demonstrated in our previous works [39,43,44] a typical property of a φ JJ is to have two critical current branches, denoted here as $I^+_{c,L}(H)$ and $I^+_{c,R}(H)$, measured for increasing [45] (superscript "+") bias current and two branches denoted as $I^-_{c,L}(H)$ and $I^-_{c,R}(H)$ for decreasing [45] (superscript "−") bias current; see Fig. 2(a). These two currents correspond to the escape of the phase out of the left "L" and the right "R" wells of $U(\psi)$; see Fig. 1. The smaller (by amplitude) of the two critical currents (at a given H) can be observed only for low enough damping. For higher damping, upon the escape from, e.g., the L well, the phase can be retrapped in the R well. Consequently one will observe $I^+_{c,R}$ when the phase will later on escape from the R well instead of $I^+_{c,L}$. In general, the damping in SIFS JJs is strongly temperature dependent and reduces for lower temperatures [46]. For our samples we estimated $T = 3.60$ K as the crossover temperature between the high and low damping regime (in a sense of observing both $I_{c,LR}$).

Our measurements were performed in a ^{3}He cryostat, equipped with a multilayer magnetic shielding. All electrical connections (wires) going to/from the sample have been filtered both at room temperature and at cryogenic temperatures. The magnetic field was applied by a coil with $\mu_0 H = \eta \cdot I_{\rm coil}$ with coil factor $\eta \sim 5\,\mu$T/mA.

The dependence of the critical current I_c on the externally applied magnetic field H at $T = 1.70$ K is shown in Fig. 2(a). The existence of two critical current branches $I^{\pm}_{c,L}$ and $I^{\pm}_{c,R}$ as well as the crossing of the branches, typical of a φ JJ, is observed. Two I_c are well visible for $-37\,\mu\text{T} \lesssim \mu_0 H \lesssim -7\,\mu$T and $18\,\mu\text{T} \lesssim \mu_0 H \lesssim 44\,\mu$T. However, for $-7\,\mu\text{T} \lesssim \mu_0 H \lesssim 18\,\mu$T for this particular JJ and T, the $I^+_{c,L}$ and $I^-_{c,R}$ branches are semistable (do not always appear), which is indicated by the dots continuing these branches; see Fig. 2(a). The traceability

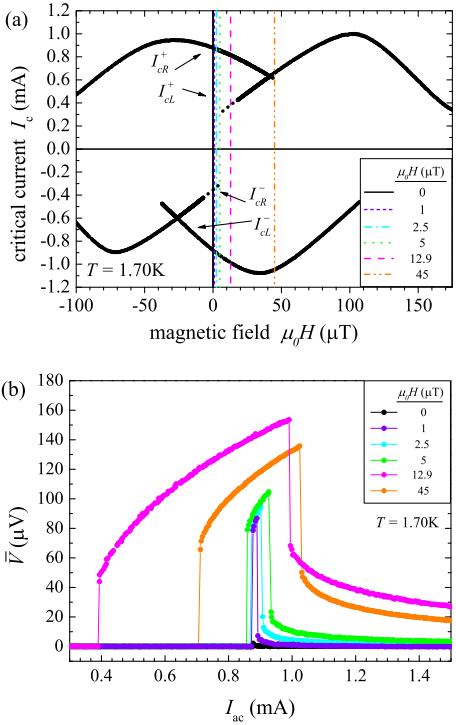

FIG. 2. (a) $I_c(H)$ curve at $T = 1.70$ K. Vertical lines in (a) correspond to the values of $\mu_0 H$, for which different rectification curves $\overline{V}(I_{ac})$ in (b) are measured. The magnetic field is applied in the plane of the JJ perpendicular to the long side of the JJ.

of the lower (by absolute value) $I_c(H)$ branches in experiment also depends on the bias current sweep sequence, i.e., depends on the well, L or R, in which the phase is trapped initially. The sweep sequences are rather different for measurements of $I_c(H)$ and rectification curves; see Figs. 2(b) and 3(b). By applying a magnetic field one can change the asymmetry between the wells of the Josephson potential energy $U(\psi)$ and create an asymmetric periodic potential required for a ratchet operation; see Fig. 1.

Here we present the results obtained in the underdamped regime at $T = 1.70$ K, where the rectification operation is strong and the rectification curves $\overline{V}(I_{ac})$ appear free from extra structures due to the presence of (half-integer zero field) steps on the current-voltage characteristics (IVCs) (see the steps, e.g., in Fig. 4 of Ref. [39]).

In our experiment we measure the rectification curves $\overline{V}(I_{ac})$, i.e., the average voltage *vs.* the amplitude of applied ac current. For this we apply a periodic bias current $I(t) = I_{ac}\sin(2\pi f t)$ with the frequency $f = 10$ Hz and the update rate of 10 000 pts/s (period $T = 100$ ms, 1000 pts/period) and

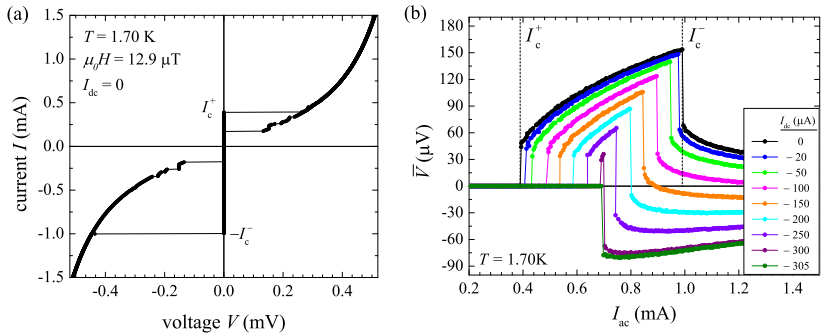

FIG. 3. φ JJ at $T = 1.70$ K and $\mu_0 H = 12.9\,\mu$T. (a) Current-voltage characteristic and (b) rectification curves for different amplitudes of the counterforce $I_{\rm dc}$. In (a) $I_c^+ \approx 389\,\mu$A, $I_r^+ \approx 171\,\mu$A and $I_c^- \approx 997\,\mu$A. The current-voltage characteristic is measured by sweeping the current from the maximum negative value of the current to the maximum positive value of the current and back. Note that, in contrast to the situation at $H = 0$ discussed in Ref. [43], here $H \neq 0$, the potential is asymmetric, and one observes lower positive I_c and higher (by absolute value) negative I_c; cf. Fig. 2(a).

we measure the voltage 1000 times with the sampling rate 10 000 samples/sec, i.e., exactly during one period, starting at an arbitrary moment of time defined by delays in hardware and software. Then the collected samples are averaged to obtain $\overline{V}$ at given $I_{\rm ac}$. The sign of $\overline{V}$ indicates the direction of motion of the phase in the Josephson potential. In the following we discuss the case of $\overline{V} > 0$, *i.e.*, $I_c^+ < |I_c^-|$, where I_c^+ or I_c^- mean the *relevant*, L or R, $I_c^{\pm}(H)$ branch; see below for details. The opposite situation ($\overline{V} < 0$) is similar.

For small $I_{\rm ac}$ the current is so small, that it does not exceed I_c^+, so that the phase remains pinned in the well and $\overline{V} = 0$. If $I_{\rm ac}$ becomes larger, i.e., $I_c^+ < I_{\rm ac} < |I_c^-|$, the voltage becomes $\overline{V} \neq 0$, because for $I_{\rm ac} > I_c^+$ the JJ jumps to the resistive branch. In the underdamped regime, due to the hysteresis on the IVC, the voltage $\overline{V}$ jumps to a finite value at the beginning of the rectification region. Then for $I_{\rm ac} > |I_c^-|$ the voltage $\overline{V}$ decreases because the junction also picks up some negative voltage during the negative semiperiod. In Fig. 2(b), the $\overline{V}(I_{\rm ac})$ curves are shown for different values of the magnetic field H, i.e., for different asymmetries of the energy potential $U(\psi)$. First, at $\mu_0 H = 0$, the rectification is absent ($\overline{V} = 0$), for any amplitude $I_{\rm ac}$ of the driving current $I(t)$. In the absence of external field the energy potential is reflection symmetric, and therefore no rectification is expected. As soon as the field is applied to the JJ, the reflection symmetry of the potential is broken and unidirectional motion of the phase occurs; see Fig. 2(b). The width of the rectification window changes with the applied magnetic field, reflecting the change in the asymmetry of the energy potential and, therefore, $I_c^{\pm}$. For $|\mu_0 H| < 10\,\mu$T we see rather narrow rectification windows due to the small difference in $I_{c,R}^+(H)$ and $|I_{c,L}^-(H)|$. For $10\,\mu\text{T} < |\mu_0 H| < 40\,\mu$T the $I_{c,L}^+$ instead of $I_{c,R}^+$ comes into play. As a result the rectification window increases substantially; see Fig. 2(b). For even larger $|\mu_0 H| \lesssim 40\,\mu$T the rectification window narrows somewhat because the difference between $|I_{c,L}^+|$ and $|I_{c,L}^-|$ decreases; see Fig. 2(a).

Up to now the ratchet shows operation in the idle regime ($I_{\rm dc} = 0$). We now apply an additional dc bias current $I_{\rm dc}$ (counterforce) to the ratchet, which tries to stop the ratchet or even move the phase in the direction opposite to the rectification direction. If the ratchet is able to overcome the counterforce $I_{\rm dc}$, it produces a mean output power $\overline{P}_{\rm out} = I_{\rm dc}\overline{V} < 0$ (i.e., the work is done by the ratchet on the current source). Furthermore one can calculate the efficiency, given by $\eta = -\overline{P}_{\rm out}/\overline{P}_{\rm in}$, where $\overline{P}_{\rm in}$ is the mean input power.

To demonstrate the operation of the ratchet against the counterforce, we have chosen the value of $\mu_0 H = 12.9\,\mu$T, where the rectification window is largest. Fig. 3(a) shows the IVC of the device for this value of H. Here the relevant $I_c^+ \equiv I_{c,L}^+(H)$ and $I_c^- \equiv I_{c,L}^-(H) < 0$, i.e. the pinning or depinning game takes place in the L well, which becomes deeper at $H > 0$, while the R well becomes more shallow and may even disappear.

The stopping force $I_{\rm stop}(I_{\rm ac})$ is defined as the current $I_{\rm dc}$ at which $\overline{V}$ (within the rectification window in the idle regime) vanishes or changes sign at a given $I_{\rm ac}$. We measured many rectification curves $\overline{V}(I_{\rm ac})$, each time increasing the amplitude of the dc current. Since we have a positive rectification, $\overline{V} > 0$, the counterforce $I_{\rm dc} < 0$ should be negative. The results are shown in Fig. 3(b). Starting from the curve with $I_{\rm dc} = 0$, one can see that by increasing the absolute value of $I_{\rm dc}$ the rectification window narrows, indicating that the additional bias actually stops the ratchet at the regions where the ratchet was not strong enough (edges of the idle rectification window). Note that the shrinkage is symmetric relative to the center of the rectification window, and this is due to the fact that the constant bias shifts up all the currents of the IVC. From these measurements we see that the at $I_{\rm dc}^{\rm off} \approx -307\,\mu$A the rectification window closes completely and the ratchet operation stops fully. The theoretical value can be calculated using our parameters (see the caption of Fig. 3) as [47] $I_{\rm dc}^{\rm off} = (I_c^+ - |I_c^-|)/2 = -304\,\mu$A, which is a rather exact coincidence with the experimental value. According to the

theory [47] the full-stop force I_{dc}^{off} depends *only* on I_c^+ and I_c^- but not on the shape of the IVC.

For given I_{dc}, the maximum efficiency is always reached at $I_{ac} = J_c^+ \equiv I_c^+ - I_{dc}$, i.e., in the beginning of the rectification window and is given by [47]

$$\eta_{max} = \frac{-2I_{dc}\left[I_{dc}\arccos\left(\frac{J_c^+}{J_c^-}\right) + \sqrt{J_c^{+2} - J_r^{+2}}\right]}{J_c^{+2}\arccos\left(\frac{J_c^+}{J_c^-}\right) + \sqrt{J_c^{+2} - J_r^{+2}}(J_r^+ + 2I_{dc})}, \quad (2)$$

where $J_r^+ = I_r^+ - I_{dc}$, with I_r^+ the return current from the resistive branch.

Using Eq. (2) and our parameters (see the caption of Fig. 3) we may plot the dependence $\eta_{max}(I_{dc})$ given by Eq. (2). This dependence (not shown) smoothly grows with $|I_{dc}|$. The maximum value of $|I_{dc}|$ that makes sense is I_{dc}^{off} measured and calculated above. At this I_{dc} the rectification window is about to close completely, but the ratchet is the most efficient with $\eta_{max} = 48\%$. This is a fairly good value, which is not much lower than the maximum efficiency of $\eta_{max} = 60\%$ observed in a specially designed vortex ratchet [16]. We stress here that our φ JJ was not optimized or designed for operation as a ratchet. It is one of two samples used in the original experimental work on φ JJs [39].

III. CONCLUSIONS

Although there were many theoretical studies on ratchets where the particle moves in an asymmetric periodic potential, the practical implementation of a simple paradigmatic system using a Josephson junction was missing, mainly because the Josephson energy in conventional junctions is reflection symmetric. Here we have demonstrated that in φ Josephson junctions this symmetry is broken and one can obtain rectification as a result of directed transport of the phase. The advantage of this system is that the asymmetry is tunable by a magnetic field H, so that one can clearly see the (dis)appearance of rectification as a function of H, as well as optimize its operation. The maximum efficiency that can be obtained with such a ratchet is rather high, considering that the parameters of the investigated junction (e.g., the asymmetry of the 0 and π part) are not optimized for the ratchet operation.

A φ JJ is only one example of constructing a system with desired nontrivial Josepshon energy profile $U(\psi)$. Following this general approach, one can try to design even more asymmetric ratchets that will provide a huge rectification window and, consequently, have higher full-stop current I_{dc}^{off} and higher efficiency η.

ACKNOWLEDGMENTS

R.M. gratefully acknowledges support by the Carl Zeiss Stiftung. This work was supported by the Deutsche Forschungsgemeinschaft (DFG) via Project No. GO-1106/5, via project A5 within SFB/TRR-21, and by the EU-FP6-COST action MP1201.

[1] P. Reimann, Brownian motors: Noisy transport far from equilibrium, Phys. Rep. **361**, 57 (2002).
[2] H. Linke, Special issue on "Ratchets and Brownian motors: Basics, experiments, and applications," Appl. Phys. A **75**, 167 (2002), guest editor.
[3] P. Hänggi, F. Marchesoni, and F. Nori, Brownian motors, Ann. Phys. **14**, 51 (2005).
[4] Peter Hänggi and Fabio Marchesoni, Artificial Brownian motors: Controlling transport on the nanoscale, Rev. Mod. Phys. **81**, 387 (2009).
[5] F. Jülicher, A. Ajdari, and J. Prost, Modelling molecular motors, Rev. Mod. Phys. **69**, 1269 (1997).
[6] F. Falo, P. J. Martínez, J. J. Mazo, and S. Cilla, Ratchet potential for fluxons in Josephson-junction arrays, Europhys. Lett. **45**, 700 (1999).
[7] E. Trías, J. J. Mazo, F. Falo, and T. P. Orlando, Depinning of kinks in a Josephson-junction ratchet array, Phys. Rev. E **61**, 2257 (2000).
[8] E. Goldobin, A. Sterck, and D. Koelle, Josephson vortex in a ratchet potential: Theory, Phys. Rev. E **63**, 031111 (2001).
[9] G. Carapella, Relativistic flux quantum in a field-induced deterministic ratchet, Phys. Rev. B **63**, 054515 (2001).
[10] G. Carapella and G. Costabile, Ratchet Effect: Demonstration of a Relativistic Fluxon Diode, Phys. Rev. Lett. **87**, 077002 (2001).
[11] G. Carapella, G. Costabile, N. Martucciello, M. Cirillo, R. Latempa, A. Polcari, and G. Filatrella, Experimental realization of a relativistic fluxon ratchet, Physica C **382**, 337 (2002).
[12] K. H. Lee, Ratchet effect in an ac-current driven Josephson junction array, Appl. Phys. Lett. **83**, 117 (2003).
[13] A. V. Ustinov, C. Coqui, A. Kemp, Y. Zolotaryuk, and M. Salerno, Ratchetlike Dynamics of Fluxons in Annular Josephson Junctions Driven by Biharmonic Microwave Fields, Phys. Rev. Lett. **93**, 087001 (2004).
[14] M. Beck, E. Goldobin, M. Neuhaus, M. Siegel, R. Kleiner, and D. Koelle, High-Efficiency Deterministic Josephson Vortex Ratchet, Phys. Rev. Lett. **95**, 090603 (2005).
[15] H. B. Wang, B. Y. Zhu, C. Gürlich, M. Ruoff, S. Kim, T. Hatano, B. R. Zhao, Z. X. Zhao, E. Goldobin, D. Koelle, and R. Kleiner, Fast Josephson vortex ratchet made of intrinsic Josephson junctions in $Bi_2Sr_2CaCu_2O_8$, Phys. Rev. B **80**, 224507 (2009).
[16] M. Knufinke, K. Ilin, M. Siegel, D. Koelle, R. Kleiner, and E. Goldobin, Deterministic Josephson vortex ratchet with a load, Phys. Rev. E **85**, 011122 (2012).
[17] S. Weiss, D. Koelle, J. Müller, R. Gross, and K. Barthel, Ratchet effect in dcSQUIDs, Europhys. Lett. **51**, 499 (2000).
[18] A. Sterck, S. Weiss, and D. Koelle, SQUID ratchets: basics and experiments, Appl. Phys. A **75**, 253 (2002).
[19] A. Sterck, R. Kleiner, and D. Koelle, Three-Junction SQUID Rocking Ratchet, Phys. Rev. Lett. **95**, 177006 (2005).
[20] A. Sterck, D. Koelle, and R. Kleiner, Rectification in a Stochastically Driven Three-Junction SQUID Rocking Ratchet, Phys. Rev. Lett. **103**, 047001 (2009).
[21] J. Spiechowicz, P. Hänggi, and J. Łuczka, Josephson junction ratchet: The impact of finite capacitances, Phys. Rev. B **90**, 054520 (2014).
[22] J. Spiechowicz and J. Łuczka, Josephson phase diffusion in the superconducting quantum interference device ratchet, Chaos **25**, 053110 (2015).

[23] J. Spiechowicz and J. Łuczka, Efficiency of the SQUID ratchet driven by external current, New J. Phys. **17**, 023054 (2015).
[24] J. E. Villegas, S. Savel'ev, F. Nori, E. M. Gonzalez, J. V. Anguita, R. Garcia, and J. L. Vicent, A superconducting reversible Rectifier that controls the motion of magnetic flux quanta, Science **302**, 1188 (2003).
[25] S. Savel'ev and F. Nori, Experimentally realizable devices for controlling the motion of magnetic flux quanta in anisotropic superconductors, Nat. Mater. **1**, 179 (2002).
[26] J. Spiechowicz, P. Hänggi, and J. Łuczka, Brownian motors in the microscale domain: Enhancement of efficiency by noise, Phys. Rev. E **90**, 032104 (2014).
[27] J. Spiechowicz and J. Łuczka, Diffusion anomalies in ac-driven Brownian ratchets, Phys. Rev. E **91**, 062104 (2015).
[28] M. O. Magnasco, Forced Thermal Ratchets, Phys. Rev. Lett. **71**, 1477 (1993).
[29] R. Bartussek, P. Hänggi, and J. G. Kissner, Periodically rocked thermal ratchets, Europhys. Lett. **28**, 459 (1994).
[30] C. R. Doering, W. Horsthemke, and J. Riordan, Nonequilibrium Fluctuation-Induced Transport, Phys. Rev. Lett. **72**, 2984 (1994).
[31] P. Jung, J. G. Kissner, and P. Hänggi, Regular and Chaotic Transport in Asymmetric Periodic Potentials: Inertia Ratchets, Phys. Rev. Lett. **76**, 3436 (1996).
[32] J. Kula, T. Czernik, and J. Łuczka, Brownian Ratchets: Transport Controlled by Thermal Noise, Phys. Rev. Lett. **80**, 1377 (1998).
[33] A. Sarmiento and H. Larralde, Deterministic transport in ratchets, Phys. Rev. E **59**, 4878 (1999).
[34] M. Barbi and M. Salerno, Phase locking effect and current reversal in deterministic underdamped ratchets, Phys. Rev. E **62**, 1988 (2000).
[35] J. L. Mateos, Chaotic Transport and Current Reversal in Deterministic Ratchets, Phys. Rev. Lett. **84**, 258 (2000).
[36] M. Kostur and J. Łuczka, Multiple current reversal in Brownian ratchets, Phys. Rev. E **63**, 021101 (2001).
[37] M. Borromeo, G. Costantini, and F. Marchesoni, Deterministic ratchets: Route to diffusive transport, Phys. Rev. E **65**, 041110 (2002).
[38] E. Goldobin, D. Koelle, R. Kleiner, and R. G. Mints, Josephson Junction with a Magnetic-Field Tunable Ground State, Phys. Rev. Lett. **107**, 227001 (2011).
[39] H. Sickinger, A. Lipman, M. Weides, R. G. Mints, H. Kohlstedt, D. Koelle, R. Kleiner, and E. Goldobin, Experimental Evidence of a φ Josephson Junction, Phys. Rev. Lett. **109**, 107002 (2012).
[40] A. Lipman, R. G. Mints, R. Kleiner, D. Koelle, and E. Goldobin, Josephson junctions with tunable current-phase relation, Phys. Rev. B **90**, 184502 (2014).
[41] M. Weides, C. Schindler, and H. Kohlstedt, Low-t_c Josephson junctions with tailored barrier, J. Appl. Phys. **101**, 063902 (2007).
[42] M. Weides, U. Peralagu, H. Kohlstedt, J. Pfeiffer, M. Kemmler, C. Gürlich, E. Goldobin, D. Koelle, and R. Kleiner, Critical current diffraction pattern of SIFS Josephson junctions with a step-like F-layer, Supercond. Sci. Technol. **23**, 095007 (2010).
[43] R. Menditto, H. Sickinger, M. Weides, H. Kohlstedt, M. Žonda, T. Novotný, D. Koelle, R. Kleiner, and E. Goldobin, Phase retrapping in a φ Josephson junction: Onset of the butterfly effect, Phys. Rev. B **93**, 174506 (2016).
[44] E. Goldobin, D. Koelle, R. Kleiner, and A. Buzdin, Josephson junctions with second harmonic in the current-phase relation: Properties of φ junctions, Phys. Rev. B **76**, 224523 (2007).
[45] Here increasing and decreasing is understood *not* by absolute value. That is $I^{+}_{c,LR}$ are measured when the bias current is swept towards positive direction (increasing), while $I^{-}_{c,LR}$ are measured when the bias current is swept towards negative direction direction (decreasing).
[46] J. Pfeiffer, M. Kemmler, D. Koelle, R. Kleiner, E. Goldobin, M. Weides, A. K. Feofanov, J. Lisenfeld, and A. V. Ustinov, Static and dynamic properties of 0, π, and 0-π ferromagnetic Josephson tunnel junctions, Phys. Rev. B **77**, 214506 (2008).
[47] E. Goldobin, R. Menditto, D. Koelle, and R. Kleiner, Model I-V curves and figures of merit of underdamped deterministic Josephson ratchets, Phys. Rev. E **94**, 032203 (2016).

Publication 4

Observation of 0–π transition in SIsFS Josephson junctions

N. Ruppelt,[1,a)] H. Sickinger,[2] R. Menditto,[2] E. Goldobin,[2] D. Koelle,[2] R. Kleiner,[2] O. Vavra,[1,b)] and H. Kohlstedt[1]

[1]*Nanoelektronik, Technische Fakultät, Christian-Albrechts-Universität zu Kiel, Kaiserstr. 2, 24143 Kiel, Germany*

[2]*Physikalisches Institut and Center for Collective Quantum Phenomena in LISA$^+$, Universität Tübingen, Auf der Morgenstelle 14, 72076 Tübingen, Germany*

(Received 15 October 2014; accepted 26 December 2014; published online 13 January 2015)

The 0–π transition in Superconductor-Insulator-superconductor-Ferromagnet-Superconductor (SIsFS) Josephson junctions (JJs) was investigated experimentally. As predicted by theory, an s-layer inserted into a ferromagnetic SIFS junction can enhance the critical current density up to the value of an SIS tunnel junction. We fabricated Nb′ | AlO_x | Nb | $Ni_{60}Cu_{40}$ | Nb JJs with wedge-like s (Nb) and F ($Ni_{60}Cu_{40}$) layers and studied the Josephson effect as a function of the s- and F-layer thickness, d_s and d_F, respectively. For $d_s = 11$ nm, π-JJs with SIFS-type $j_c(d_F)$ and critical current densities up to $j_c^{\pi} = 60\,A/cm^2$ were obtained at 4.2 K. Thicker d_s led to a drastic increase of the critical current decay length, accompanied by the unexpected disappearance of the 0–π transition dip in the $j_c(d_F)$ dependence. Our results are relevant for superconducting memories, rapid single flux quantum logic circuits, and solid state qubits. © *2015 AIP Publishing LLC*. [http://dx.doi.org/10.1063/1.4905672]

The introduction of a ferromagnet into the barrier of a Josephson junction (JJ) can lead to a π-JJ.[1] Over the last years, in-depth studies were performed to theoretically and experimentally analyze the critical current density in Josephson junctions in dependence on the ferromagnetic (F) layer properties, e.g., in SFS and SIFS junctions (S: superconductor and I: insulator).[2–4] Apart from addressing some fundamental questions, such as pair breaking mechanisms or the proximity effect at SF interfaces, novel promising applications are expected.[5–9] If properly designed, SF based Josephson junctions may enhance the design flexibility in superconducting circuitry and solid state qubits.[10–12] In particular, they offer new perspectives for the important field of non-volatile superconducting memories.[13,14] In general, low values of critical current density j_c and characteristic voltage $V_c = I_c R_N$ (I_c: critical current and R_N: normal resistance) limit the switching time $\tau \sim 1/V_c$ of rapid single flux quantum logic (RSFQ) elements and lead to a large Josephson penetration depth[15] $\lambda_J \sim \sqrt{1/j_c}$ and short coherence times of quantum states.[13] The all-metallic SFS JJs intrinsically have a very low V_c although j_c can be large.[2,16] In SIFS, π-JJs with significantly larger $V_c = 40\,\mu V$ and $j_c = 30\,A/cm^2$ have been achieved but both values are still two orders of magnitude smaller than for SIS JJs.[4,17] Recently, it was proposed to use Superconductor-Insulator-superconductor-Ferromagnet-Superconductor (SIsFS) instead of SIFS JJs.[18] The thin s-layer helps to recover superconductivity, which is suppressed by the I- and F-layers. First experiments compared SIsS and SIsFS junctions and presented similar j_c and $V(I)$ characteristics, which are only slightly modified by the F-layer.[18,19] Theory also predicts an influence of the s-layer on the 0–π transition.[20–22] In this paper, we present a detailed electric transport study on SIsFS junctions with the focus on the variation of the s-layer and F-layer thicknesses.

The Nb′|AlO_x|Nb|$Ni_{60}Cu_{40}$|Nb (SIsFS) layer sequence (from bottom to top) was *in-situ* deposited on $3 \times 8\,cm^2$ Si|SiO_2 wafer stripes in an Oerlikon Univex 450B cluster tool system by using 4-in. DC magnetron sputter sources. The base pressure of the system was 4×10^{-7} mbar. For the Nb′ bottom layer, a 3 × [Nb(40 nm)|Al(3 nm)|] Nb(40 nm)|Al(7 nm) multilayer sequence was sputtered to achieve a low surface roughness.[23] Subsequently, the top Al was oxidized in a pure oxygen atmosphere. A Nb s-layer, a $Ni_{60}Cu_{40}$ F-layer, and 40 nm Nb completed the sandwich structure. Details on the fabrication process can be found elsewhere.[24] The ferromagnet $Ni_{60}Cu_{40}$ was used to obtain SIFS π-JJs comprising large critical current densities and high normal state resistances.[4]

To systematically study the SIsFS junction behaviour depending on the thicknesses of the F-layer d_F and the s-layer d_s, the junctions were fabricated in two ways. In a first set (F-wedge), the samples were composed by a d_F wedge and a constant thickness d_s. The latter was varied from run to run. Vice versa in a second set of samples (s-wedge), d_F was kept constant and d_s was deposited as a wedge. To obtain wedges of the ferromagnet and the superconductor, those layers were deposited off-centered.[4,25] X-ray reflectivity (XRR) measurements in θ–2θ configuration were performed to determine the thickness and hence the deposition rate r for various calibration points along the radial distance x from the target center. For the Nb and $Ni_{60}Cu_{40}$ films, we obtained a smooth and monotonic thickness gradient along the wafer stripes, as shown in Fig. 1 for $Ni_{60}Cu_{40}$. The inset shows XRR data from two points located 38 mm apart from each other. The F-wedge samples presented in this paper were fabricated in the region marked by a dashed line. A similar approach was applied to calibrate the intermediate Nb layer

a)Electronic mail: nru@tf.uni-kiel.de
b)Present address: Experimentelle und Angewandte Physik, Universität Regensburg, Universitätsstr. 31, 93053 Regensburg, Germany.

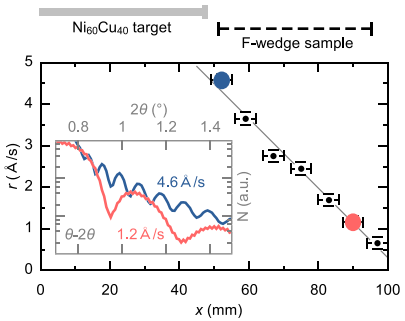

FIG. 1. $Ni_{60}Cu_{40}$ deposition rate r vs. radial distance from the target center x. F-wedge JJs were fabricated in a region (├- - -┤), which exhibits a quasi-linear rate gradient. Inset: XRR in θ–2θ alignment, corresponding to bold dots in main graph.

thickness d_s. The Nb deposition rate for the s-wedge samples varied between 0.75 Å/s and 4 Å/s. In the F-wedge JJs, the I-layer was oxidized by using parameters that lead to SIS junctions with $j_c = 7\,\mathrm{kA/cm^2}$ at 4.2 K. For the s-wedge JJs, the I-layer oxidisation parameters were the same as those we used for the fabrication of SIS reference junctions with $j_c = 1.2\,\mathrm{kA/cm^2}$.

An electric characterization of individual Josephson junctions was done in a liquid helium dip-stick equipped with a coil, to produce a homogeneous magnetic field along the junction width w. Junctions with areas $(l \times w)$ $10 \times 10\,\mu\mathrm{m}^2$ and $50 \times 10\,\mu\mathrm{m}^2$ were wire bonded in a four point arrangement. Current–voltage curves $V(I)$ and critical current versus magnetic field dependencies $I_c(H)$ were recorded at 4.2 K. A demagnetization procedure prior to the measurement resulted in a homogeneous and maximized critical current through the junction as indicated by a Fraunhofer-like $I_c(H)$ dependence. Therefore, a damped oscillating magnetic field sweep starting at a maximum amplitude of 20 mT was applied at a temperature between 10 K and 15 K. We would like to emphasize that without this particular magnetic treatment non-reproducible $I_c(H)$ with reduced j_c occurred, especially for large d_F (>7 nm). To account for the influence of remanent magnetization of the F-layer on the measurement, the critical current of a junction and its $V(I)$ were not recorded at zero applied field but at the maximum of the $I_c(H)$ pattern.

Josephson junctions with various combinations of d_s and d_F were studied. Representative $V(I)$ and $I_c(H)$ dependencies for SIFS structures (Figs. 2(a) and 2(b)) and SIsFS with $d_s = 30$ nm (Figs. 2(c) and 2(d)) demonstrate a broad variation in the junction characteristics such as hysteresis and j_c caused by variations in d_F and d_s. The normal resistance R_N was $\sim 0.3\,\Omega$ for all $10 \times 10\,\mu\mathrm{m}^2$ junctions. The s-layer assisted to maintain SIS-like $V(I)$ characteristics for JJs with $d_F \approx 2$ nm (Fig. 2(c)) and, except for a slight decrease of the subgap resistance, also up to several nm of $Ni_{60}Cu_{40}$ (Fig. 2(d)).

The dependence of the critical current density j_c on the thickness of the ferromagnetic interlayer d_F (F-wedge) is shown in Fig. 3 for d_s ranging from 0 to 60 nm. For SIFS ($d_s = 0$) junctions, $j_c(d_F)$ shows a distinct minimum at $d_F = 5.8$ nm

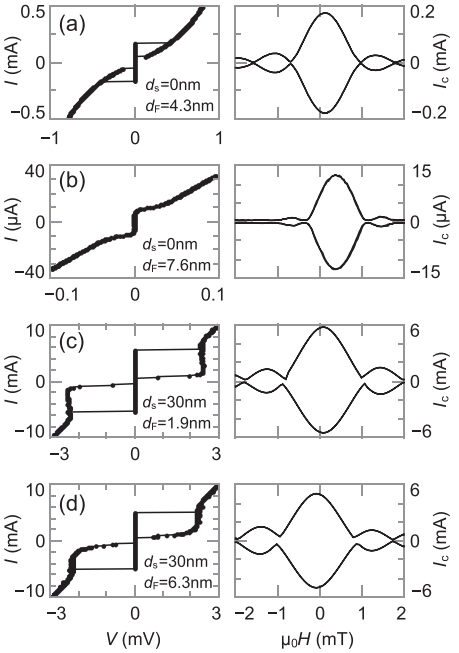

FIG. 2. Current–voltage characteristics $V(I)$ and magnetic field dependence $I_c(H)$ for different layer thicknesses d_s and d_F (junction area $10 \times 10\,\mu\mathrm{m}^2$). Labels (a)–(d) correspond to data points in Fig. 3.

indicating the cross over from the 0 to π ground state. A similar feature is observed for series of junctions with $d_s \leq 11$ nm. They all exhibit a well pronounced cusp-like dip in $j_c(d_F)$, which is considered as an unambiguous indicator for a 0–π transition. For increasing d_s, we notice a tendency of the $j_c(d_F)$ dependence towards the upper right corner of Fig. 3, i.e., the 0–π transition shifts by $\Delta d_F = 1$ nm from $d_s = 0$ nm to 11 nm and j_c rises overall.

At $d_s = 13$ nm and above the enhancement in j_c with increasing d_s persists, however, the 0–π transition disappeared or cannot be resolved unambiguously. In addition, the junction characteristics became sensitive to the history of magnetic treatment. For $d_s \leq 11$ nm, the demagnetization procedure reliably led to a Fraunhofer pattern, a maximum critical current amplitude and, most likely, to a well defined magnetic state. Although junctions with thicker d_s could also show a Fraunhofer pattern, the maximum critical current amplitude was very sensitive to the magnetic history of the junction.

For $d_s = 30$ nm and 60 nm, the critical current density was practically independent of d_F. Obviously, the AlO_x tunnel barrier limits the critical current of those junctions to approximately $7\,\mathrm{kA/cm^2}$. For junctions with $d_s = 60$ nm, the $V(I)$ curve and $I_c(H)$ resembled pure SIS characteristics (see Fig. 2(c)) for all d_F under investigation.

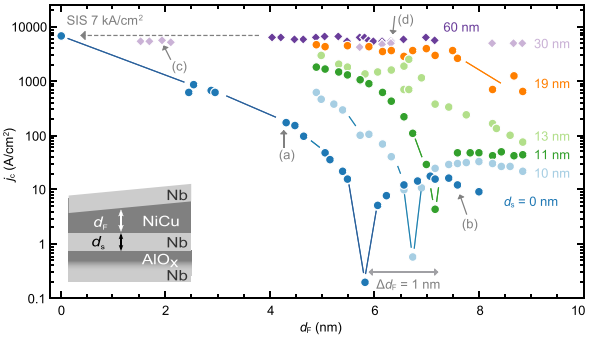

FIG. 3. Critical current density j_c vs. the $Ni_{60}Cu_{40}$ thickness d_F for Nb′ | AlO_x | Nb | $Ni_{60}Cu_{40}$ | Nb Josephson junctions ($10 \times 10\,\mu m^2$) with d_s from 0 nm to 60 nm (F-wedge). Shift of 0–π transition dip indicated by Δd_F. Electrical characteristics for junctions labeled with (a)–(d) are presented in Fig. 2. Inset: layer sequence for F-wedge series with constant d_s and thickness gradient in d_F.

The $j_c(d_F)$ dependencies for $d_s \leq 11$ nm are in good qualitative agreement with the theoretical predictions. Apparently, the thin s-layer in proximity to the F-layer behaves like a normal metal (n) and shifts the 0–π transition towards larger d_F, while j_c is enhanced.[22] Furthermore, the Nb interlayer reduces the suppression of the critical current density caused by the ferromagnetic layer until for $d_s \geq 30$ nm the critical current density reaches the value of pure SIS junctions with the same tunnel barrier. Calculations also predict a d_F induced 0–π transition up to large values of d_s, where equal critical current densities occur in 0 and π junctions.[20] However, in our experiments no evidence for such a π-JJ with SIS like j_c was found. In fact, the maximum j_c, clearly identified in a π junction, is a factor 100 smaller than predicted.

In the following, we present results on s-wedge type junctions, as shown in Fig. 4. For this investigation, the critical current density of pure SIS reference junctions was set to 1.2 kA/cm^2 representing the upper limit for j_c. We assume that, despite the change of the maximum j_c, the results of F-wedge and s-wedge junctions can be compared qualitatively. Indeed, the $j_c(d_s)$ curves in Fig. 4 consistently follow a trend that can be expected from Fig. 3. For any d_s between 4 nm and 14 nm, the value of j_c decreases from $d_F = 3.1$ nm down to a minimum at 5.8 nm but rises again at $d_F = 6.3$ nm. With larger d_s all $j_c(d_s)$ converge towards the maximum value which is defined by the SIS reference junction. The transition between regions that are d_F-dependent and regions that are d_F-independent occurs around $d_s = 15$ nm over a width of about $\Delta d_s \approx 3$ nm. Our experimental data shown in Fig. 4 for various d_F closely resembles the shape of several theoretical $I_cR_N(d_F)$ curves that vary in the magnitude of the ferromagnetic exchange energy instead.[19]

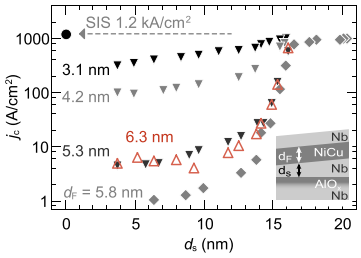

FIG. 4. Critical current density j_c vs. s-layer thickness d_s for series with different F-layer thickness d_F (s-wedge). Junction areas are $50 \times 10\,\mu m^2$ or $10 \times 10\,\mu m^2$. Inset: layer sequence for s-wedge series with thickness gradient in d_s.

In conclusion, we systematically investigated Nb-based SIsFS Josephson junctions by using a wedge deposition technique. The s-layer thickness d_s had a significant influence on the critical current density j_c of the junctions without affecting the normal resistance which is mainly defined by the AlO_x tunnel barrier. For a F-layer thickness $d_F < 9$ nm, $V(I)$ characteristics and critical current densities similar to SIS tunnel junctions could be realized. In addition, F-layer thickness induced 0–π transitions were observed for $d_s \leq 11$ nm. This allowed to realize SIsFS π junctions with $j_c = 60$ A/cm^2, i.e., a twofold increase compared to corresponding SIFS junctions. However, j_c in the π junctions is at least two orders of magnitude lower than in a corresponding SIS junction and does not show tunnel junction $V(I)$ characteristics. Methodically, the wedge technology is a suitable approach to optimize thickness dependent junction parameters with respect to the specific field of use. SIsFS junctions might be an interesting element for a number of applications, for example, as lumped π shifter or memory in superconducting logic circuits and in self biased solid state qubits.

This work has been funded by Deutsche Forschungsgemeinschaft (DFG) within the project "Semifluxons in ferromagnetic Josephson junctions" KO 1953/11-1 and GO 1106/3-1. H.S. gratefully acknowledges support by the Evangelisches Studienwerk Villigst e.V. and R.M. gratefully acknowledges support by the Carl Zeiss Stiftung.

[1]A. I. Buzdin, L. N. Bulaevskii, and S. V. Panyukov, JETP Lett. **35**, 178 (1982).
[2]V. V. Ryazanov, V. A. Oboznov, A. Y. Rusanov, A. V. Veretennikov, A. A. Golubov, and J. Aarts, Phys. Rev. Lett. **86**, 2427 (2001).
[3]T. Kontos, M. Aprili, J. Lesueur, F. Genêt, B. Stephanidis, and R. Boursier, Phys. Rev. Lett. **89**, 137007 (2002).
[4]M. Weides, M. Kemmler, E. Goldobin, D. Koelle, R. Kleiner, H. Kohlstedt, and A. Buzdin, Appl. Phys. Lett. **89**, 122511 (2006).
[5]A. I. Buzdin, Rev. Mod. Phys. **77**, 935 (2005).

[6]E. Terzioglu and M. R. Beasley, IEEE Trans. Appl. Supercond. **8**, 48 (1998).
[7]O. Mielke, T. Ortlepp, B. Dimov, and F. H. Uhlmann, J. Phys.: Conf. Ser. **97**, 012196 (2008).
[8]L. B. Ioffe, V. B. Geshkenbein, M. V. Feigel'man, A. L. Fauchère, and G. Blatter, Nature **398**, 679 (1999).
[9]T. Yamashita, K. Tanikawa, S. Takahashi, and S. Maekawa, Phys. Rev. Lett. **95**, 097001 (2005).
[10]O. Mielke, T. Ortlepp, P. Febvre, and F. Uhlmann, IEEE Trans. Appl. Supercond. **19**, 621 (2009).
[11]T. Ortlepp, O. Mielke, J. Kunert, and H. Toepfer, Physica C **470**, 1955 (2010).
[12]A. K. Feofanov, V. A. Oboznov, V. V. Bol'ginov, J. Lisenfeld, S. Poletto, V. V. Ryazanov, A. N. Rossolenko, M. Khabipov, D. Balashov, A. B. Zorin, P. N. Dmitriev, V. P. Koshelets, and A. V. Ustinov, Nat. Phys. **6**, 593 (2010).
[13]V. V. Ryazanov, V. V. Bol'ginov, D. S. Sobanin, I. V. Vernik, S. K. Tolpygo, A. M. Kadin, and O. A. Mukhanov, Phys. Procedia **36**, 35 (2012).
[14]E. Goldobin, H. Sickinger, M. Weides, N. Ruppelt, H. Kohlstedt, R. Kleiner, and D. Koelle, Appl. Phys. Lett. **102**, 242602 (2013).
[15]A. Barone and G. Paternò, *Physics and Applications of the Josephson Effect* (Wiley, New York, 1982).
[16]V. V. Ryazanov, V. A. Oboznov, A. S. Prokofiev, V. V. Bolginov, and A. K. Feofanov, J. Low Temp. Phys. **136**, 385 (2004).
[17]G. Wild, C. Probst, A. Marx, and R. Gross, Eur. Phys. J. B **78**, 509 (2010).
[18]T. I. Larkin, V. V. Bol'ginov, V. S. Stolyarov, V. V. Ryazanov, I. V. Vernik, S. K. Tolpygo, and O. A. Mukhanov, Appl. Phys. Lett. **100**, 222601 (2012).
[19]I. Vernik, V. Bol'ginov, S. Bakurskiy, A. Golubov, M. Kupriyanov, V. Ryazanov, and O. Mukhanov, IEEE Trans. Appl. Supercond. **23**, 1701208 (2013).
[20]S. V. Bakurskiy, N. V. Klenov, I. I. Soloviev, V. V. Bol'ginov, V. V. Ryazanov, I. V. Vernik, O. A. Mukhanov, M. Y. Kupriyanov, and A. A. Golubov, Appl. Phys. Lett. **102**, 192603 (2013).
[21]S. V. Bakurskiy, N. V. Klenov, I. I. Soloviev, M. Y. Kupriyanov, and A. A. Golubov, Phys. Rev. B **88**, 144519 (2013).
[22]D. M. Heim, N. G. Pugach, M. Y. Kupriyanov, E. Goldobin, D. Koelle, R. Kleiner, N. Ruppelt, M. Weides, and H. Kohlstedt, e-print arXiv:1310.0567v2 [cond-mat.supr-con].
[23]H. Kohlstedt, F. König, P. Henne, N. Thyssen, and P. Caputo, J. Appl. Phys. **80**, 5512 (1996).
[24]M. Weides, K. Tillmann, and H. Kohlstedt, Physica C **437–438**, 349 (2006).
[25]N. Ruppelt, O. Vavra, H. Sickinger, E. Goldobin, D. Koelle, R. Kleiner, and H. Kohlstedt, Appl. Phys. A **116**, 229 (2014).